CHALMERS
UNIVERSITY OF TECHNOLOGY

Shape Optimization of High Voltage Electrodes

Master's thesis in Electric Power Engineering

JUNIOR SHEMA

DEPARTMENT OF ELECTRICAL ENGINEERING

CHALMERS UNIVERSITY OF TECHNOLOGY
Gothenburg, Sweden 2023
www.chalmers.se

MASTER’S THESIS 2023

Shape optimization of high voltage electrodes

JUNIOR SHEMA

Department of Electrical Engineering
CHALMERS UNIVERSITY OF TECHNOLOGY
Göteborg, Sweden 2023

Shape optimization of high voltage electrodes

JUNIOR SHEMA

Master 's thesis 2023
Department of Electrical Engineering
Chalmers University of Technology
SE- 412 96 Göteborg
Sweden
Telephone: + 46 (0) 31- 772 1000

Typeset in MS Word

Gothenburg, Sweden 2023

Shape optimization of high voltage electrodes.

Junior Shema
Department of Electrical Engineering
Chalmers University of Technology

Abstract

Electrostatic screens and electrodes used in high voltage apparatuses and in test setups in high voltage laboratories are essential for proper operation of the equipment and for performing high voltage withstand tests. Electrostatic fields generated on their surfaces must be minimized to prevent parasitic discharges in surrounding air especially under conditions of limited space. To realize this, shape of the electrodes can be optimized in a way that the maximum electric field strength is kept below the critical level corresponding to the initiation of breakdown in air.

In the thesis, the optimization methods provided in COMSOL Multiphysics software were examined and shape optimization was employed in the electrostatic problem for minimizing the maximum field strength. Several 2D study cases reflecting typical electrode shapes providing different field enhancement factors were implemented. The effects of various parameters in the optimization algorithms on the shapes of the electrodes and respective reductions of the maximum field were analyzed. The influence of the proximity of the boundaries to the energized electrodes was also investigated and best practices for selecting numerical parameters for the optimization were established. Furthermore, 3D scanning of the real 400 kV high voltage divider equipped with a toroidal electrostatic screen was performed using Scaniverse software installed on iPhone. The obtained scan was cleaned up and imported into COMSOL Multiphysics for conducting electrostatic field calculations. The procedure developed with the 2D study cases was used for shape optimization of the 3D high voltage divider to demonstrate the validity of the method for real scale high voltage devices.

Acknowledgements

I would like to express my deep gratitude to my examiner Prof.Yuriy Serdyuk for his dedication in helping me understand the project regardless of the workload, busy schedule he had. His prior knowledge and expertise in high voltage engineering was indeed of great help.

Thanks to the collaboration between Chalmers and Nexans Norway AS, I acquired this opportunity of doing my master's degree project which greatly helped me evolve, gain knowledge about the scientific phenomena related to flashovers, corona in which I believe will have a positive impact in my future career as an electrical engineer.

Finally, I would also like to thank my family in helping me throughout this master's programme by providing me with the necessary mental support, encouragement needed for me to overcome challenges that I faced in my daily academic life. I dedicate this achievement to them.

Junior Shema, Gothenburg, March 2024.

CONTENTS

1 Introduction. 13
- 1.1 Background. 13
- 1.2 Problem statement. 13
- 1.3 Aim. 13
- 1.4 Objectives. 13

2 Literature review 15
- 2.1 Electrostatic fields in HV equipment. 15
- 2.2 Electrostatic field mapping. 17
  - 2.2.1 Topology optimization. 18
- 2.3 Optimization for mitigating strong electric fields. 18
  - 2.3.1 Schweiger factor. 19
  - 2.3.2 Uniform field arrangement. 19
  - 2.3.3 Rogowski profile. 20
- 2.4 3D-scanning. 21
  - 2.4.1 How to obtain better 3D-scans. 22
  - 2.4.2 The clean-up of scans. 22

3 Method and results. 25
- 3.1 Model set up and results. 25
  - 3.1.1 2D- circles & squares at the center of the box. 25
    - 3.1.1.1 Mesh adjustments. 27
    - 3.1.1.2 Es-study of 2D- circles & squares (symmetric case). 28
    - 3.1.1.3 Shape optimization of circles & squares (at the center). 29
  - 3.1.2 2D-circles & squares (non-symmetric case). 48
    - 3.1.2.1 Es-study of the 2D-circles & squares (at the corner). 50
    - 3.1.2.2 Shape optimization of circles & squares (at the corner). 51
  - 3.1.3 3D-voltage divider. 61
    - 3.1.3.1 3D-voltage divider at the center. 61
    - 3.1.3.2 The boundary conditions. 61
    - 3.1.3.3 Mesh adjustments. 62
    - 3.1.3.4 Es-study of 3D-voltage divider (center). 63
    - 3.1.3.5 Shape optimization of 3D-voltage dividers at the center. 65
    - 3.1.3.6 3D-voltage divider at the corner. 68
    - 3.1.3.7 Es-study of the 3D-voltage divider (at the corner). 68
    - 3.1.3.8 Shape optimization of 3D-voltage dividers (at corner). 69

4 Discussion. 71
- 4.1 3D-scanning. 71
- 4.2 Shape optimization. 71
  - 4.2.1 2D- circles (symmetric case). 71
  - 4.2.2 2D-circles (corner). 72
  - 4.2.3 2D-squares. 72
    - 4.2.3.1 Side-side (symmetric case). 72
    - 4.2.3.2 Corner-corner (symmetric case). 72
    - 4.2.3.3 Side-side squares (corner). 73
    - 4.2.3.4 Corner-corner squares (corner case). 73
  - 4.2.4 Voltage divider. 73

5 Conclusion and suggestions for the future work. 75

References. 77

LIST OF FIGURES

Figure 1: Source of Electric field (From Kuchler, High voltage engineering, 2018). 15
Figure 2: FEM discretization (From Kuchler, High voltage engineering 2018)..17
Figure 3: Topology optimization of a bracket geometry (from COMSOL webpage). 18
Figure 4: Rogowski profile (From Kuffel & Zaengl, High voltage engineering fundamentals (2nd edition), (2000))..20
Figure 5: Voltage divider with unwanted reflections vs the cleaned-up geometry. 22
Figure 6: Cleaned up geometry of the high voltage transformer. 23
Figure 7: High voltage transformer with un-wanted reflections. 23
Figure 8: Scanned 3D-sphere...24
Figure 9: Cleaned up spheres using mesh mixer. 24
Figure 10: 2D-circles at the center...25
Figure 11:2D side-side squares at the center 26
Figure 12: 2D corner-corner squares at the center...26
Figure 13: Meshing of 2D- squares & circles at the center of the box..27
Figure 14: Electrostatic study of 2D-circles at the center of the box. 28
Figure 15: Electrostatic study of 2D- side- side squares at the center of the box. 28
Figure 16: Electrostatic study of 2D corner-corner squares at the center of the box. 29
Figure 17: The selected boundaries of the 2D-circles to be optimized. 31
Figure 18: The displacement of the boundaries using the polynomial boundary method at dmax=0.07 [m] & n=1...31
Figure 19: Shape optimization of 2D-circles using polynomial boundary method at dmax= 0,07 [m] & n=1....32
Figure 20: Boundaries selected for shape optimization using the polynomial boundary method at dmax=0.07[m] & n=1..32
Figure 21: Overall displacement of the boundaries using the polynomial boundary method at dmax=0.07 [m] & n=1...33
Figure 22: Shape optimization of 2D-circles (with fixed boundaries) at dmax= 0,07 [m] and n=1. 33
Figure 23: Boundaries selected for shape optimization. 34
Figure 24: Overall displacement of the boundaries after shape optimization...34
Figure 25: Shape optimization at dmax= 0.07 [m], Rmin=medium. 35
Figure 26: Shape optimization of circles (with fixed boundaries) using the free-shape boundary method. 36
Figure 27: Overall change of shape of the boundaries after shape optimization using the free-shape boundary method. 36
Figure 28: Shape optimization (with fixed boundaries) using free-shape boundary method...............................37
Figure 29: Boundaries selected for shape optimization. 37
Figure 30:Overall change of shape of the boundaries at dmax=0.075 [m] & n=2..38
Figure 31: Shape optimization at dmax= 0.075 [m] & n=2. 38
Figure 32: Convergence error message from COMSOL caused by having a large dmax, small Rmin. 39
Figure 33: Boundaries selected for shape optimization. 40
Figure 34: The displacement of the boundaries at dmax=0.1 [m] & n=2 40
Figure 35: Shape optimization of side-by-side squares at dmax= 0.1 [m] and n= 2. 41
Figure 36: Electric field distribution on the surface of the side-side squares (at the center of the box). 41
Figure 37: Shape optimization of side-by-side squares (free-shape boundary) 42
Figure 38: Boundary displacements of side-by-side squares (free-shape boundary)...43
Figure 39: Electric field distribution of the side-side squares (at the center of the box) using the free-shape boundary method. 44
Figure 40: Boundaries selected for shape optimization. 44
Figure 41: Boundary displacement of corner-corner squares (polynomial boundary)......................................45
Figure 42: Shape optimization of corner-corner squares using polynomial boundary..45
Figure 43: Boundary displacement of corner-corner squares (polynomial boundary)..46
Figure 44: Shape optimization of corner-corner squares using free-shape boundary (all corners fixed).............47
Figure 45: The E.factor distribution for corner-corner squares (at the center of the box). 48
Figure 46: Boundary conditions for side-side squares & circles. 48
Figure 47: Boundary conditions for corner-corner squares (at the corner). 49
Figure 48: Meshing of circles (at the corner)...49
Figure 49: Meshing of corner-corner squares (at the corner)..49
Figure 50: Meshing of side-side squares (at the corner). 49
Figure 51: Es-study of circles at the corner of the box. 50
Figure 52: Es-study of side-side squares at the corner of the box...50

Figure 53: Es-study of corner-corner squares at the corner of the box. 51
Figure 54: Boundaries selected for shape optimization. 51
Figure 55: Boundary displacement of circles (polynomial boundary). 52
Figure 56:Shape optimization of circles (at the corner of the box) using polynomial boundary. 52
Figure 57: Boundaries selected for shape optimization. 53
Figure 58: Boundary displacement of circles with fixed boundaries (using free-shape boundary method). 54
Figure 59: Shape optimization of circles (at the corner) using free-shape method. 54
Figure 60: Boundaries selected for shape optimization. 55
Figure 61: Boundary displacement for side-side squares (polynomial boundary). 56
Figure 62: Shape optimization of side- side squares (at the corner of the box) using polynomial boundary. 56
Figure 63:Boundaries selected for shape optimization. 57
Figure 64: Boundary displacement for corner-corner squares 58
Figure 65: Shape optimization of corner-corner squares. 58
Figure 66: Electric field distribution on the surface of corner-corner squares versus iteration number. 59
Figure 67: The formulation of the objective function (E-factor) in the shape optimization solver settings. 60
Figure 68: The formulation of the objective function (electric field strength) in the solver settings. 60
Figure 69: Test set-up of the voltage divider in COMSOL. 61
Figure 70: Finalized geometry of the voltage divider with boundary conditions. 62
Figure 71: Meshing of the voltage divider at the center of the box. 63
Figure 72: Es-study of voltage divider at the center of the box. 64
Figure 73: (Bottom view) of the es-study of voltage divider at the center of the box. 64
Figure 74: (Top view) of the es-study of voltage divider at the center of the box. 65
Figure 75: (Top view) of the optimized voltage divider at the center. 66
Figure 76: (Side view) of the optimized voltage divider at the center. 66
Figure 77: Inner view of the voltage divider. 67
Figure 78: Optimized voltage divider (center) with dmax= 0,2 [m] and Rmin= small. 67
Figure 79: Meshing of the voltage divider (at the corner). 68
Figure 80: Es-study of voltage divider at the corner of the box. 69
Figure 81: (Front view) of shape optimization of the voltage divider. 69
Figure 82: (Inner view) of shape optimization of the voltage divider. 70
Figure 83: (Top view) of shape optimization of the voltage divider. 70

LIST OF TABLES

Table 1: Pros and cons & applications of 3D-scanning 21
Table 2: Different types of Shape optimization solvers. 30
Table 3: Results showing the shape optimization of circles located at the center of the box using the free-shape boundary method. 35
Table 4: Results showing the shape optimization of circles located at the center of the box using the polynomial boundary method. 39
Table 5: Data showing the variation of electric field strength versus successive iterations using polynomial boundary. 41
Table 6: Results of shape optimization of side-by-side squares located at the center of the box using the polynomial boundary method. 42
Table 7: Results showing the shape optimization of side-by-side squares located at the center of the box using the free-shape boundary method. 43
Table 8: Results of shape optimization of corner-corner squares located at the center of the box using the polynomial boundary method. 46
Table 9: Results of shape optimization of corner-corner squares at the center of the box using the free-shape boundary method. 47
Table 10: Results of shape optimization of circles at the center of the box using the polynomial boundary method. 53
Table 11: Results of shape optimization of circles (at the corner) using free-shape boundary method. 55
Table 12: Results of shape optimization of side-side squares (at the corner) using polynomial boundary method. 57
Table 13: Results of shape optimization of corner-corner squares using polynomial boundary method (at the corner). 59

1. Introduction

This thesis aims to explore the shape optimization of high voltage electrodes. More specifically it aims to study different techniques required to solve problems related to having oversized high voltage equipment and test setups enclosed in tight laboratory spaces, to ensure reliable operation when conducting high voltage tests. This thesis is part of a collaboration between Chalmers and Nexans Norway AS focusing on establishing best practices in shape optimization of high voltage electrodes via computer simulations. Hence, results and conclusions from the thesis are intended to serve as contribution to the development of optimized test setups and equipment. This chapter begins with an overview of the background that frames the thesis. Following this is the problem statement which describes why the study should be conducted. Finally, the thesis' purpose, specification of the objectives needed to fulfil it is described.

1.1 Background

Normally, high voltage laboratories are equipped with test setups, equipment which can vary in sizes ranging from small to bigger equipment, necessary to conduct different laboratory tests. Various laboratories can have different dimensions depending on the size and the number of equipment to be accommodated. However, intermediate (not big enough) test setups and equipment are needed to facilitate conducting high voltage tests. Different 3D-optimization techniques based on a computational approach are used in the design of 3D-optimized shapes to solve the issues related to having oversized equipment in tight spaces.

1.2 Problem statement

The main questions to be answered are;

- How can shape optimization be used to optimize the design of HV electrodes?
- How can it be run to gain the maximal impact at minimal computational time/resource expenditure?
- Are the final shapes relevant and in what way do they reflect a geometric optimum?
- Will it make sense to 3D print the new shapes? i.e., can the 3D-shapes be manufactured in a cost-efficient manner?

1.3 Aim

The main idea is to perform a study with the purpose of acquiring knowledge about the state-of- the art inspection and computation. Various steps including 3D-scanning of the high voltage laboratory whereby important connections are computed to generate an optimized shape that meets the fixed stress criteria all over the whole electrode surface with minimal material usage.

1.4 Objectives

Specific tasks to be implemented to achieve the above-mentioned aim are briefly outlined below;

- To investigate capabilities of the optimization module in COMSOL Multiphysics software for shape optimization of high voltage electrodes.
- To test simple scanning tools for recording 3D-geometrically complex small-scale HV set-up and generating geometry files that can be imported into FEM calculation software.
- To analyse feasibility of performing shape optimization using scanned 3D images.

2 Literature review

This chapter covers the analysis of literature related to the thesis topic with the purpose to provide a brief comprehension of important background theory. It outlines a description of the electrostatic fields in HV equipment, methods of mitigating strong electric field enhancement in engineering designs of high voltage electrodes, and a description of how 3D-scanning and electrostatic field mapping by means of the Finite Element Method (FEM) works.

2.1 Electrostatic fields in HV equipment

Electrostatic fields are defined as steady electric fields produced by stationary electric charges [1]. In this section, the main idea is to explain theories that mainly describe how high voltage electrodes behave under the influence of high voltage electric field stresses in relation to their engineering design. Furthermore, for a clear understanding of electrostatic fields in ambient air, it is important describing the origin of electric field stress, the numerical field calculations in relation to the finite element method used in computing electric field stresses.

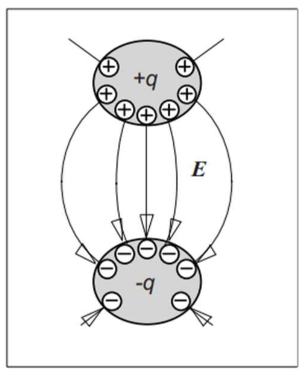

Figure 1: Source of Electric field (From Kuchler, High voltage engineering, 2018).

It is known that in high voltage engineering, high voltage apparatus makes use of insulations such as solids, liquids, gases, vacuums, or a combination of all these as clearly illustrated in in modern engineering applications, the necessity of using high voltage AC or DC in research laboratories, and in the transmission of electricity from the source until the final consumer is something very common. However, this calls for advanced research in fields of high voltage engineering like insulation systems, given the fact that technology is ever evolving.

According to [1], electric field strength is defined as a ratio of mechanical force to the positive test charge. This means that the electric field strength will be in the same direction as the electric force, F applied on the positive test charge, q^+ [Coulombs]. This is however contrary to the case of a negative charge, q^- because here the electric field strength acts in the opposite direction to the mechanical force applied. Therefore, as illustrated in [1], the electric field strength, E is described mathematically in equation (2.1) as;

$$\vec{E} = \frac{\vec{F}}{q^+} \tag{2.1}$$

where; E is a vector quantity, Electric field strength in [N/C], F is vector quantity, electric force in Newtons [N] , q is scalar quantity, charge in Coulombs [C]

In relation to the theory of electric field strength described in [1], it is characterised by having electric field lines originating from positive and negative charges which act as sources and sinks of the electric field; as described in the figure 1.Additionally, other sources of electric field strength exist but such depend on time as for time-varying magnetic fields inducing electric fields; which are the basis of Maxwell's equations. However, the most relevant of Maxwell's equations is "Gauss law for electric fields" as explained in [1]expressed mathematically in equation (2.2). It describes what happens to electrically charged objects placed in a region where electric field appears to be active. Here the net electric field entering and leaving a defined volume of space is not balanced, because it is scaled by the amount of charges existing within that volume of space. This is represented by the space charge density term, ρ [C/m^3] whereby the net electric field is now determined by the relative permittivity, ε_r [F/m] and the permittivity of free space, ε_o [F/m] [1].

$$\nabla \cdot \vec{E} = \frac{\rho}{\varepsilon_r \varepsilon_0} \tag{2.2}$$

The capacitive electric field is here calculated from the electric scalar potential field, VI. The electric scalar potential field is important in determining the electric field, where E defined as the gradient of the electric potential, V (i.e., $\vec{E}$ = -∇V). Based on the Poisson's equation to be derived it is possible to ultimately find the Laplace expression as in the equation (2.5) [1] [2].

The electric field strength, E can be expressed in terms of the gradient of the electric potential, V as;

$$\vec{E} = -\nabla V \tag{2.3}$$

The Poisson equation which states "the Laplacian of the electric potential is equivalent to the ratio of the volume charge density to the permittivity of the medium with a change of sign" is determined as in equation (2.4) [1] [2].

$$\nabla^2 V = -\frac{\rho_v}{\varepsilon} \tag{2.4}$$

In a source- free region but also no permittivity gradients, the Poisson equation in the equation (2.4) becomes the Laplace's equation as described in the equation (2.5). The electrostatics problem formulation involves setting up of the boundary conditions needed to calculate field quantities like the electric displacement field, electrostatic field strength, etc. This explains why it is important to understand the basic electrostatic theory behind this problem. In the "*charge conservation node"*, that is where theories related to Gauss' law are added such that constitutive relations of electrostatic fields can be applied in the FEM calculation of electric field strength [1] [2].

$$\nabla^2 = 0 \tag{2.5}$$

2.2 Electrostatic field mapping

Numerical field calculations are applied when calculating field stresses in complex insulation arrangements, this method of analytically calculating the magnitude of electric field strength is attributed to the application of Maxwell's equations over a specific interval of points created because of discretizing a volume into smaller individual surfaces that can be split into upper and lower boundaries of an integration, thus allowing the calculation of various field quantities. However, numerical field calculations in engineering designs can be used in various computational approaches including; the FEM (Finite Element Method); Integral Equation Method; FDM, Monte-Carlo Method, etc, which make use of differential equations in describing electric fields, hence making them important tools for researchers, developers, and designers in the field of high voltage engineering. However, the focus of the thesis is to use the FEM approach in the optimization and the electrostatic study of high voltage electrodes.

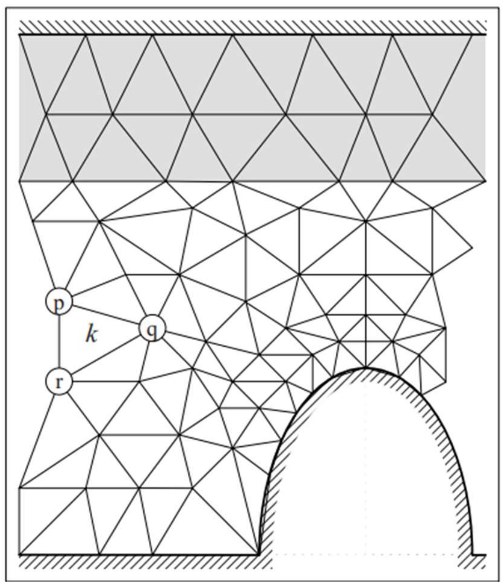

Figure 2: FEM discretization (From Kuchler, High voltage engineering 2018).

Finite element method is a powerful computational tool for performing numerical calculations. It has been widely used in solving complex engineering problems in the fields related to electromagnetics, solid mechanics, fluid mechanics. The finite element method approaches complex problems by simply using the discretization of the whole volumes as illustrated in figure 2, this technique involves the breaking down of the whole volume into smaller element shapes connected to each other at nodes (p, q, r), thus the whole discretized volume is referred to as mesh.

Several element shapes can be used in the discretization of volumes such as surface or 2D elements which include shapes like triangles, quadrilaterals [1]. Such a method of discretization is specifically suitable for problems involving complex structures, thin surfaces. Solid elements including cuboids, pyramids are suitable in solving problems related to 3D bodies. Other possible way of discretization is the use of line elements. It is after discretization that the finite element method starts computing different shapes of how the structure will change by constantly moving the nodes until an optimal solution is reached. This process can be described as an iteration because when errors occur either the parameters are adjusted or the mesh around the geometry of interest is refined. The summarised steps taken by the FEM in solving for any type of engineering problems is listed below as:

- Defining the problem; which involves defining the relevant material properties as well as the boundary conditions, defining the relevant physics.
- Discretization of the whole volume into smaller finite elements.
- Run the study, by applying suitable solver options depending on the type of problem.
- Modification of the parameters and the validation of the results.

2.2.1 Topology optimization

Topology optimization consists of the re-arrangement of the distribution of materials that make up a given structure, this method of optimization is performed with a purpose of obtaining a final optimized structure that is cost-beneficial, stiff, with a maximal performance by applying constraints, boundary conditions on the original structure that is to be optimized. The topology optimization algorithm involves setting an objective function and set of constraints (optional) defined in the topology optimization interface which will generate new optimized structures with design variables characterized by the presence, absence of materials from the original structure as shown in the figure 3 in solid mechanics whereby a bracket geometry' s topology is optimized to create holes in the structure such that the total weight, cost of the material is minimized [3].

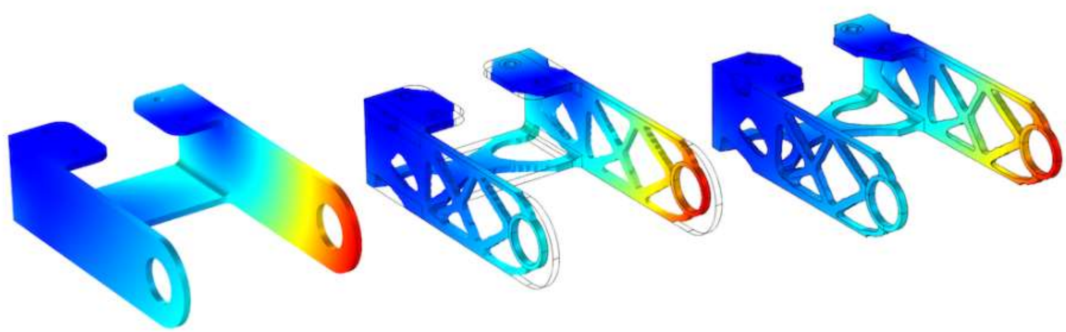

Figure 3: Topology optimization of a bracket geometry (from COMSOL webpage).

2.3 Optimization for mitigating strong electric fields

In this part, field distributions and breakdown in various kinds of fields in different media will be addressed as well as breakdown under uniform field conditions. That is because it is easier to predict breakdown processes that under uniform field conditions but in practice, uniform field conditions seldom apply and for non-uniform fields the exact mechanism by which a breakdown may progress until catastrophic failure which might occur can be complex.

Assuming a parallel plate capacitor with a dielectric material of a suitable permittivity and breakdown strength. If now needed to utilize the material to its fullest capability, voltage will be continuously applied hence the material withstands the applied voltage at which the material is stressed, until it reaches the breakdown strength. If the field is uniform, high voltages can be achieved across the capacitor plates; as the voltage is increased, the field in most of the material is below the breakdown strength of the dielectric material [2] [4].

However there exists a region close to the tip where the field is high because of local field intensification and within that region if the electric field strength exceeds the breakdown strength of the material, partial discharges occur hence degradation and deterioration of the neighbouring material proceeds. Therefore, voltage is applied such that local electric field is not above the dangerous level [4].

2.3.1 Schweiger factor

As perfectly uniform field cannot be achieved a certain degree of non-uniformity is to be accounted for. For this reason, the Schweiger Factor, η is introduced as a measure of the non-uniformity of the field as defined in equation (2.6);

$$\mathrm{H} = \frac{E_{mean}}{E_{max}} = \frac{V}{dE_{max}} \tag{2.6}$$

The Schweiger factor, or the field efficiency factor, is defined as a ratio of the average to the maximum value of the electric field strength [2]. $E_{\mathbf{mean}}$ is obtained by calculating the average of the electric field at each point of the entire volume of the dielectric which is close to the mean of an average field; calculated as *v/d*. Thus, in a uniform field distribution, a voltage *v* is applied across the capacitor plates whereby; the field is constant everywhere equivalent to the mean value of the field which is *v/d* [2]. However, in a non-uniform field, the value of the electric field strength will deviate from the mean value. The maximum electric field does not necessarily happen at a predestined point in fact it is difficult to predict where the maximum value will occur. Thus, computation of the electric field is needed from which the field efficiency factor can be derived. Here uniform electric fields will yield a Schweiger factor equal to unity, and hence the electrical optimization process shall approach unity as the computational steps progress. On the other hand, for severely non-uniform fields, the Schweiger factor is reduced, and this fractional value may approach zero in the worst-case examples typically for infinitely sharp corners in the mesh, sharp needle tips, etc.

2.3.2 Uniform field arrangement

It is important to design electrodes in any insulation system such that nearly- uniform fields are available everywhere and when impossible field intensifications, characterized by a local maximal field Emax should be as close to the average electric field as possible. This requires choosing electrode geometries appropriately such that the field is uniform. High voltage tests in the lab typically use uniform, or on purpose non-uniform electrode arrangements such as parallel plate assemblies, rod-plane gap, rod-rod gap, sphere-sphere gap, etc. While ideal parallel plate capacitors arrangement provides an ideal field distribution such uniform field distribution will only be obtained in between the capacitor plates [2]. However, at the edges of the plates, instead a concentration of field lines will occur and that will depend upon the radius of curvature of the edges, thus the smaller the radius, the higher will be the concentration of field lines and higher will be the local field intensification. This intensification may well exceed local dielectric breakdown strength of adjacent air causing a flashover along the surface. This will happen nowhere close to the critical breakdown strength of the material, and the average value of the electric field strength will be low. To avoid this there are proposals to profile the parallel plates in such a way that the local field intensification can be minimized. This means that it is not zero or perfectly uniform, but it will have uniform field between the plates while at the edges the field can be reduced. Such profiles addressed in the next section [2] [4].

2.3.3 Rogowski profile

For axially symmetric systems shown in figure 4 describing the Rogowski profile follows the analytical function introduced by Maxwell where z and w are complex coordinates in the z-plane and w-plane respectively as defined below.

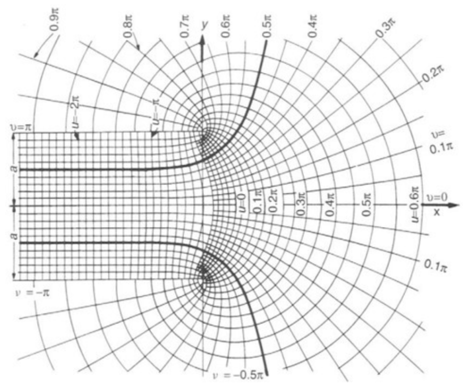

Figure 4: Rogowski profile (From Kuffel & Zaengl, High voltage engineering fundamentals (2nd edition), (2000))

Assuming two infinite parallel plates in the w-plane;

$$v = \pm\pi = constant \qquad (2.7)$$

Assuming the horizontal lines between the parallel plate electrodes are equipotential lines;

$$v = const \text{ with } -\pi < v < +\pi \qquad (2.8)$$

The perpendicular lines to these equipotential lines are the field lines in the w-plane, representing a uniform field distribution.

$$u = const \text{ with } -\infty < u < +\infty \qquad (2.9)$$

Since, the Rogowski profile models electrodes in such a way that they lie along the equipotential v-lines choosing ($v = \pm\pi$) to be equipotential along which the electrodes lie in the z-plane [2]. These lines appear to be equivalent to an electric field distribution for parallel plates which can no longer go up to infinity, but which will be terminated at x=0. Along the line x=0, if electrodes within this region, a perfectly uniform field distribution will be obtained. Similarly, from -inf to x=0, a uniform field distribution will also occur. However, at the edges of $v = +\pi$ and $v = -\pi$, there will be a high concentration of field lines [2].

Breakdown due to local field enhancements at these two points is likely, hence this concentration of field lines not acceptable. Conclusively, the parallel plates placed at $v = \pm\pi$, do not fulfil the requirements for obtaining a uniform field distribution. However, the field enhancement decreases when moving away from the equipotential lines at $v = \pm\pi$ towards the centre [2].

2.4 3D-scanning

3D-scanning refers to the transformation of physical objects into digital information by the help of using a camera or any other equipment that uses light detection and ranging (LIDAR); sensors or Lasers to generate the coordinate positions of a surface. The physical object is digitally recreated by the help of coordinate positions that are created at the scanned surface locations, the created point cloud is later compiled together to form a mesh that covers the surface of the physical object with a high degree of detail and accuracy, hence forming a newly built digitized object [5].

Physical objects within a few meters are typically scanned using a short-range scanner, these objects can vary from a tiny up to fully- built high voltage setup while a long-range scanner is typically needed for large objects, big spaces that are beyond the range of 1[m]. For this project, a mobile-based software known as Scaniverse that uses the LiDAR technology is used for generating digitalized high voltage electrodes like voltage dividers, etc. From this process an STL file containing the scanned physical high voltage electrode as a surface mesh is generated. However, 3D-scanning has advantages and disadvantages and is used for a range of applications summarized in the table below.

Table 1: Pros and cons & applications of 3D-scanning

Pros of 3D-scanning	Cons of 3D- scanning	Applications
Fast	Low degree of accuracy for some techniques	Education, art, Medical and industrial uses, Animations, construction, cinema production
Ease of use	Periodical upgrading of features for proper function	
More reliable mesh generation compared to photogrammetry.	Significantly affected by the reflection from shinny objects	

There are also other scanning methods such as;

- **Laser scanners**: They perform the scanning task by capturing surface components of the physical object, however the only difference with the LIDAR technology is that they are suitable for projects requiring high accuracy [5].

- **Laser pulse-based 3D scanning technology:** It performs scanning by applying the speed of light and the sensor in a way that millions of pulses from the Laser are sent to the surface of the physical object whereafter they are reflected to the sensor thus enabling the capturing of surface components of the high voltage electrodes. In addition to this, a rotating mirror enables this kind of scanning method to collect data in 360 degrees [5].

2.4.1 How to obtain better 3D-scans

Below, a summary describing how to obtain good quality 3D-scans using the Scaniverse software is provided;

- **Properly adjusting the scanning distance of the camera from the real object**: It is advisable to maintain a range of 0.8-1.5 [m] from the scanned object because for the mostly featureless high voltage components it is advantageous for the whole object to fit-in in the screen of the phone. This enables the phone LiDAR to track its position better thus preventing un-conventional placements of the camera that are most of the times prone to scanning errors.
- **Minimal lighting in the room**: An indirect light intensity range of 100-200 [lumens] is normally advisable, this allows the preventing glare which reduces the quality of the scans.
- **Avoiding abrupt movements of the camera**: Sudden movements of the camera may cause a delay of 2-5 [seconds] in the response to the scanning of objects by the light sensor. Thus, it is recommended to slowly turn the camera for the sensor to adjust to changes in position.

2.4.2 The clean-up of scans

Step1: Importing the scan in Meshmixer. There are cases when the geometry must be redesigned using Meshmixer.

Step2: Apply the "***smooth model***" feature, this will allow the use of the ***"brush***" function on to the surface of the scan. This is more less like sculpting the object itself such that the surfaces are uniform as shown in the figure 6.

Step3: Export or save the .STL file for further studies.

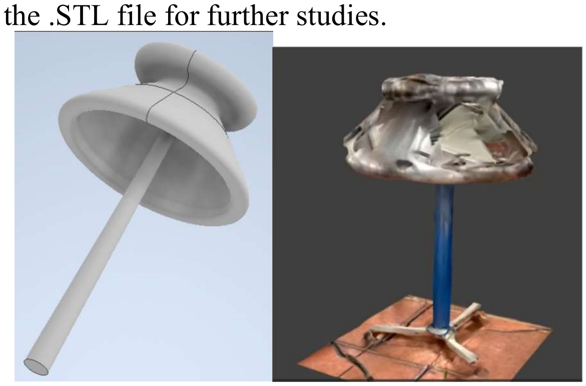

Figure 5: Voltage divider with unwanted reflections vs the cleaned-up geometry.

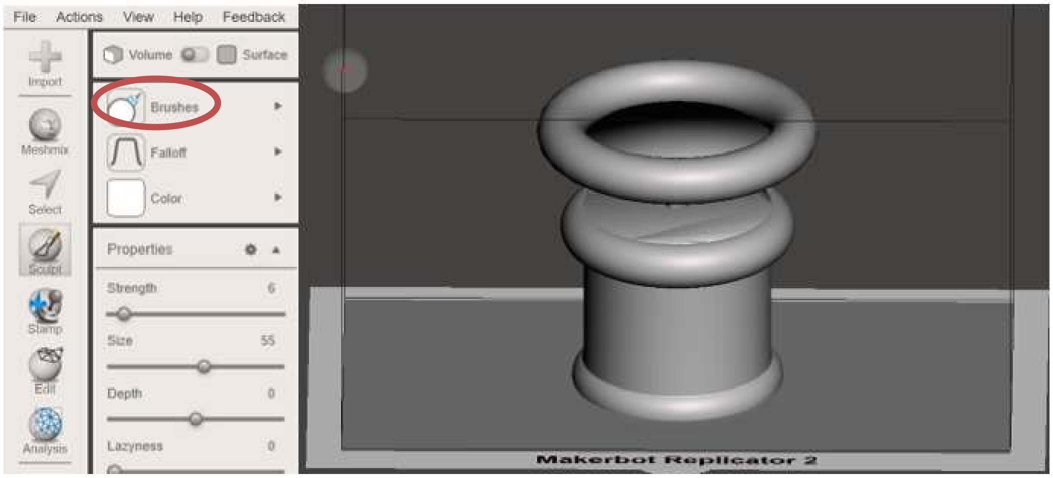

Figure 6: Cleaned up geometry of the high voltage transformer.

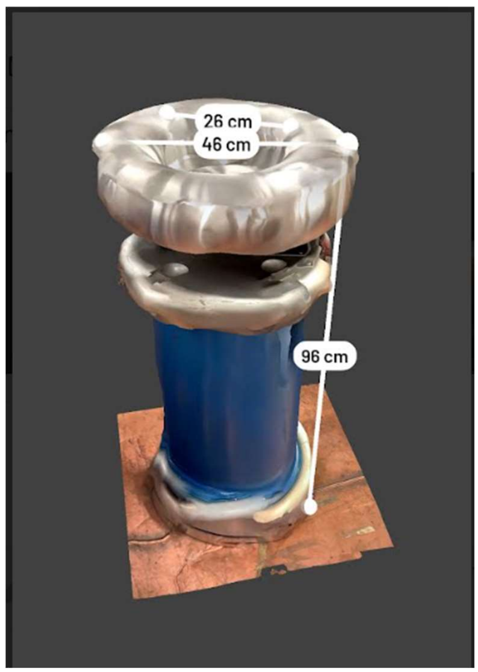

Figure 7: High voltage transformer with un-wanted reflections.

Scans of 3D-spheres have problems in their scans such as having bumps and un-wanted reflections from their surfaces due to the incoming light intensity in the high voltage laboratory as shown in the figure 8.

The clean-up of the spheres in mesh mixer software is not complicated since it has a few in-built basic geometries for instance spheres, trapeziums, etc. Therefore, it was only a matter of re-drawing the spheres with the same dimensions as the physical ones as shown in the figure 9.

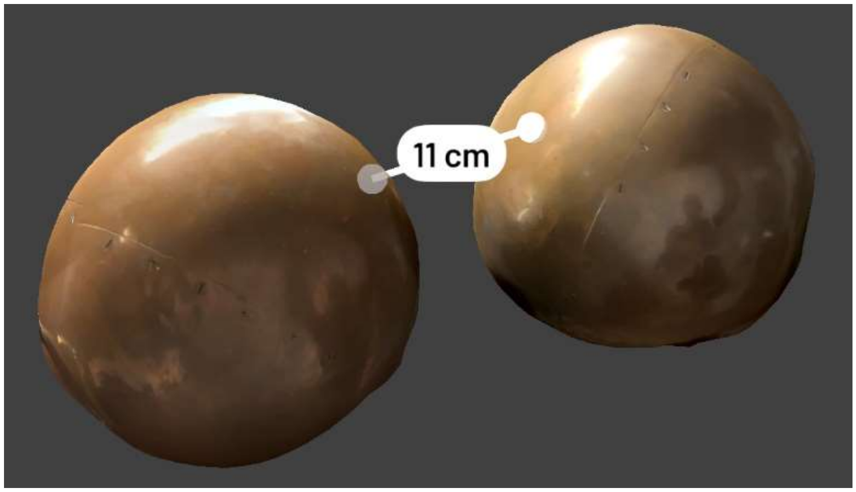

Figure 8: Scanned 3D-sphere.

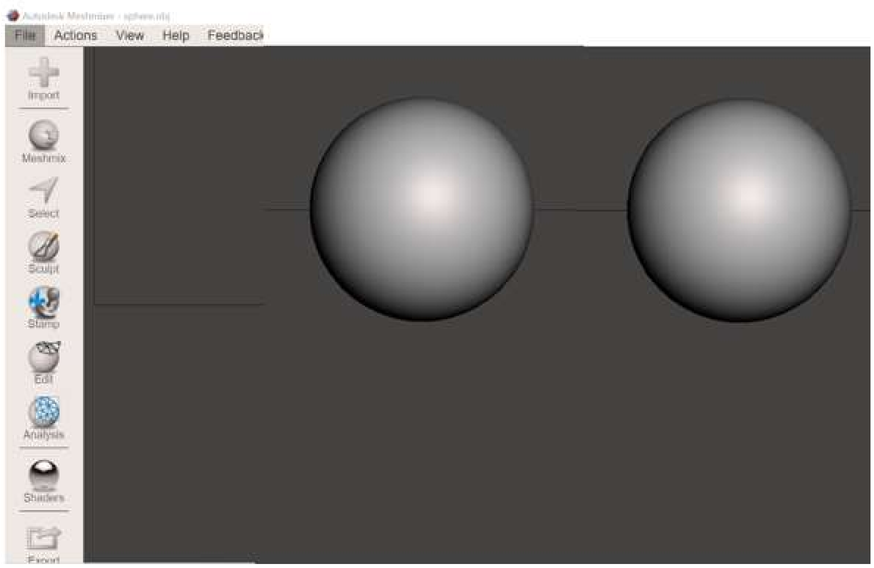

Figure 9: Cleaned up spheres using mesh mixer.

3 Method and results

In this section, the focus is based on the methods used for implementing the thesis objectives. It mainly comprises of the geometries of the test-cases used in studying the behavior of the electric field strength by considering their symmetrical and un-symmetrical cases, their boundary conditions, the formulation of the optimization problem. This will therefore form a basis of concluding and discussing about the suitable design parameters needed in obtaining optimized shapes with a minimized electric field strength on their surfaces.

3.1 Model set up and results

The points of discussion in this section include the development of a methodology that helps in the analysis of the electrostatic study of the 2 different test cases involving the two 2D-spheres & squares located at different positions in an enclosed box and 3D-voltage divider.

3.1.1 2D- circles & squares at the center of the box

The electrostatic study of 2D- circles of diameter *0.1 [m]* & squares of side *0.005 [m*] enclosed in a box of length *0.5 [m]* and height *0.035 [m]* are shown in the figures 10 to12 below. The 2D- geometries are assigned a higher relative permittivity, $\varepsilon_r = 80$. The average and maximum values of the electric field strength in the air medium are used to establish the field efficiency factor. Therefore, the field efficiency factor is set as the objective function for the optimization, and it should be close to unity.

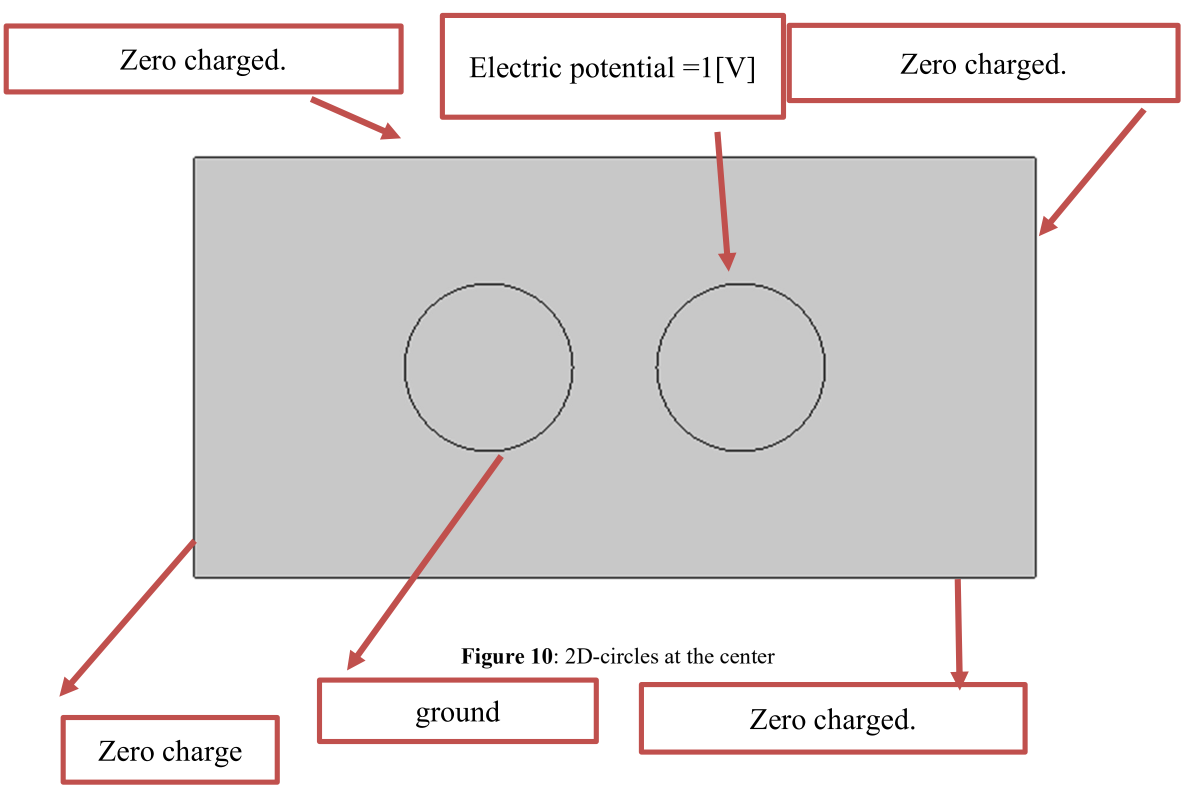

Figure 10: 2D-circles at the center

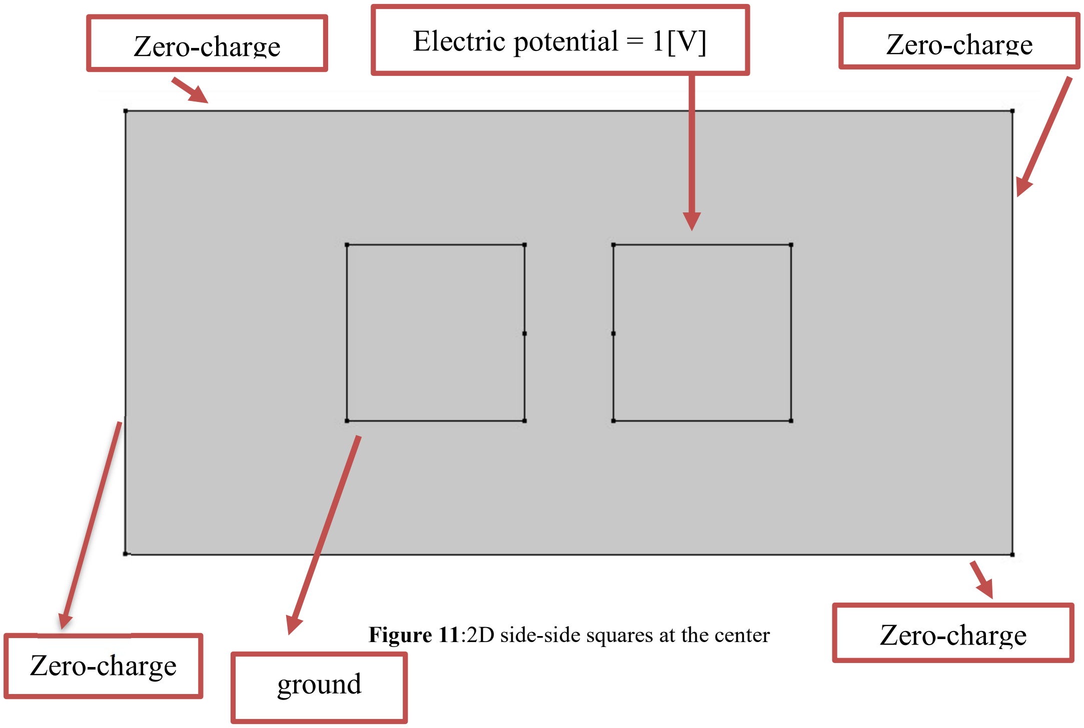

Figure 11:2D side-side squares at the center

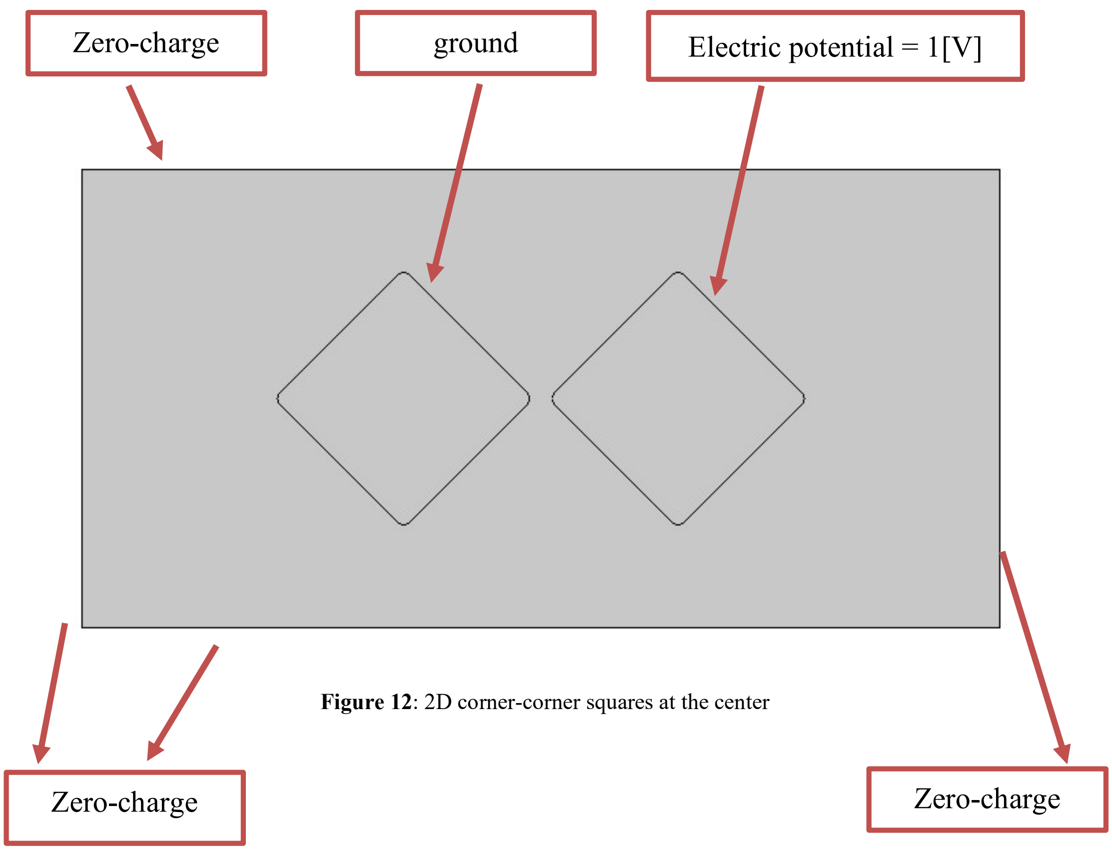

Figure 12: 2D corner-corner squares at the center

3.1.1.1 Mesh adjustments

The mesh on the boundaries of the 2D-geometries is refined to a much smaller mesh element to enhance the electrostatic and optimization study results.

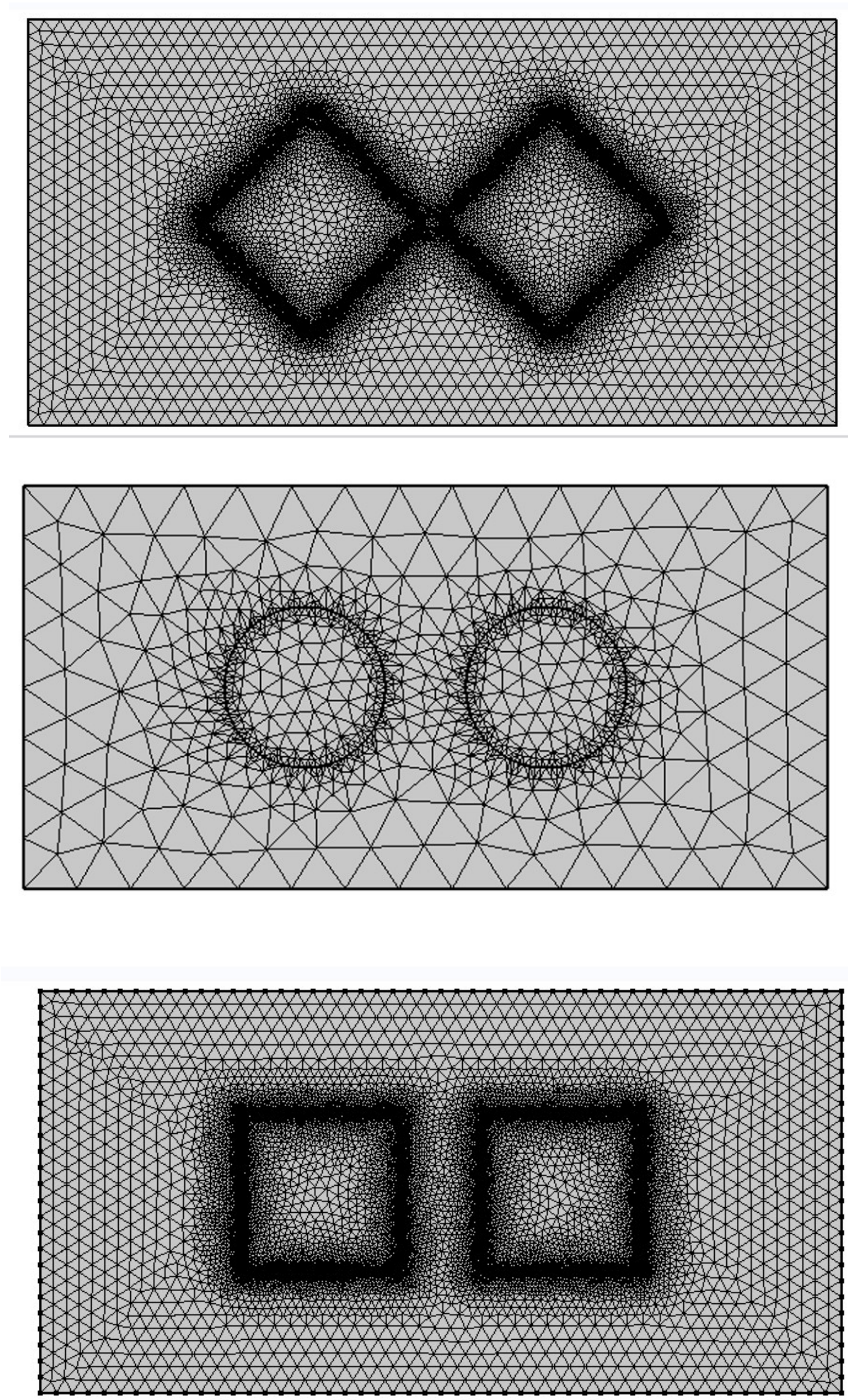

Figure 13: Meshing of 2D- squares & circles at the center of the box.

3.1.1.2 Es-study of 2D- circles & squares (symmetric case)

A pure electrostatic study allows the calculation of the maximum electric field, which serves as the reference in performing shape optimization. From the figure 14, the reference maximum electric field stress is 6.52 [V/m].

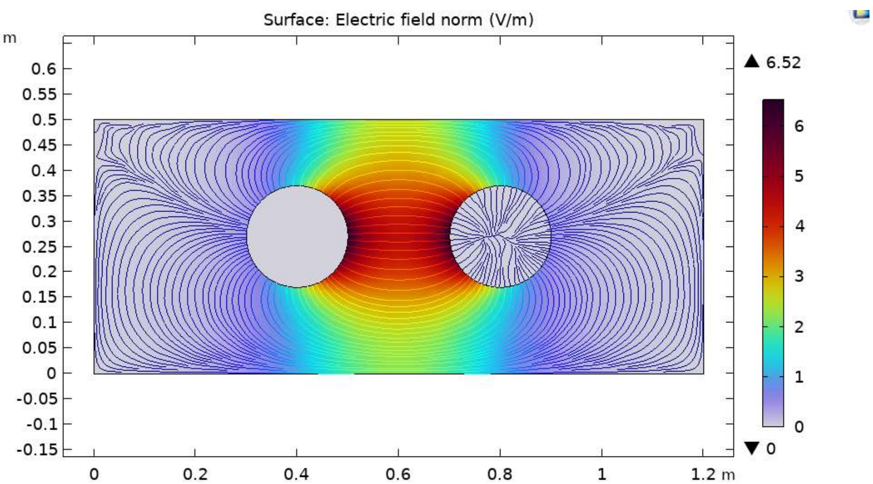

Figure 14: Electrostatic study of 2D-circles at the center of the box.

The electrostatic study of 2D- side by side squares placed at the center of the box is shown in the figure 15. The electric field strength is stronger at the corners of the squares because of sharp corners which have a higher surface charge density. The maximum electric field of the 2D-squared electrodes is expected to be slightly close to the sharp corners. Therefore, the reference maximum electric field strength is 30.3 [V/m] as shown in figure 15.

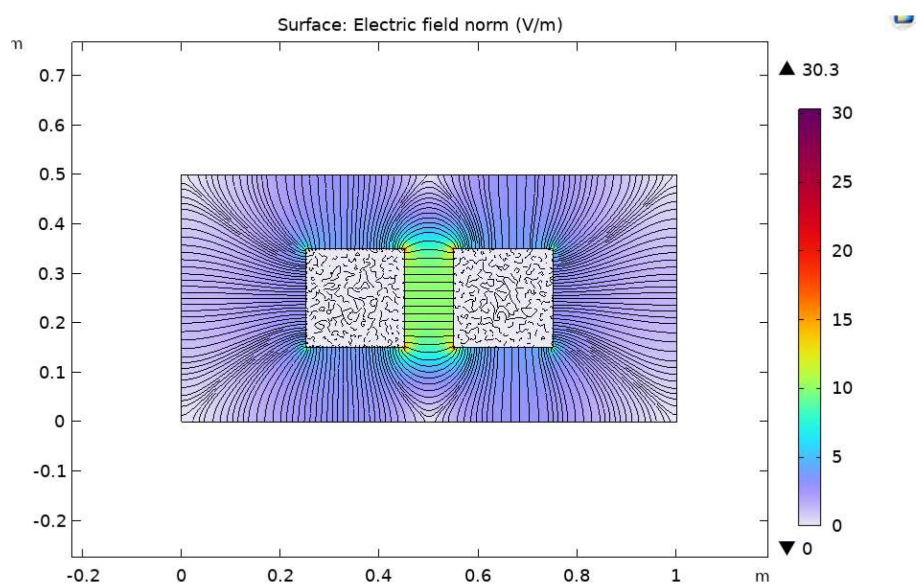

Figure 15: Electrostatic study of 2D- side- side squares at the center of the box.

For the corner-corner adjacent squares, there is almost no concentration of field lines around the corners except in the region between the electric potential and the ground. Field enhancements at sharp corners are minimized by modifying the initial geometry of the squares whereby a slight curvature of radius = 0,001 [m] is introduced at the sharp corners as shown in the figure 16 below.

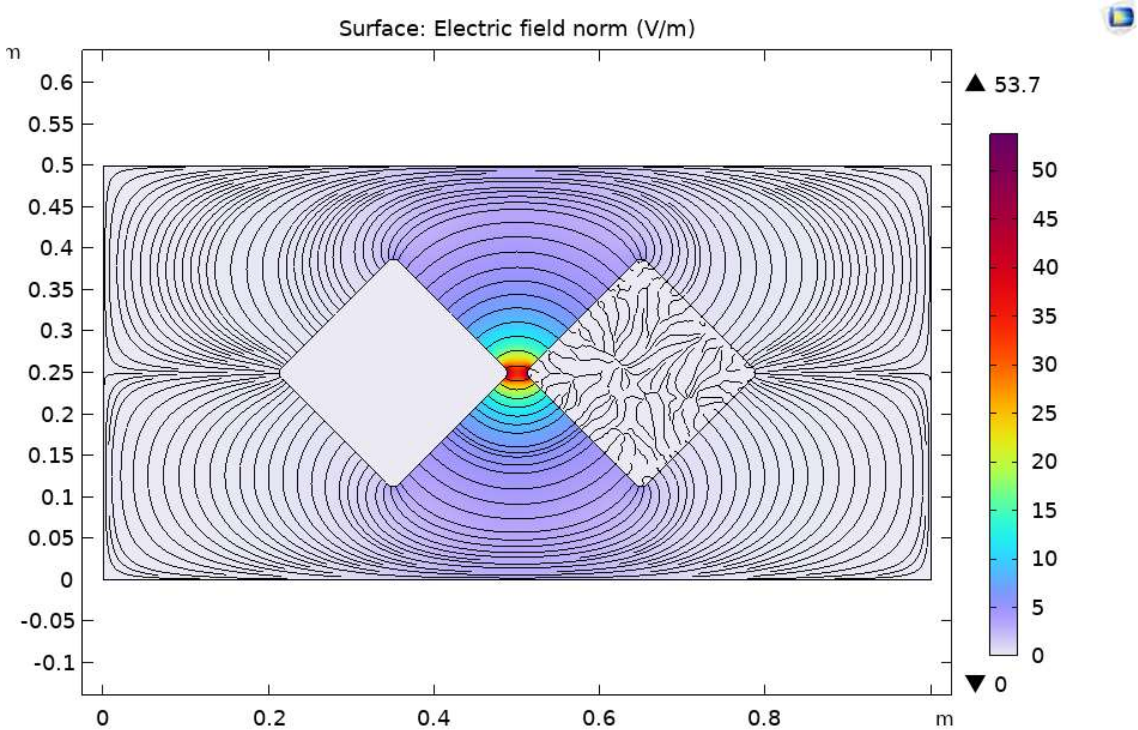

Figure 16: Electrostatic study of 2D corner-corner squares at the center of the box.

3.1.1.3 Shape optimization of circles & squares (at the center)

The shape optimization of 2D-spheres is performed by adding a "free-shape domain" to the domain of the sphere to allow the control variables features in the "polynomial boundary & free-shape boundary method" perform optimization on the boundaries. Boundaries that are not part of the "polynomial boundary & free shape boundary" list of selected boundaries are fixed. The polynomial boundary method uses *maximum displacement, dmax* to regulate the change of the original geometry whereby the default value in 2D is 0.07 [m] while for 3D is 0.5 [m]. Additionally, the polynomial boundary method uses the *type of polynomial* feature that contains a set of equations like the *Bernstein, Lagrange* equations; these are mathematical expressions that define how curved the edges of the boundaries of the optimized shape appears depending on the *order, n* of the Bernstein, Lagrange polynomial equations [3] [6]. Their mathematical formulation is based on the binomial expression below.

$$(x + a)^n = \sum_{k=0}^{n} \binom{n}{k} x^k a^{n-k} \quad (2.12)$$

Where.

combination formula = $\frac{n!}{k!(n-k)!}$

n= degree of freedom of the polynomial
k= number of choices in the sample space to choose from
a, x = variables.

The free-shape boundary method consists of the *maximum displacement (dmax)*, *filter size (Rmin)* to perform shape optimization. The filter size allows the filtering of data to improve the model performance. Therefore, the formulation of the shape optimization algorithm requires adding features outlined below.

1. **Probe selection**: The objective function is added by selecting a boundary probe which calculates the maximum electric field strength on the boundaries of the 2D-geometries. Depending on the type of optimization problem, the objective function is formulated by scaling the electric field strength using the *E-factor (field efficiency factor*).

2. **Shape Optimization solver**: There are several types of optimization solvers in COMSOL to choose from depending on the type of problem as described in the table.

Table 2: Different types of Shape optimization solvers.

Types of solvers	Names	Description
Gradient- based solvers	SNOPT	This optimizer is suitable for non-linear problems [6].
	IPOPT	Uses interior points to solve non-linear problems.
	MMA	It is robust compared to the rest of the gradient-based solver [6]. It is accurate and efficient.
Gradient- free solvers	Nelder-mead, BOBYQA (Bound optimization by quadratic approximation), the Coordinate search solver, COBYLA (Constrained optimization by linear approximation), etc.	Well-known for versatility in the prediction of outcomes from the raw data input [6].
Other type	Levenberg Marquardt solver	It is designed to solve objective functions involving least square types [6].
	Monte Carlo	Relatively slower in choosing data points used in the analysis of the objective function [6].

1. **Using polynomial boundary method at dmax= 0,07 [m] and n= 1**

The electric field strength calculated after the shape optimization of 2D-circles at the center of the box is 5.68 [V/m] as shown in the figure 19. The shape of the optimized circle is flat because COMSOL constructs new shapes of boundaries (Bezier curves) based on Bernstein polynomial equation.

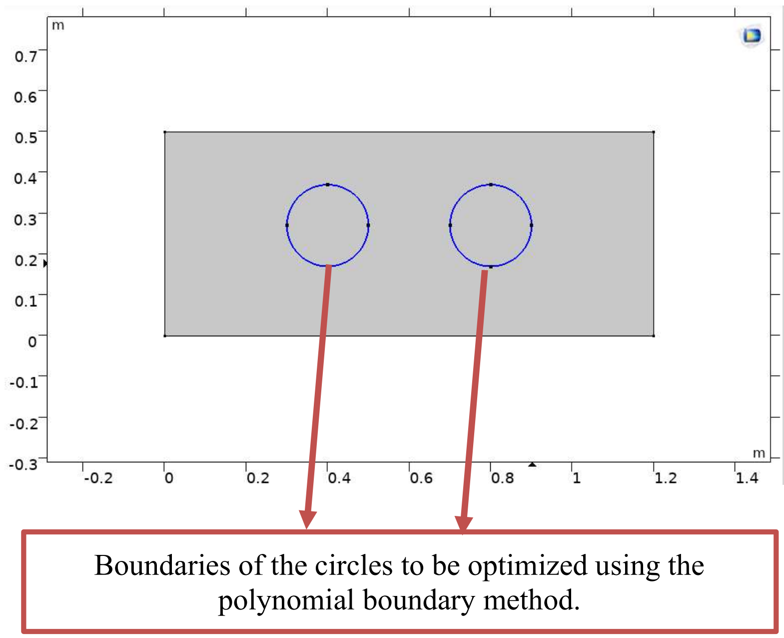

Figure 17: The selected boundaries of the 2D-circles to be optimized.

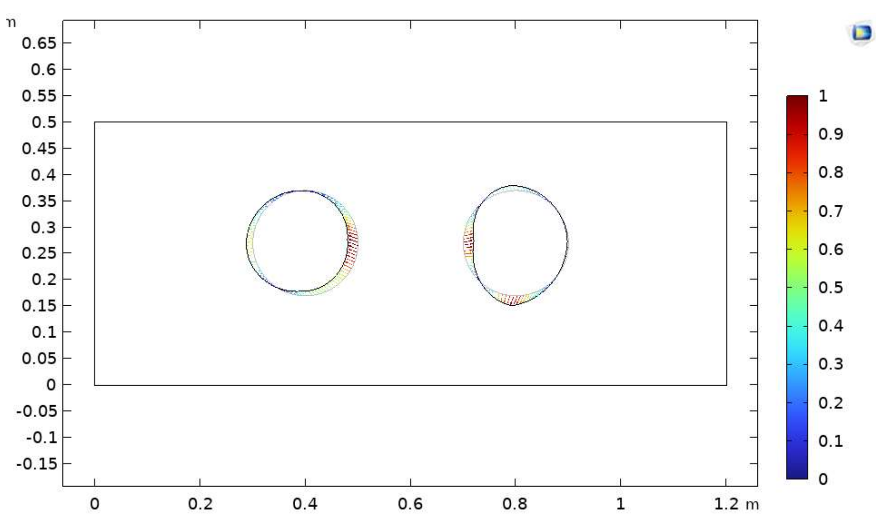

Figure 18: The displacement of the boundaries using the polynomial boundary method at dmax=0.07 [m] & n=1.

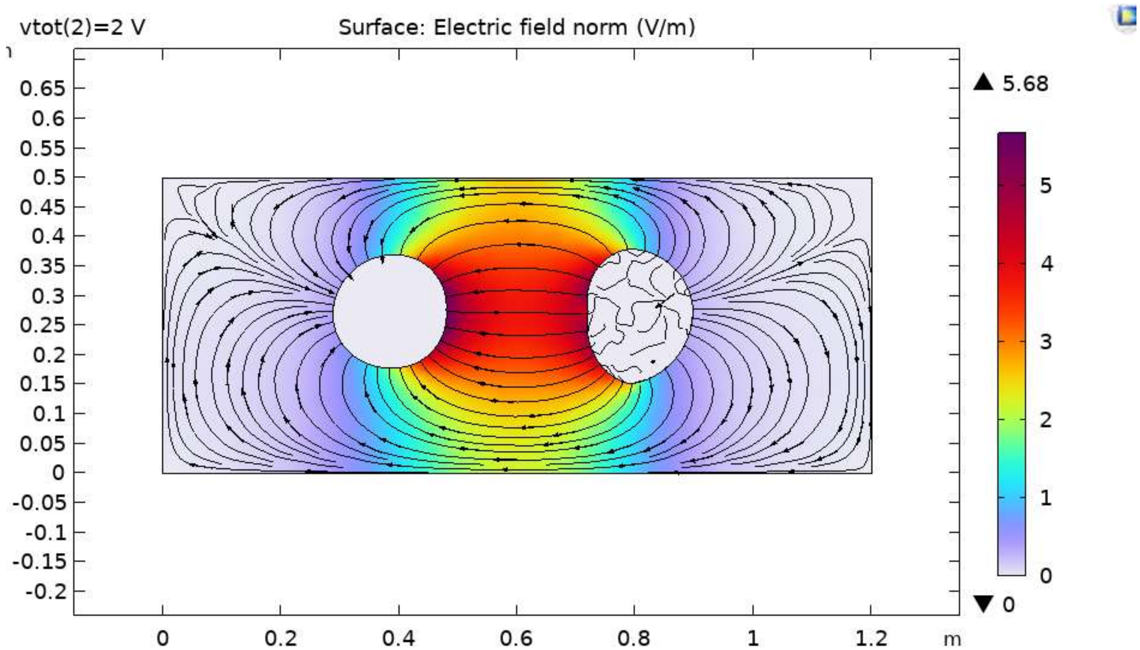

Figure 19: Shape optimization of 2D-circles using polynomial boundary method at dmax= 0,07 [m] & n=1.

However, to evaluate the flexibility of this method, some boundaries are fixed while others are subjected to shape optimization. In the figure 20, the blue boundaries describe those selected for shape optimization.

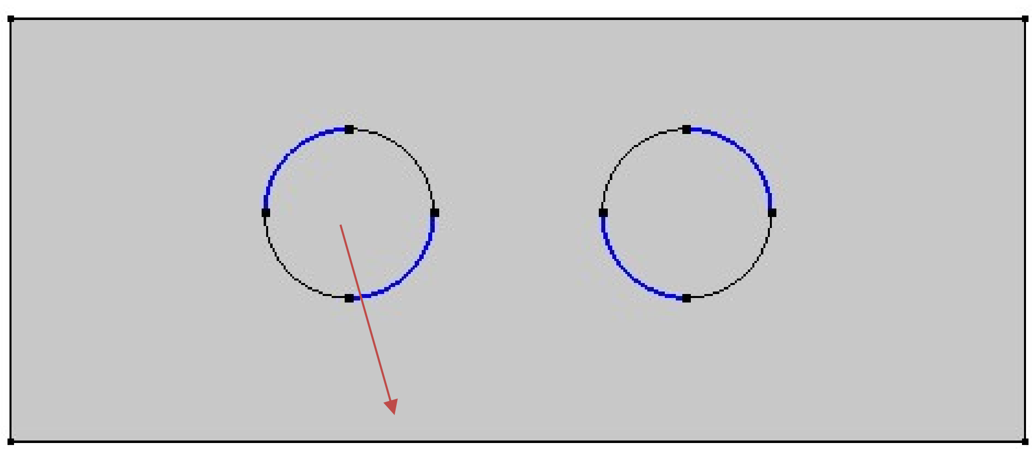

Selected boundaries for shape optimization using the polynomial boundary method.

Figure 20: Boundaries selected for shape optimization using the polynomial boundary method at dmax=0.07[m] & n=1.

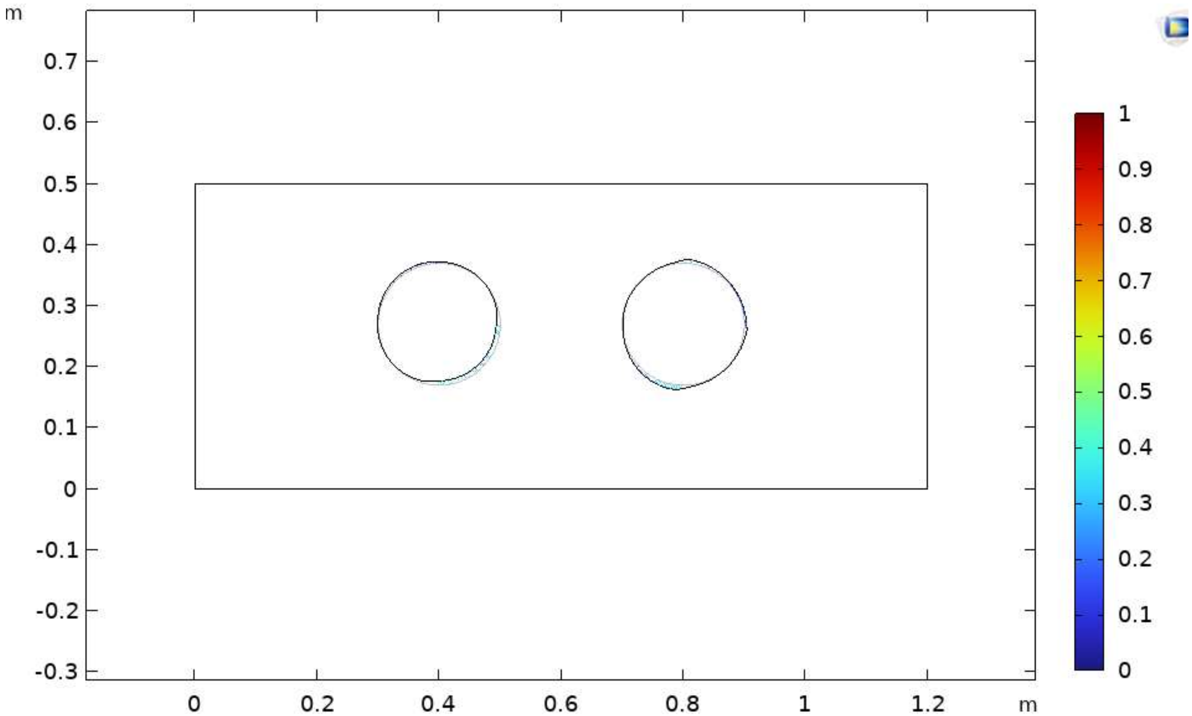

Figure 21: Overall displacement of the boundaries using the polynomial boundary method at dmax=0.07 [m] & n=1.

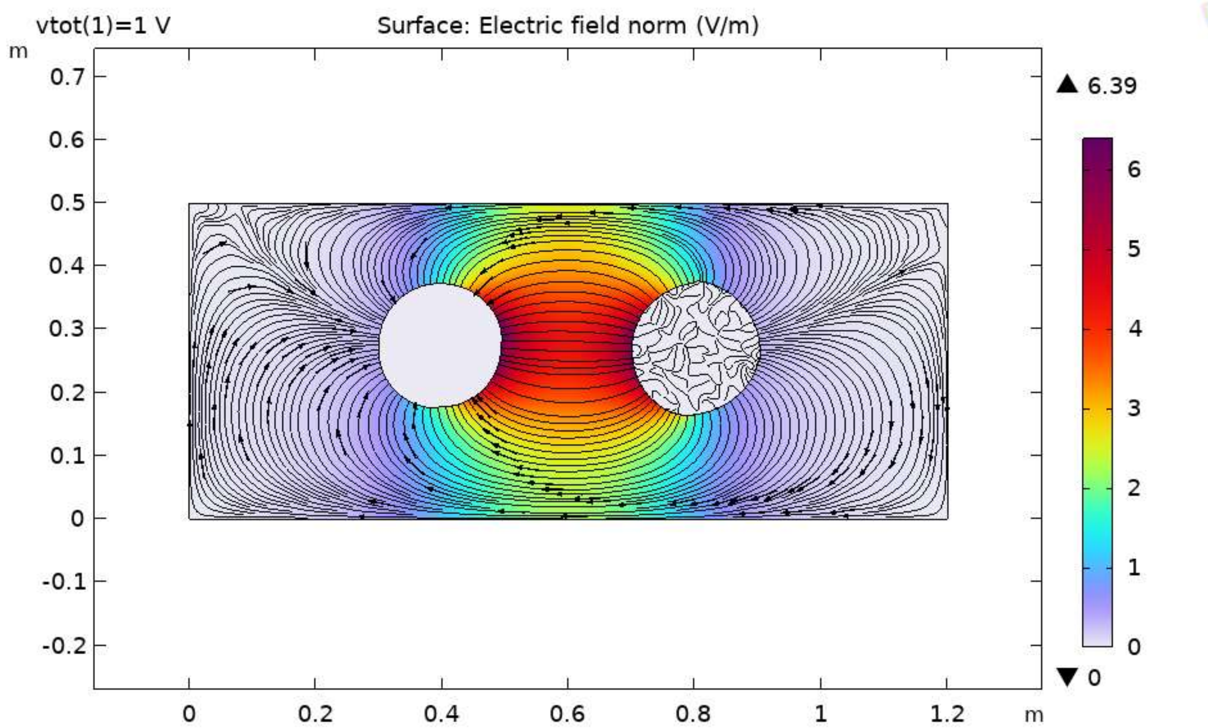

Figure 22: Shape optimization of 2D-circles (with fixed boundaries) at dmax= 0,07 [m] and n=1.

2. **Using the free-shape boundary method at dmax = 0.07 [m], Rmin=medium.**

The electric field strength calculated after the shape optimization of 2D-circles at the center of the box is 6.24 [V/m] as shown in the figure 25. The elapsed time of computation is 26 [minutes] because the SNOPT solver takes long to select the initial values used in optimization solver settings. However, this issue is solved by increasing the value of the tolerance of the optimal solution under the solver settings that results in a significant decrease of the elapsed time of computation.

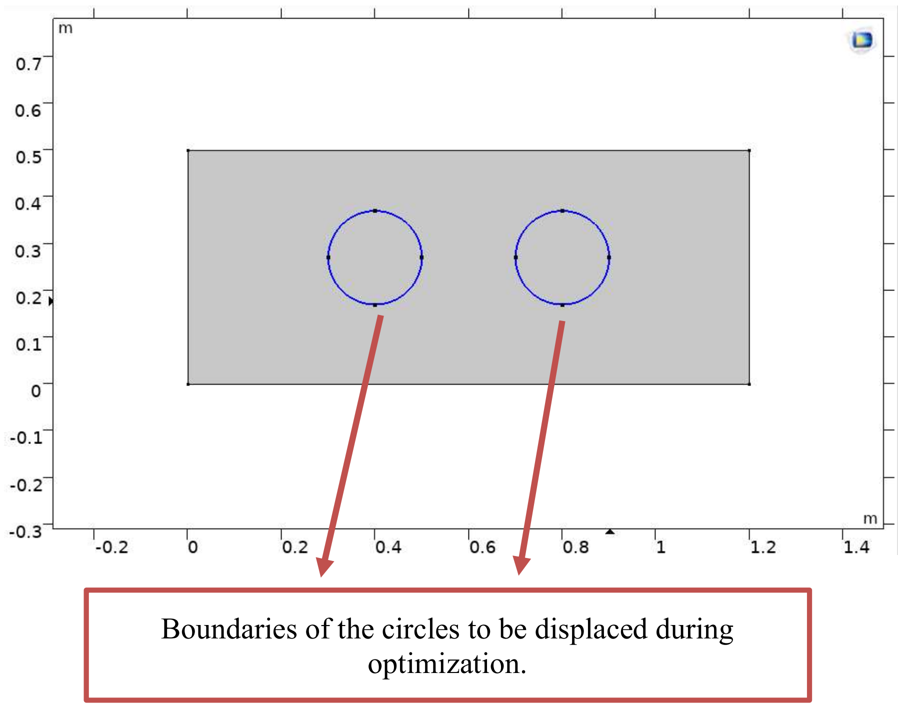

Figure 23: Boundaries selected for shape optimization.

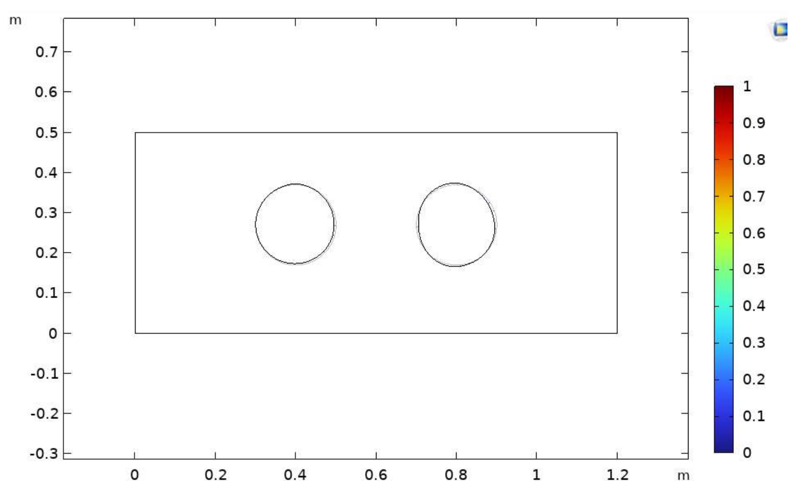

Figure 24: Overall displacement of the boundaries after shape optimization.

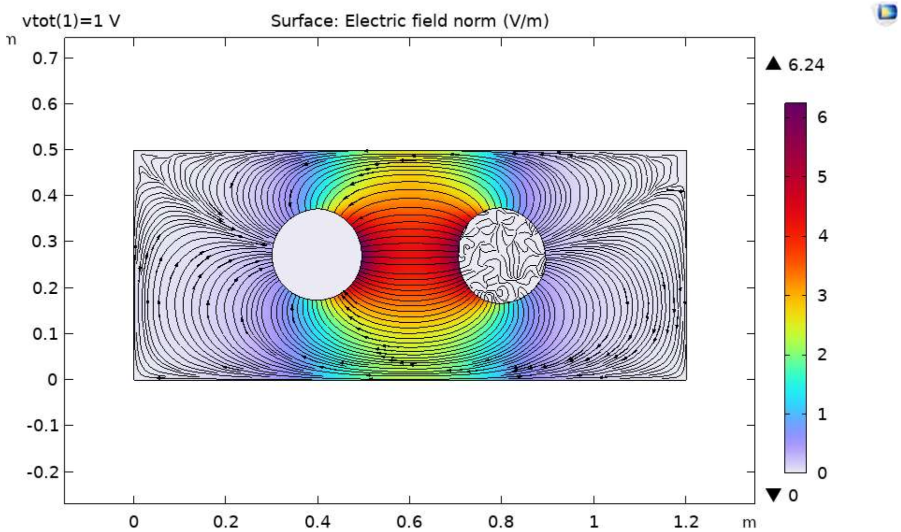

Figure 25: Shape optimization at dmax= 0.07 [m], Rmin=medium.

The findings from several simulations using the free-shape boundary method and the polynomial boundary method are shown in the table of results, as this will allow the discussion about the:

- The initial area of the geometries before optimization and the optimized area obtained after optimization thus forming the basis of calculating the percentage change in the geometries.
- The initial and optimized maximum electric field strength which is measured on the surface of the geometries using boundary probes.

Table 3: Results showing the shape optimization of circles located at the center of the box using the free-shape boundary method.

Minimum filter size, Rmin	dmax, [m]	Initial area, [m^2]	Optimized area, [m^2]	% change in the area	Initial max E-field, [V/m]	Optimized max E-field, [V/m]	Elapsed time, [min]
Rmin = large	0.07	0.062	0.068	9.6	**6.52**	4.12	6
	0.075		0.069	11.2		4.96	5
	0.08		0.070	12.9		4.97	8
Rmin = medium	0.07		0.065	4.83		6.33	4
	0.078		0.066	5.22		3.40	3
	0.089		0.063	1.61		3.45	3
Rmin = small	0.07		0.063	1.61		3.50	2
	0.081		0.063	1.61		2.70	1
	0.091		0.063	1.61		3.90	1

By keeping some boundaries fixed as shown in the figure 26, it is expected that the maximum electric field strength after optimization slightly decreases compared to when the entire geometry is selected as it was the case in the figure 25. The type of iteration solver used here is “Nelder -mead” since it is a gradient free- solver that relies on the selection of several control variable points on the geometry to generate expansions and/or contractions such that the worst points in the sequence are improved, thus resulting in changes of the maximum electric field strength.

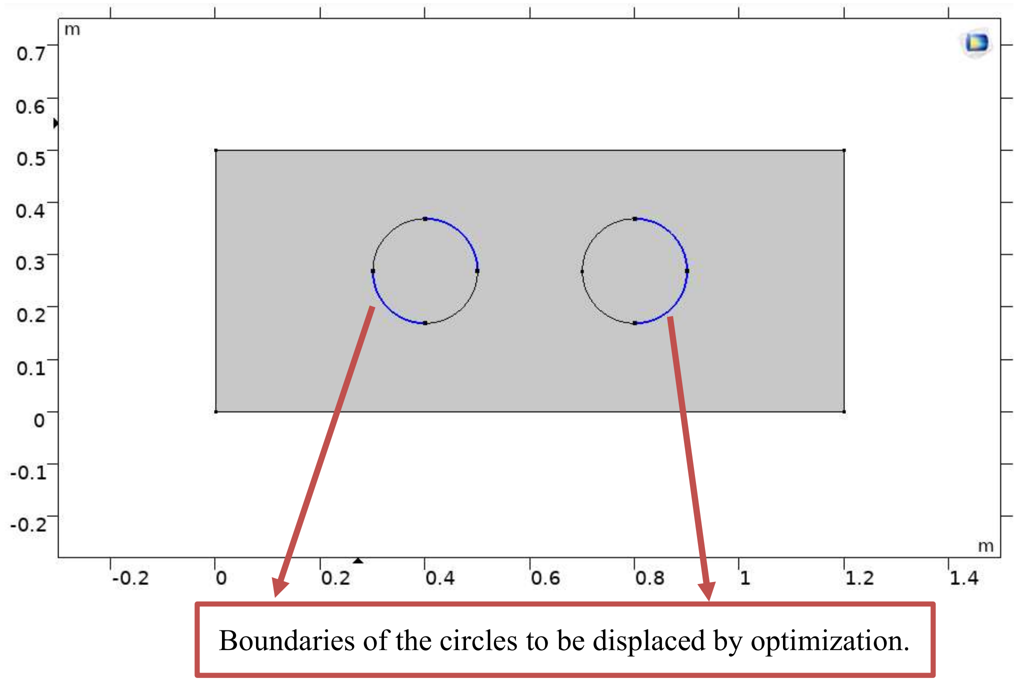

Figure 26: Shape optimization of circles (with fixed boundaries) using the free-shape boundary method.

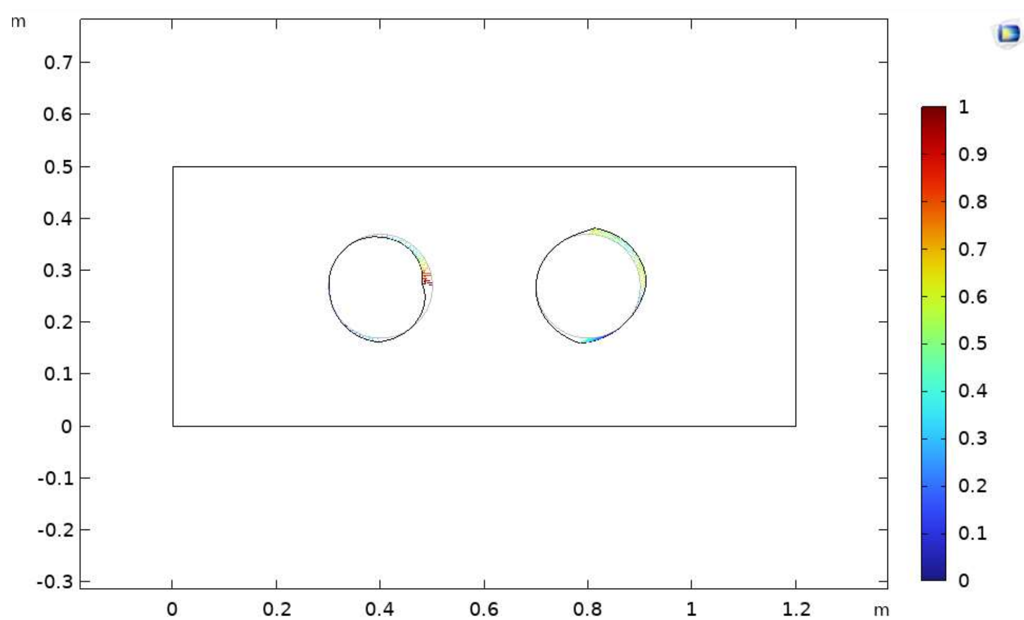

Figure 27: Overall change of shape of the boundaries after shape optimization using the free-shape boundary method.

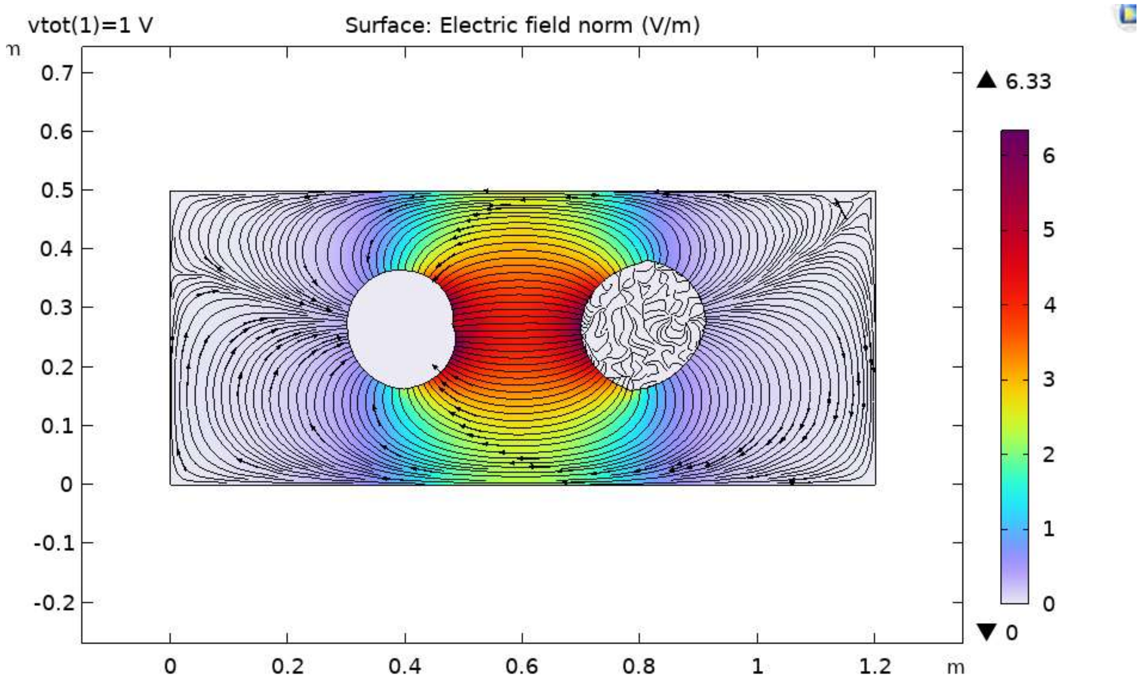

Figure 28: Shape optimization (with fixed boundaries) using free-shape boundary method.

3. Using the polynomial boundary method at dmax = 0.075 [m], n=2

By increasing the maximum displacement and the order of the Bernstein equation the geometry of the optimized circle undergoes significant shape change whereby the elapsed time is 2 [minutes] which is relatively faster because of running the simulation with the MMA optimization solver known for its robustness to deal with large control variables.

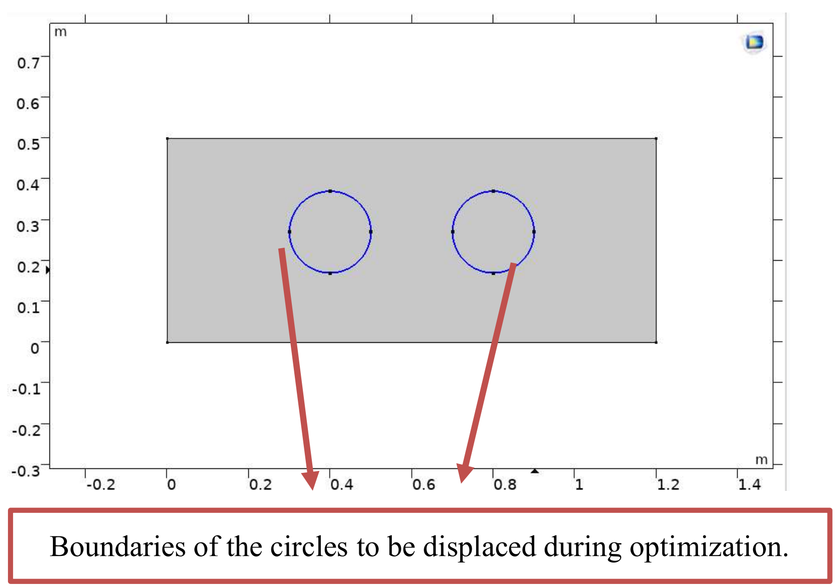

Figure 29: Boundaries selected for shape optimization.

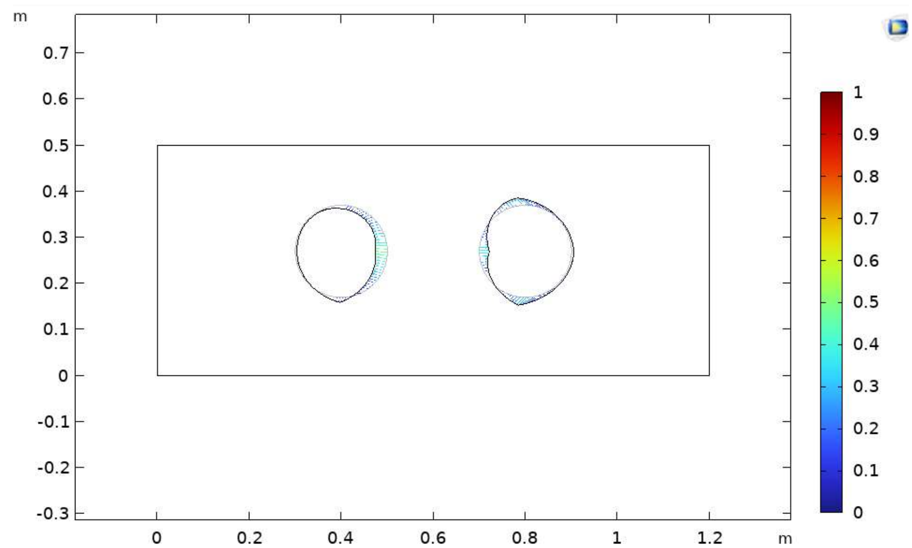

Figure 30:Overall change of shape of the boundaries at dmax=0.075 [m] & n=2.

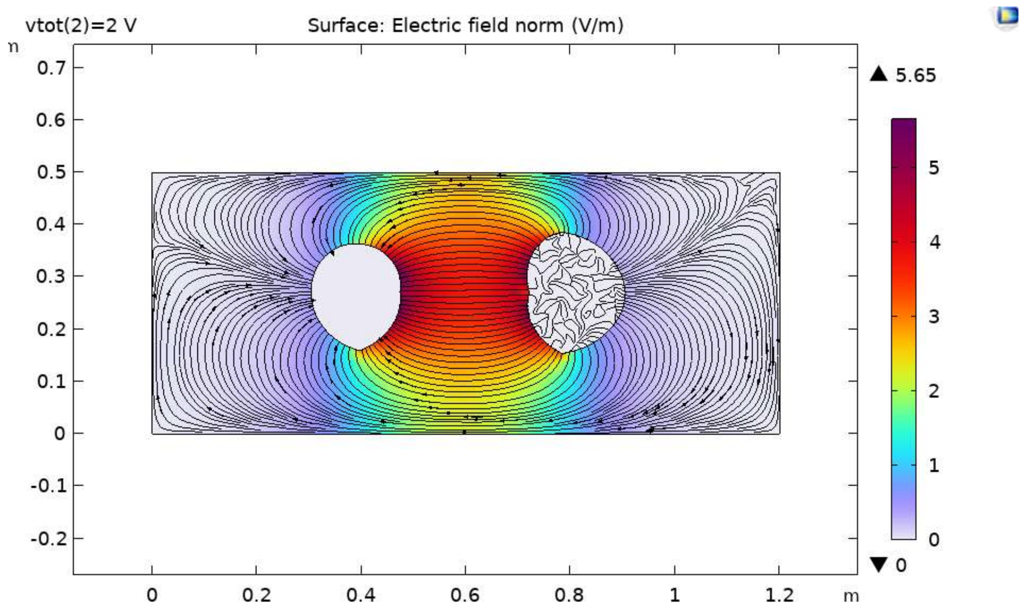

Figure 31: Shape optimization at dmax= 0.075 [m] & n=2.

The change in the shapes of circles at the center of the box, is governed by the control variables of the free-shape boundary method like the filter size, maximum displacement as described in the table 3 which results in the relative decrease of the electric field strength. Additionally, the table 4 describes how the polynomial boundary method affects the decrease in the electric field strength and the overall change in the shape.

Table 4: Results showing the shape optimization of circles located at the center of the box using the polynomial boundary method.

Bernstein order, n	dmax, [m]	Area before opt, $[m^2]$	Area after opt, $[m^2]$	% change in the area	Max E-field before opt, [V/m]	Max E-field after optimization, [V/m]	Elapsed time, [min]
	0.07		0.067	8		5,68	1,0
n=1	0,075		0,063	1.61		5,6	1,0
	0,08		0,063	1,61		5,58	1,0
	0,07	0,062	0,064	3,22	6,52	6.18	2.0
n=2	0,078		0,064	3,22		5,15	3,1
	0,089		0.065	4.83		5.11	3.0
	0,07		0,066	6,45		5.52	4,1
n=3	0,081		0,065	4.83		4.12	4.1
	0,091		0,063	1,61		5,22	5,2

Conclusively, the minimum filter size must be within a range of 1.5 to 2 times the selected maximum displacement hence should be carefully selected not to generate error messages shown in the figure 32, caused by having a very large dmax and a very small filter size, *Rmin* resulting in having the returned solutions that are not converged [7] [8].

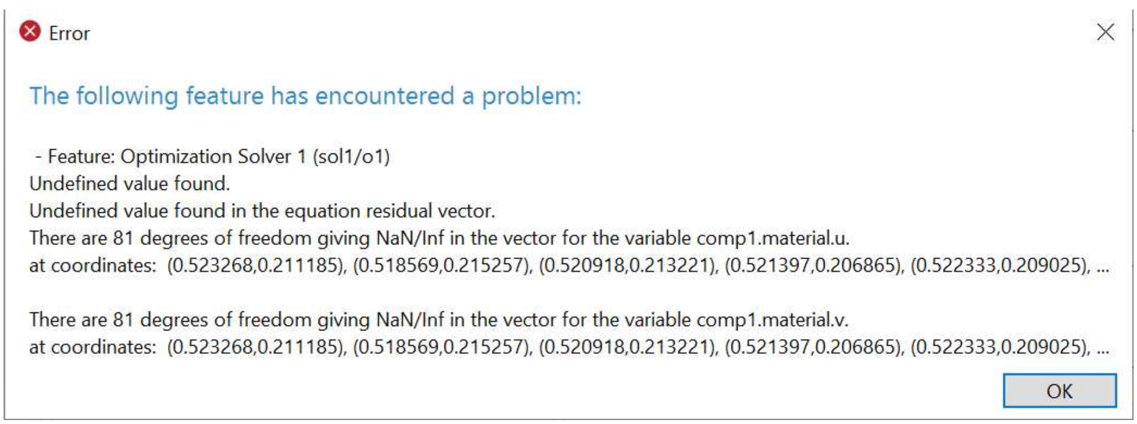

Figure 32: Convergence error message from COMSOL caused by having a large dmax, small Rmin.

For the 2D-side by side squares, the initial geometry of the squares has "2 fixed points at the center" to allow boundaries of the square to be more flexible to move outwards to minimize the chances of having field enhancements at the sharp corners as shown in the electric field plot obtained after shape optimization in the figure 35.

1. **Using polynomial boundary at dmax= 0.1 [m], n=2**

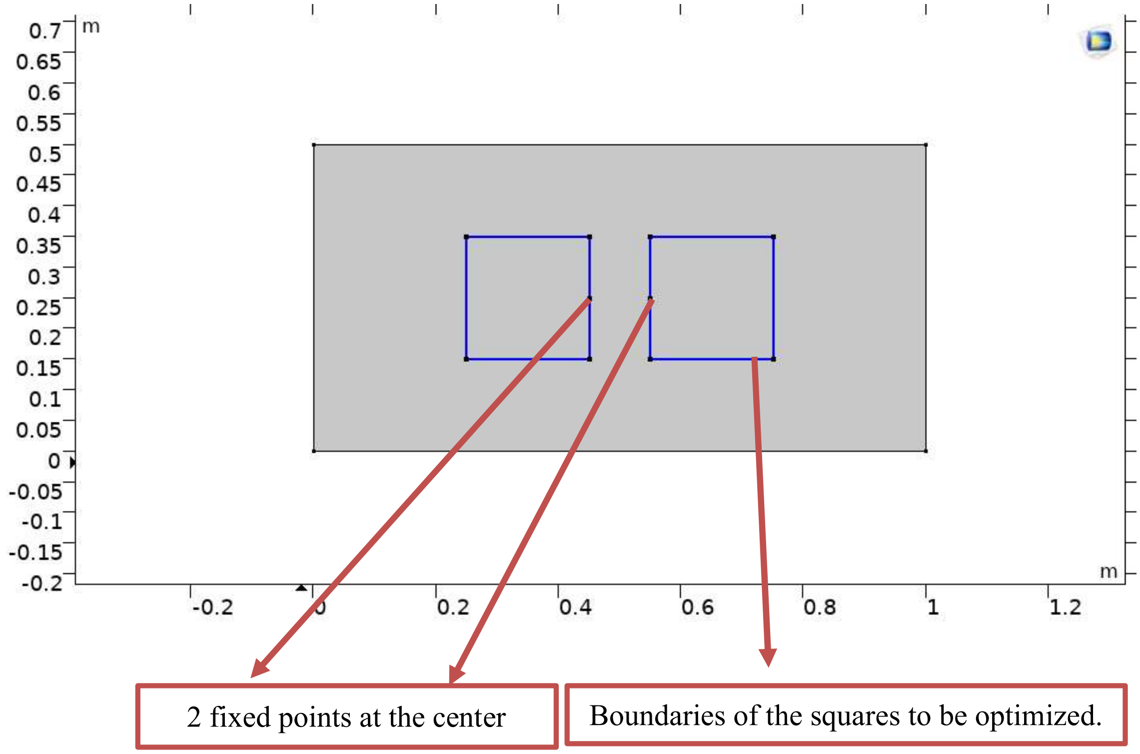

Figure 33: Boundaries selected for shape optimization.

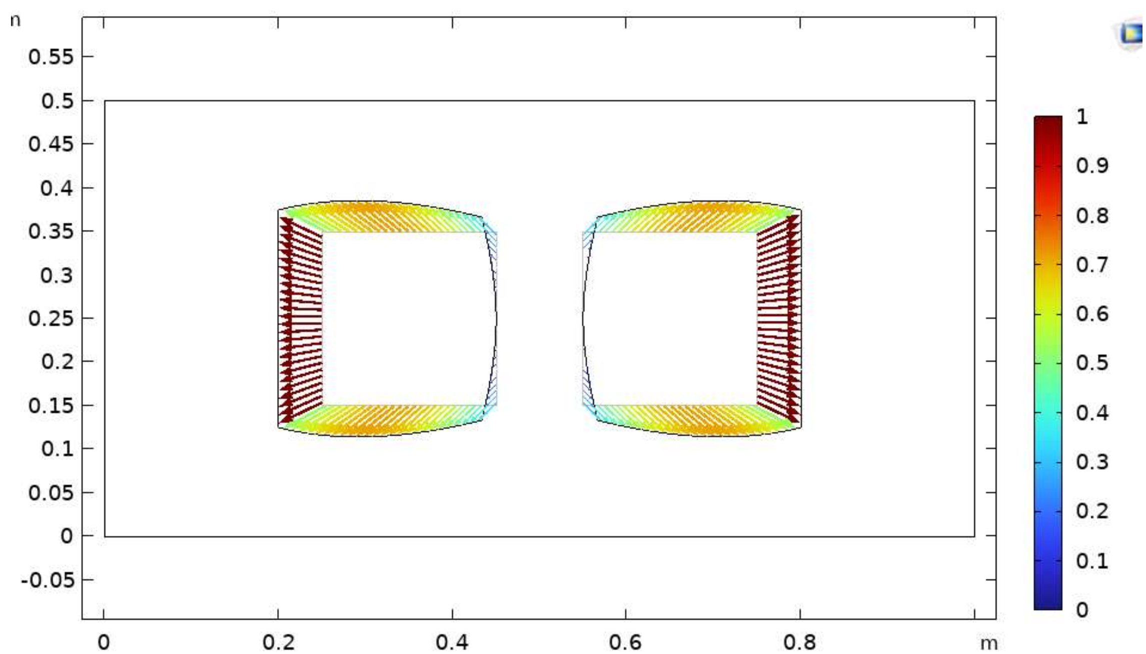

Figure 34: The displacement of the boundaries at dmax=0.1 [m] & n=2

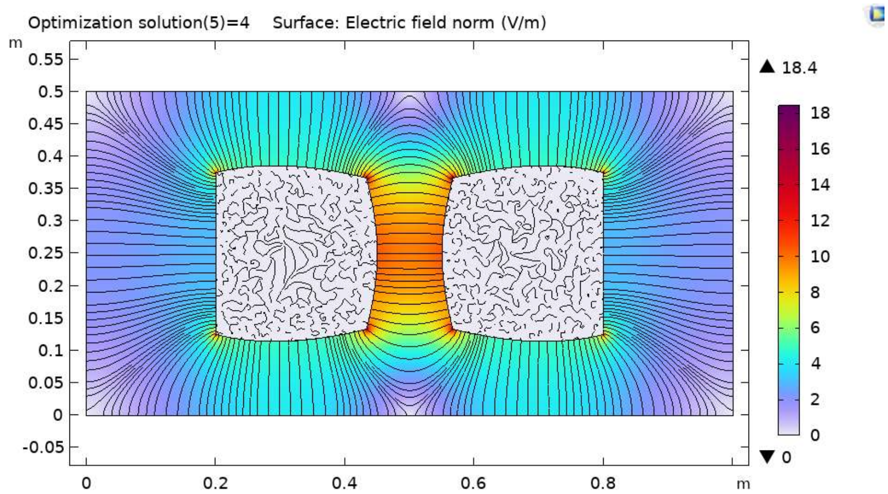

Figure 35: Shape optimization of side-by-side squares at dmax= 0.1 [m] and n= 2.

The electric field strength distribution on the surface of the squares is shown in the figure 36. At the start of the optimization process, the electric field strength measured by boundary probe is higher on the surface of the squares due to the presence of sharp corners in the initial geometry thus as several iterations in the optimization are performed, the sharp corners become curved hence there will be a decrease in the magnitude of electric field strength until an optimal solution is reached as shown in the table 5.

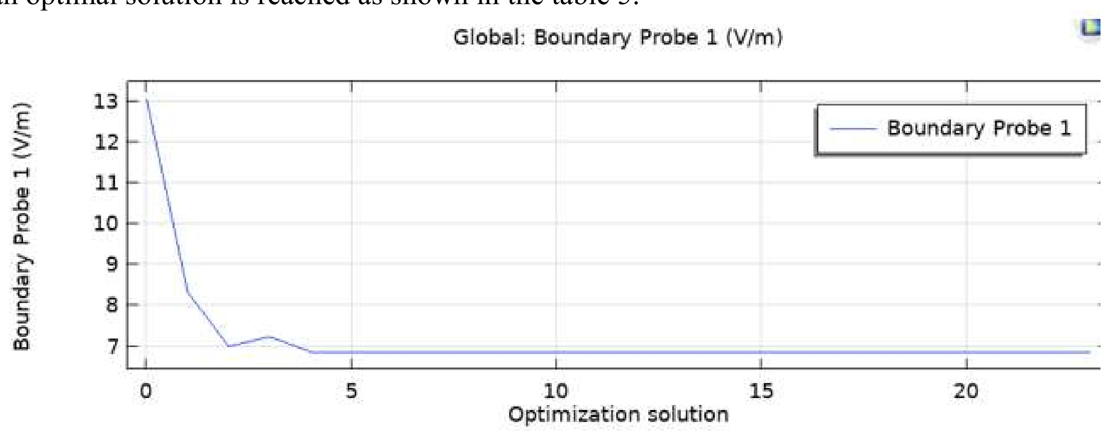

Figure 36: Electric field distribution on the surface of the side-side squares (at the center of the box).

Table 5: Data showing the variation of electric field strength versus successive iterations using polynomial boundary.

Iterations, n	Electric field strength, [V/m]
n=0	13
n=1	12
n=2	10
n=3	9
n=4-25	7

Table 6: Results of shape optimization of side-by-side squares located at the center of the box using the polynomial boundary method.

Bernstein order, n	dmax, [m]	Initial area, [m^2]	Optimized area, [m^2]	% change in the area	Initial max E-field, [V/m]	Optimized max E-field, [V/m]	Elapsed time, [min]
	0.1		0.082	2.50		18,4	11
n=2	0.2		0.083	3.75		18.4	12
	0.3		0.085	6.25		12.3	14
	0.1	0,08	0.081	1.25	30.9	13.0	27
n=3	0.2		0.082	2.50		11.6	31
	0.3		0.083	3.75		17.9	30
	0.1		0.082	2.50		22.8	23
n=3	0.2		0.089	11.25		17.4	18
	0.3		0.090	12.50		15.7	15

2. Using free-shape boundary at dmax= 0.09 [m], Rmin=small

With the same fixed points as the previous case, the boundaries of the optimized geometry will not be displaced that much due to a relatively small maximum displacement and a small filter size as shown in the figures 37 & 38.

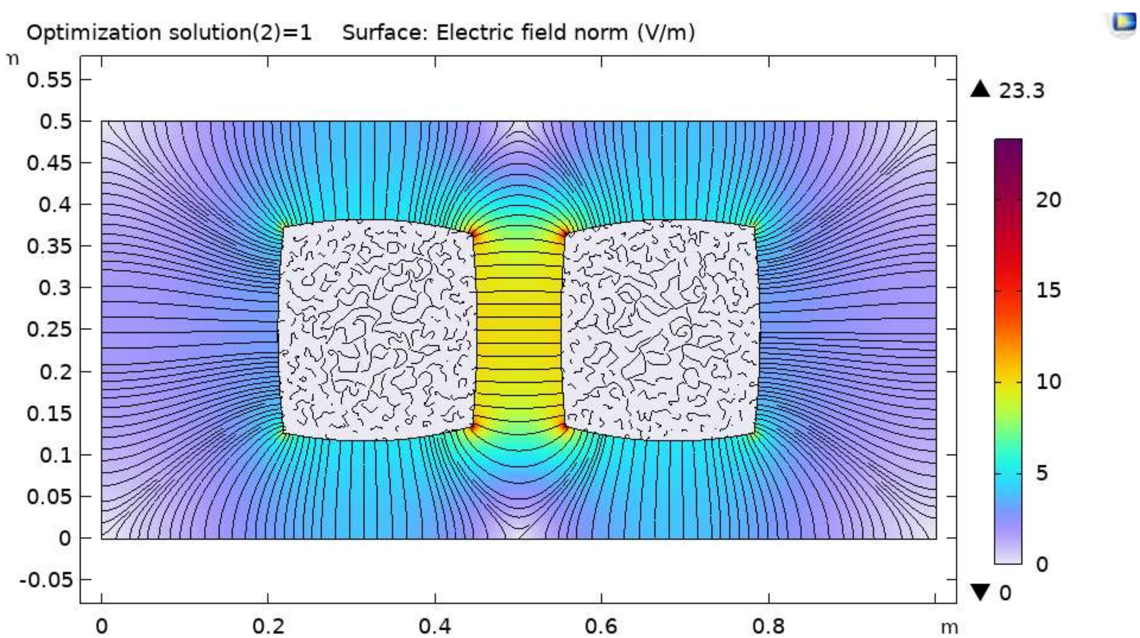

Figure 37: Shape optimization of side-by-side squares (free-shape boundary)

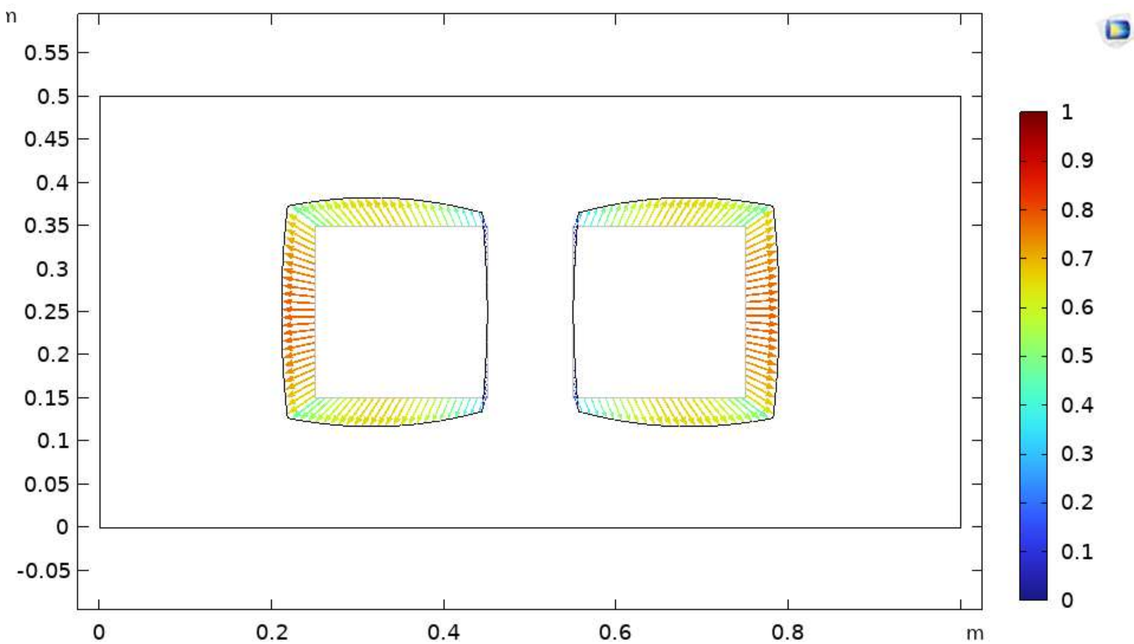

Figure 38: Boundary displacements of side-by-side squares (free-shape boundary)

Table 7: Results showing the shape optimization of side-by-side squares located at the center of the box using the free-shape boundary method.

Minimum filter size, Rmin	dmax, [m]	Initial area, $[m^2]$	Optimized area, $[m^2]$	% change in the area	Initial max E-field, [V/m]	Optimized max E-field, [V/m]	Elapsed time, [min]
	0.07		0.10	25,0		15.10	6
Rmin = large	0.08		0.11	37.5		14.94	5
	0.09		0.11	37.5		14.97	8
	0.07	0.08	0.09	12.5		18.90	7
Rmin = medium	0.08		0.09	12.5	30.9	18.40	7
	0.09		0.10	25.0		18.45	5
	0.07		0.11	37.5		19.50	9
Rmin = small	0.08		0.09	12.5		18.70	6
	0.09		0.09	12.5		23.30	4

The E-factor (objective function) is obtained by taking the ratio of the average to the maximum electric field strengths. In the figure 39, at the start of optimization (i.e., at optimization solution=0), the E-factor is minimal, thus the electric field strength on the surface of the squares is maximum, as the optimization progresses the E-factor starts to increase until the optimal solution is achieved hence overcoming the influence of the maximum electric field strength on the surface of the squares. When the shape optimization converges to a solution at the 4th iteration, a constant value of the E-factor is achieved hence the maximum electric field on the surface of the squares is minimized to an optimal solution.

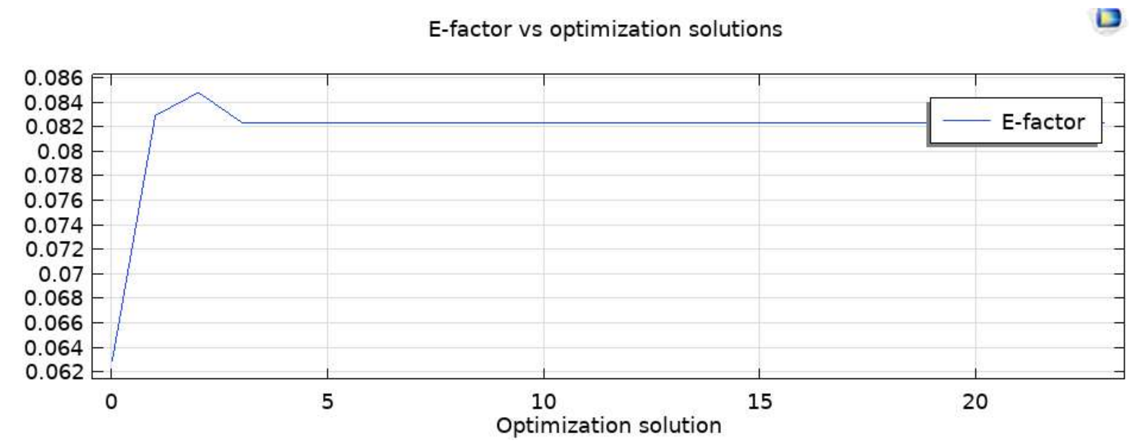

Figure 39: Electric field distribution of the side-side squares (at the center of the box) using the free-shape boundary method.

The shape optimization for corner-corner squares is done by fixing a point on the edges to allow the boundaries move freely hence allow the deformation of the boundaries as shown in the figures 40-42.

1. **Using the polynomial boundary at dmax= 0.05 [m], Bernstein order, n=2**

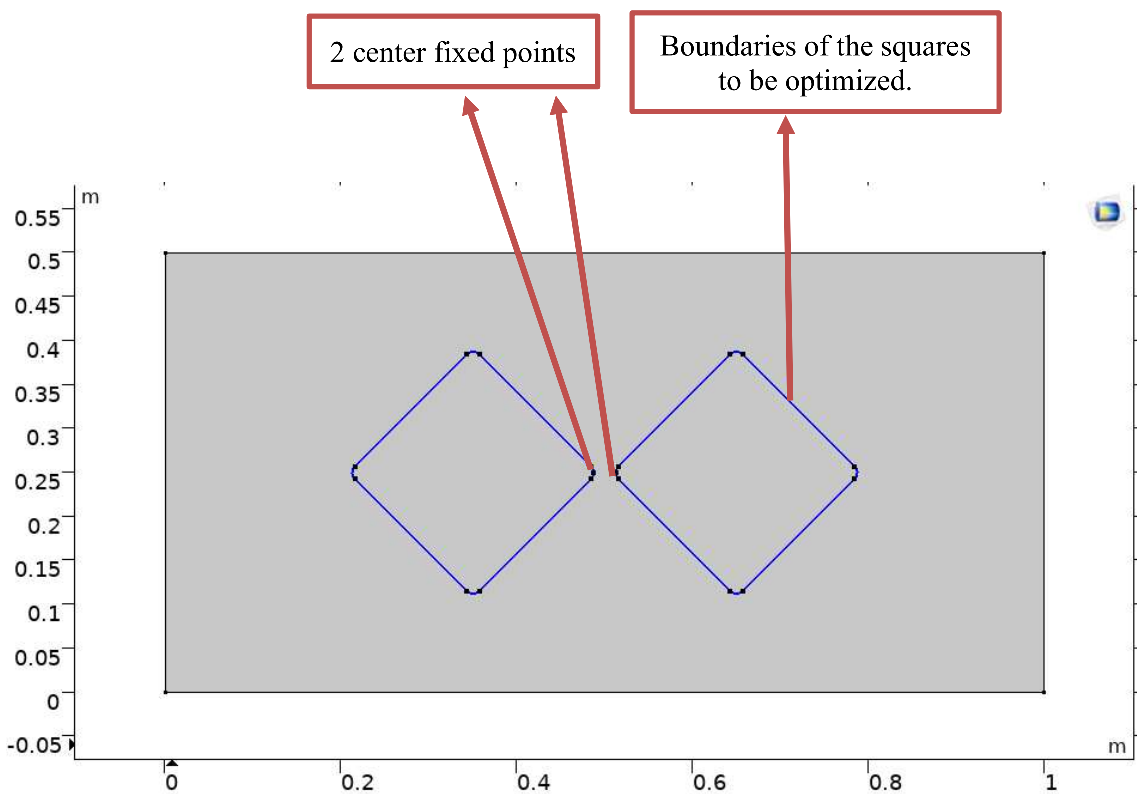

Figure 40: Boundaries selected for shape optimization.

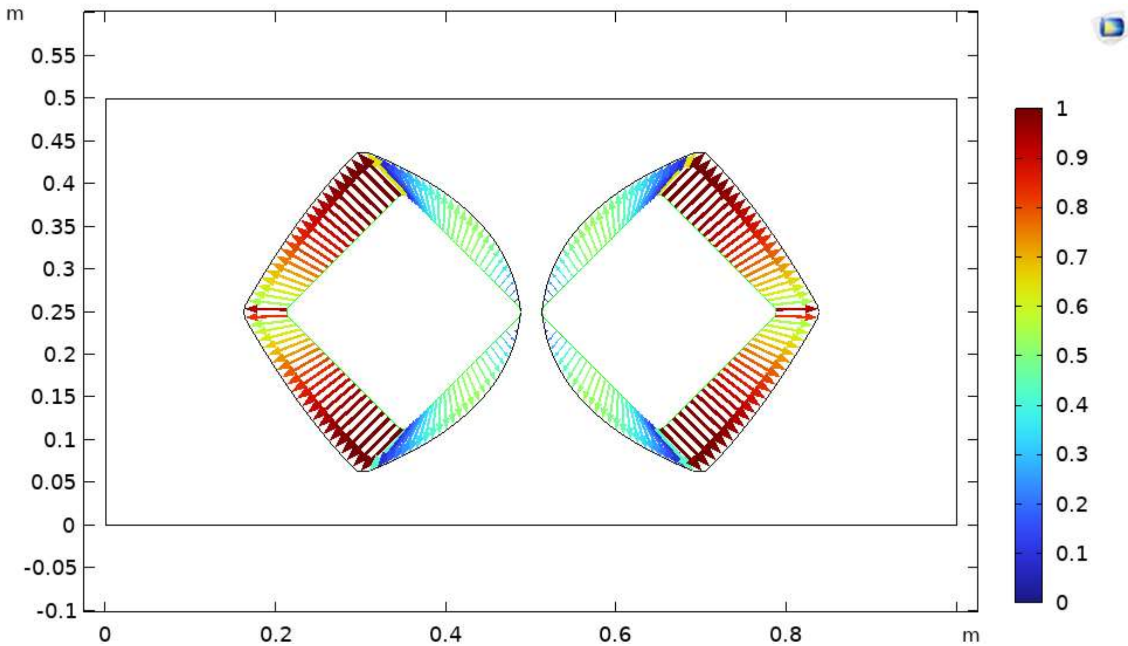

Figure 41: Boundary displacement of corner-corner squares (polynomial boundary).

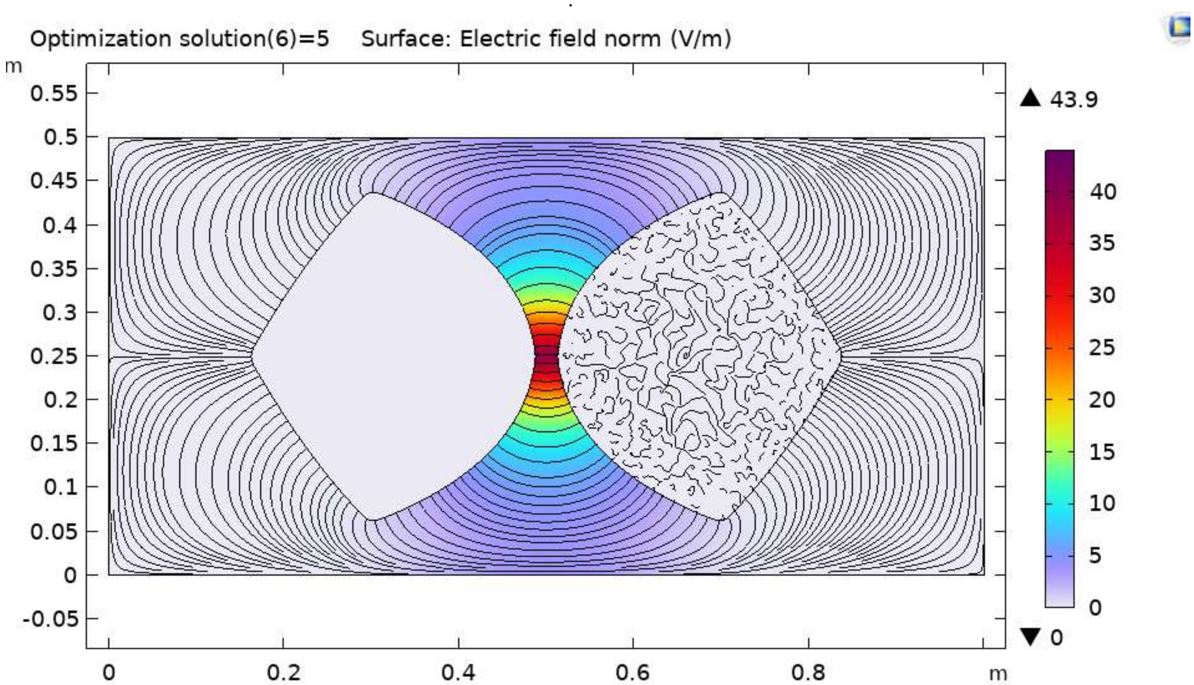

Figure 42: Shape optimization of corner-corner squares using polynomial boundary.

Table 8: Results of shape optimization of corner-corner squares located at the center of the box using the polynomial boundary method.

Bernstein order, n	dmax, [m]	Area before opt, [m^2]	Area after optimization, [m^2]	% change in the area	Max E-field before opt, [V/m]	Max E-field after opt, [V/m]	Elapsed time, [min]
n=2	0.050	0.079	0.080	1.26	**53.7**	43.8	6
	0.055		0.081	2.53		48.0	6
	0.060		0.082	3.79		42.3	7
n=3	0.050		0.080	1.26		35.5	11
	0.055		0.084	6.32		36.1	13
	0.060		0.085	8.10		36.1	15
n=4	0.050		0.095	11.1		36.5	22
	0.055		0.095	11.1		26.5	15
	0.060		0.083	5.06		26.5	12

2. **Using the free-shape boundary method at dmax= 0.05 [m], Rmin= medium with all points in the corners fixed.**

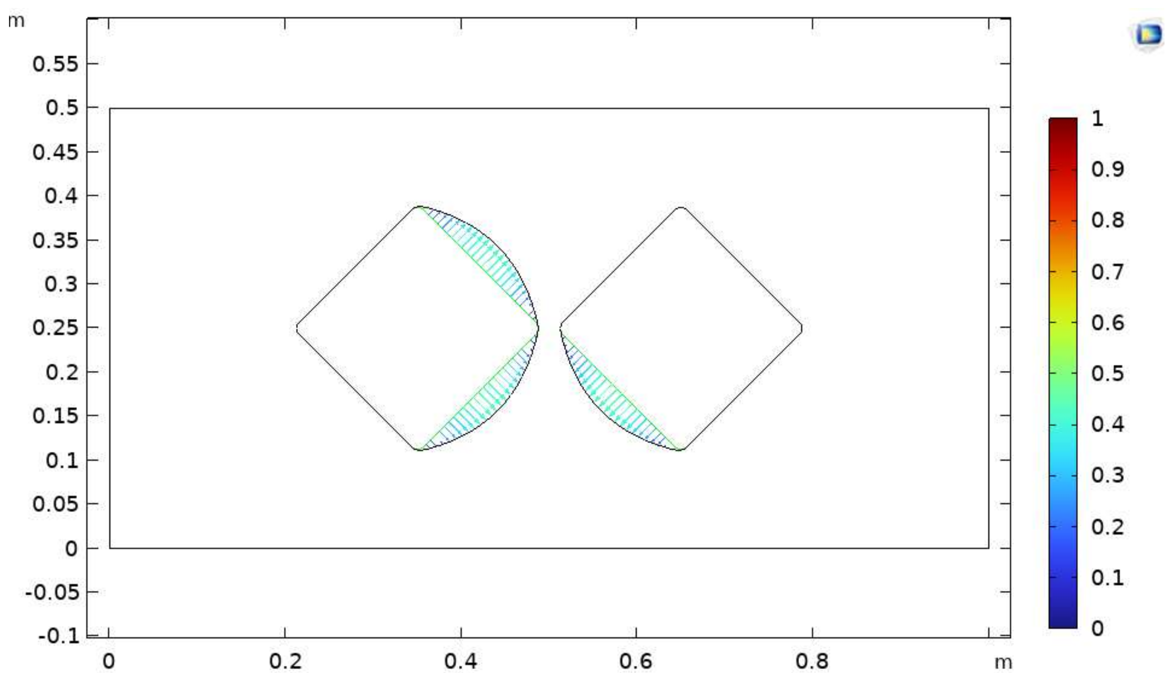

Figure 43: Boundary displacement of corner-corner squares (polynomial boundary).

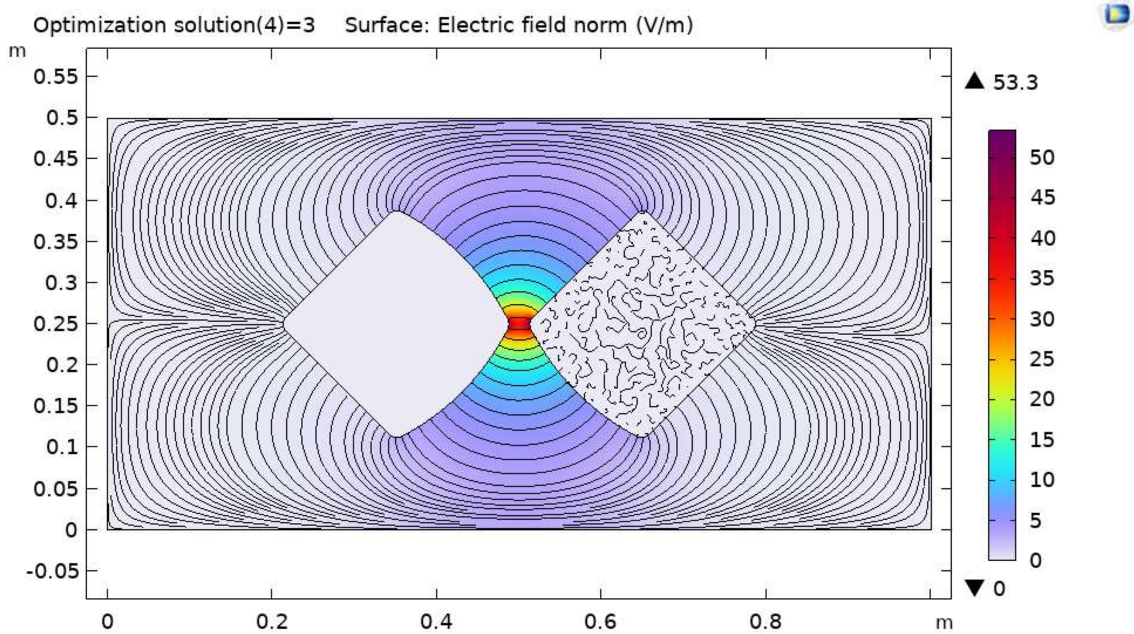

Figure 44: Shape optimization of corner-corner squares using free-shape boundary (all corners fixed)

Table 9: Results of shape optimization of corner-corner squares at the center of the box using the free-shape boundary method.

Minimum filter size, Rmin	dmax, [m]	Initial area, [m^2]	Optimized area, [m^2]	% change in the area	Initial max E-field, [V/m]	Optimized max E-field, [V/m]	Elapsed time, [min]
Rmin = large	0.05	0.08	0.082	25.0	53.7	51.10	6
	0.06		0.084	37.5		44.94	5
	0.07		0.082	37.5		34.97	8
Rmin = medium	0.05		0.083	12.5		53.30	7
	0.06		0.084	12.5		48.40	7
	0.07		0.085	25.0		38.45	5
Rmin = small	0.05		0.081	37.5		39.50	9
	0.06		0.090	12,5		38.70	6
	0.07		0.082	12.5		27.90	4

The objective function for corner-corner squares is to maximize the E-factor. From the figure 45 below, at the start of the optimization process the E-factor is minimal, due to the maximum electric field strength; as the optimization progresses towards the optimal solution where the electric field strength is minimum; the E-factor increases until the third iteration where the E-factor is no longer increasing.

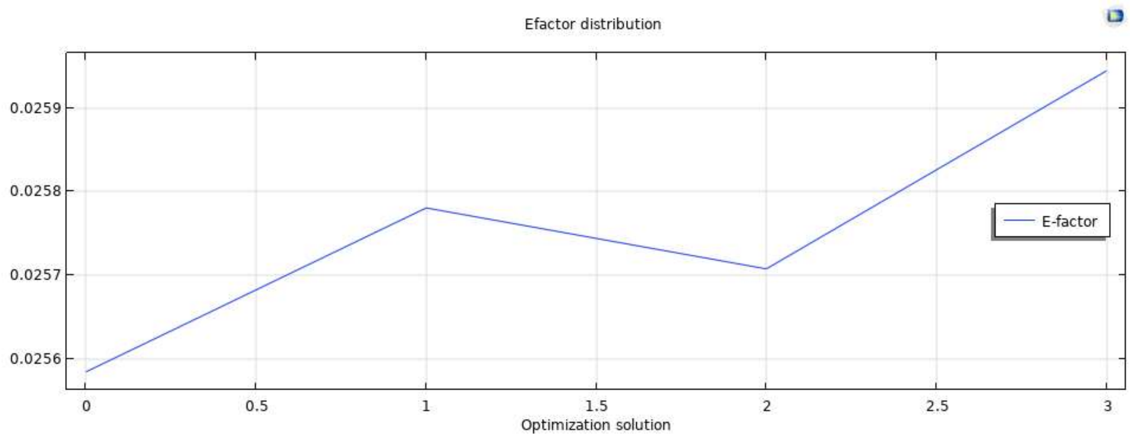

Figure 45: The E.factor distribution for corner-corner squares (at the center of the box).

3.1.2 2D-circles & squares (non-symmetric case)

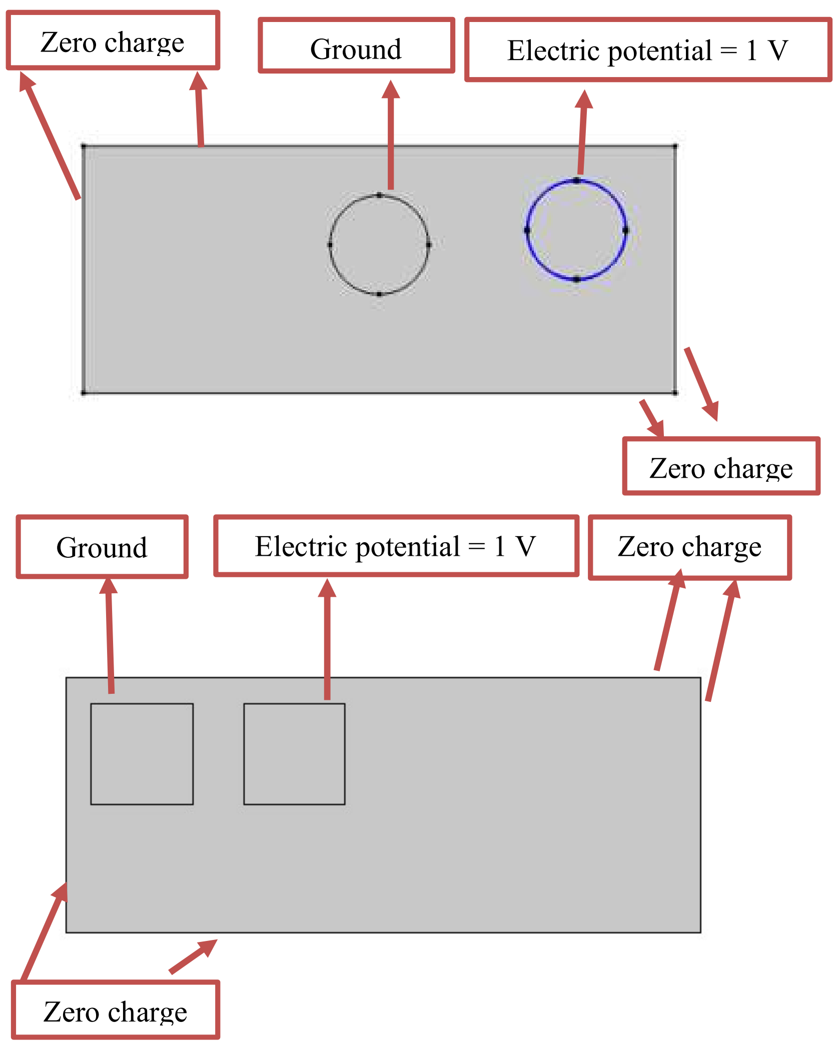

Figure 46: Boundary conditions for side-side squares & circles.

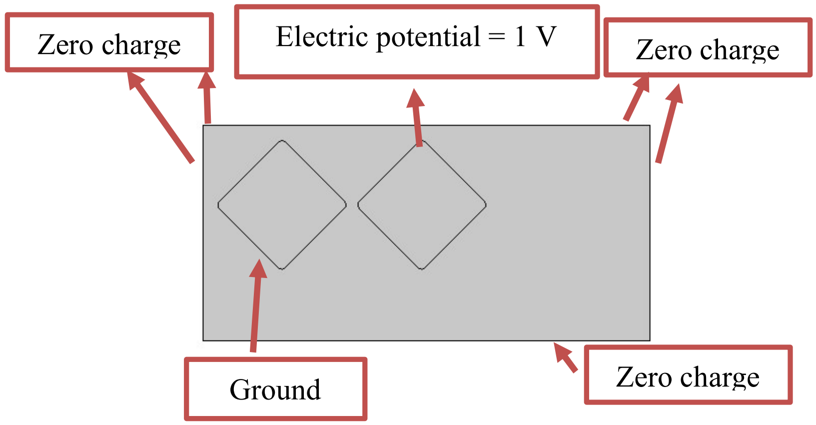

Figure 47: Boundary conditions for corner-corner squares (at the corner).

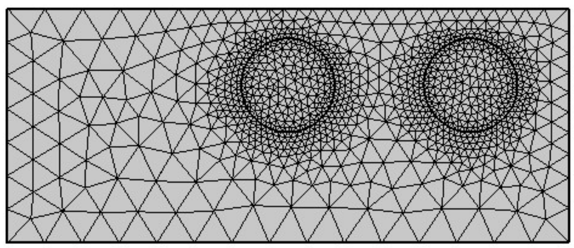

Figure 48: Meshing of circles (at the corner).

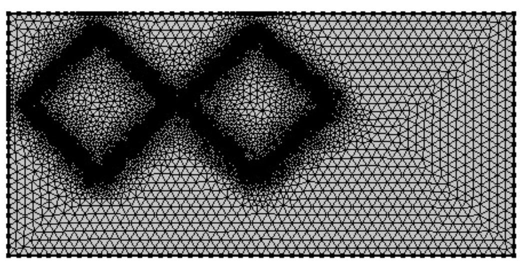

Figure 49: Meshing of corner-corner squares (at the corner).

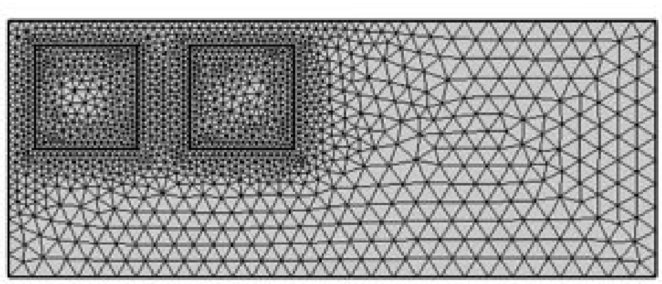

Figure 50: Meshing of side-side squares (at the corner).

3.1.2.1 Es-study of the 2D-circles & squares (at the corner)

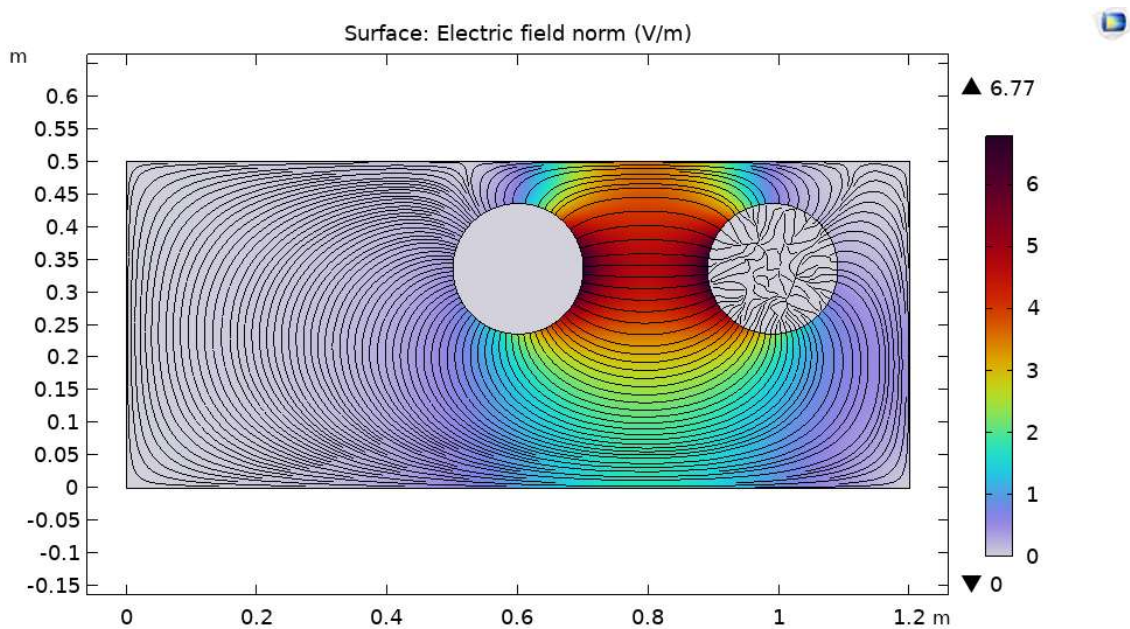

Figure 51: Es-study of circles at the corner of the box.

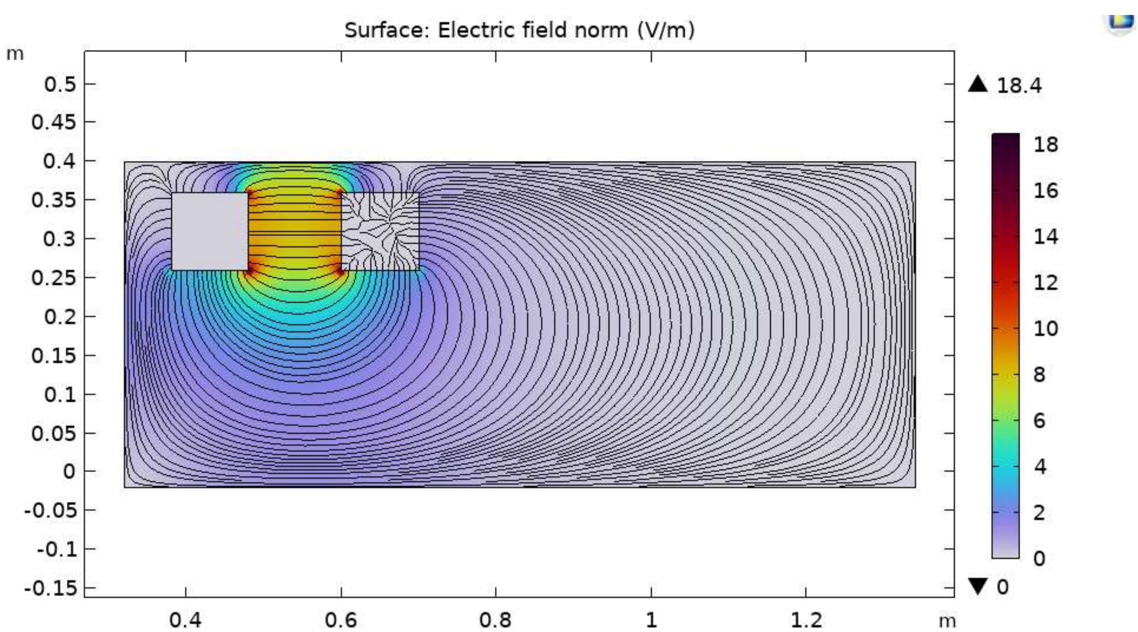

Figure 52: Es-study of side-side squares at the corner of the box.

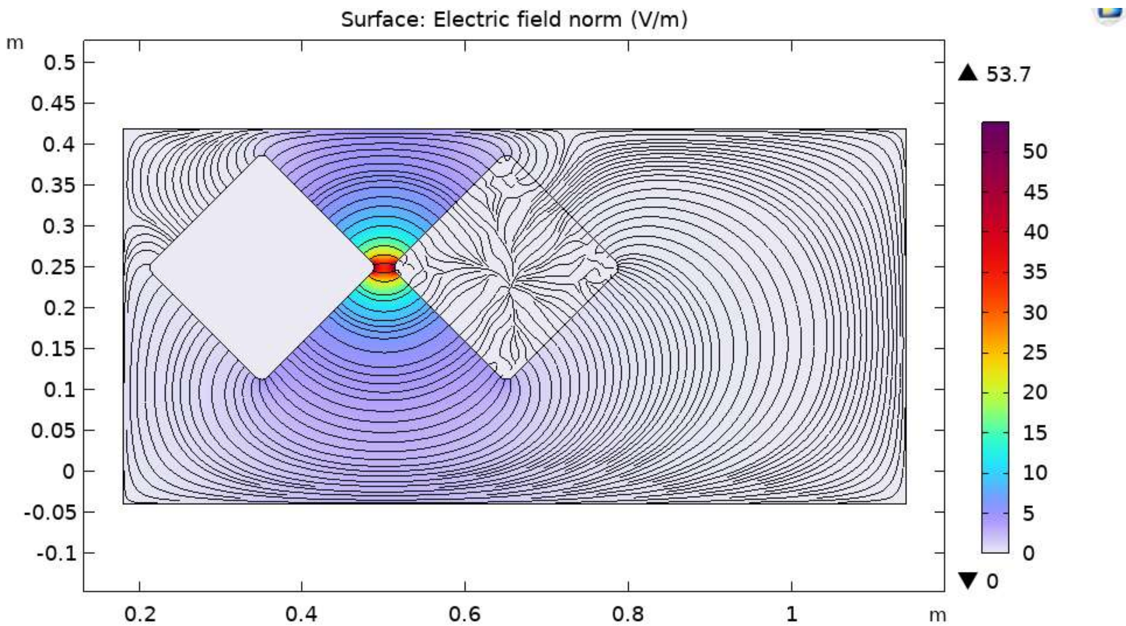

Figure 53: Es-study of corner-corner squares at the corner of the box.

3.1.2.2 Shape optimization of circles & squares (at the corner)

The shape optimization of 2D-circles and squares is done by adding a "free-shape domain" to the shape optimization algorithm to enable control variables in the "polynomial boundary" and the "free-shape boundary" perform optimization on the selected boundaries of the respective geometries [8].

1. **Using the polynomial boundary at dmax= 0.07[m], n=2**

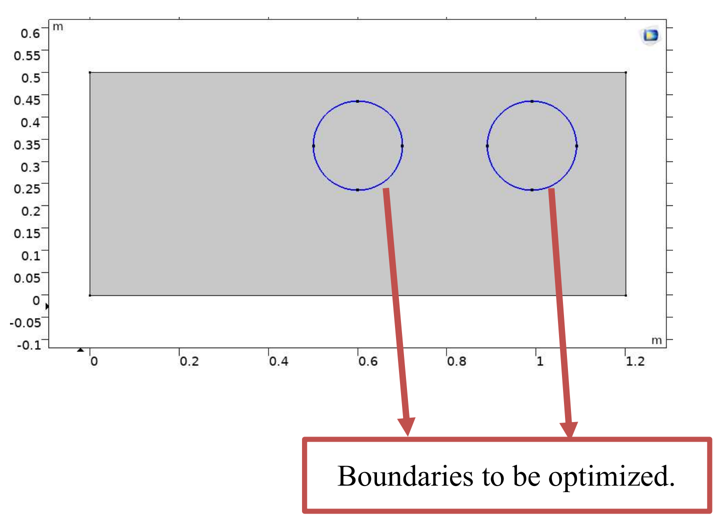

Figure 54: Boundaries selected for shape optimization.

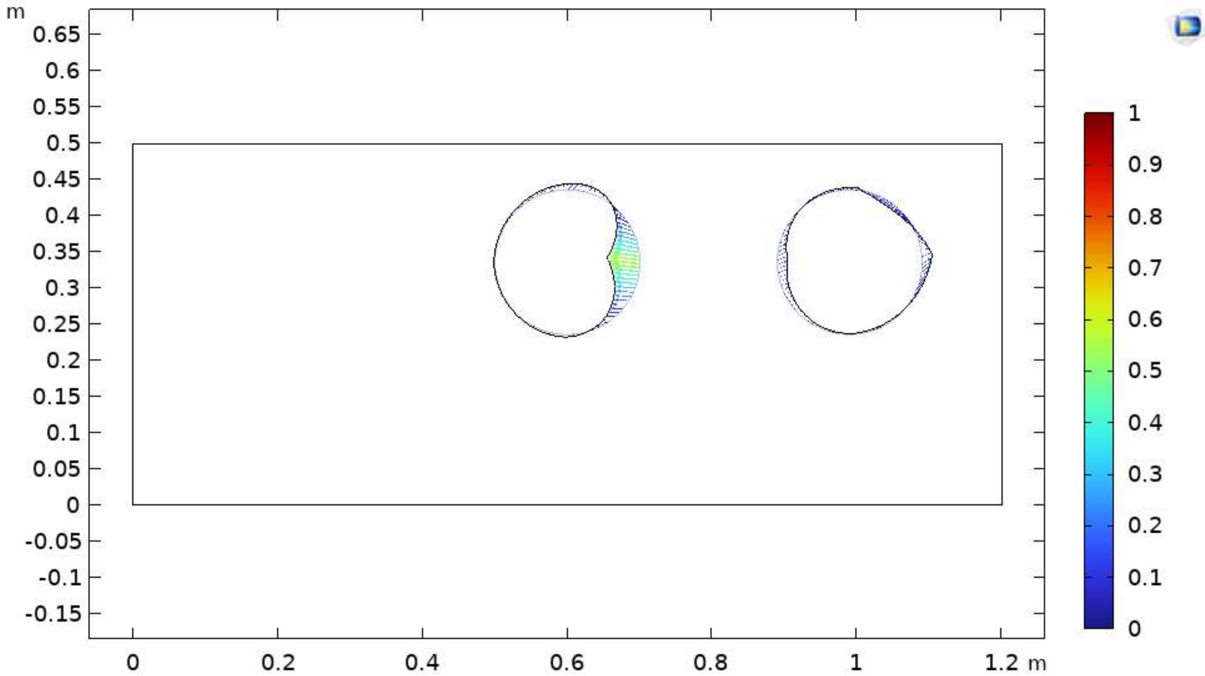

Figure 55: Boundary displacement of circles (polynomial boundary).

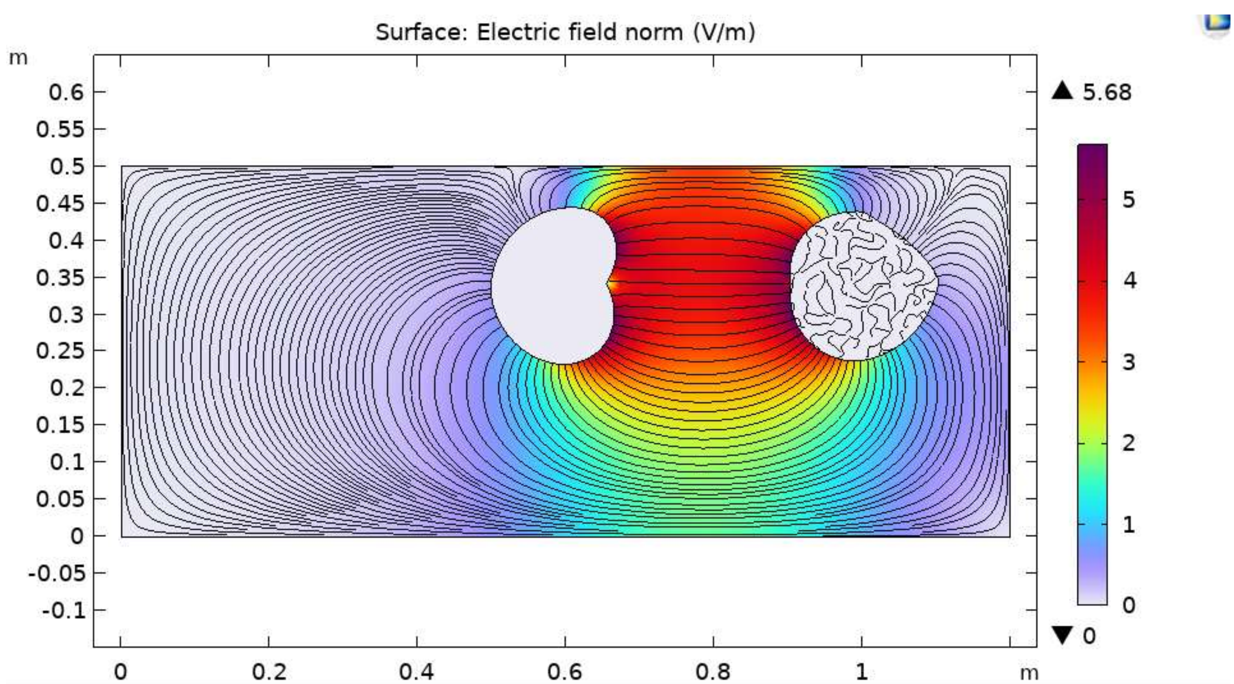

Figure 56:Shape optimization of circles (at the corner of the box) using polynomial boundary.

Table 10: Results of shape optimization of circles at the center of the box using the polynomial boundary method.

Bernstein order,n	dmax, [m]	Area before opt, [m^2]	Area after optimization, [m^2]	% change in the area	Max E-field before opt, [V/m]	Max E-field after opt, [V/m]	Elapsed time, [min]
n=2	0.050	**0.052**	0.058	11.5	**6.77**	6.3	15
	0.065		0.059	13.4		5.0	16
	0.070		0.058	11.5		5.7	7
n=3	0.050		0.055	5.76		4.5	11
	0.065		0.054	3.82		5.1	13
	0.080		0.056	7.70		4.1	15
n=4	0.052		0.055	5.76		3.5	12
	0.055		0.055	5.76		3.5	15
	0.060		0.054	3.82		4.5	12

2. Using the free-shape boundary at dmax= 0.07[m], Rmin=large

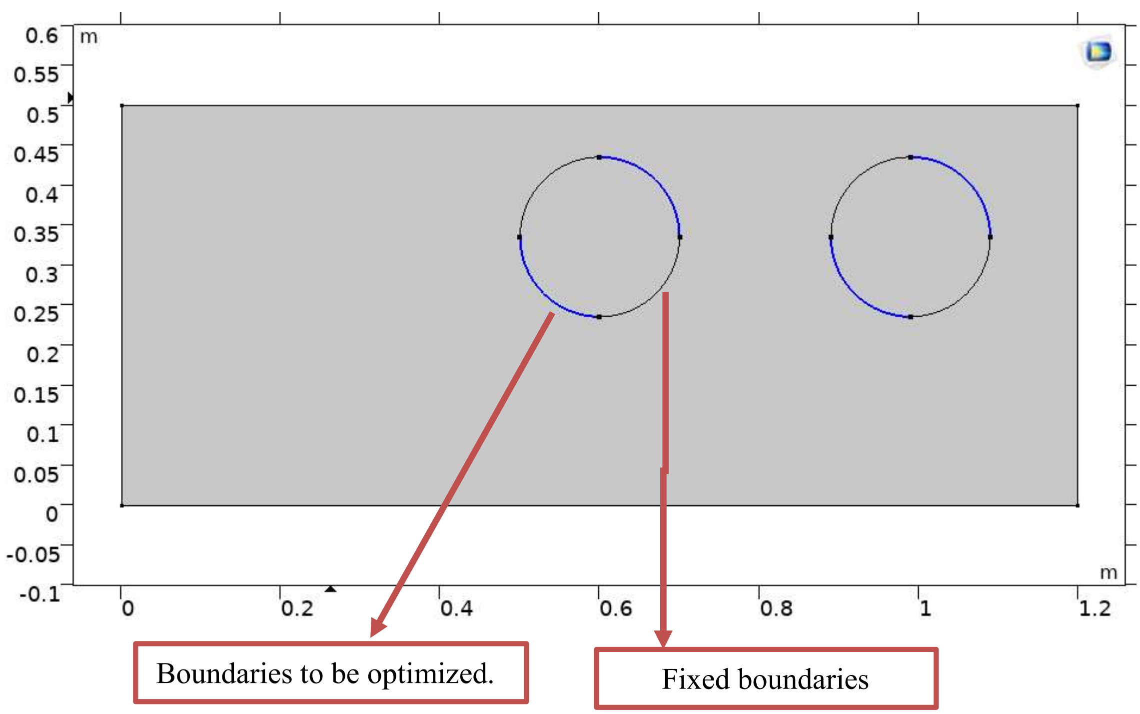

Figure 57: Boundaries selected for shape optimization.

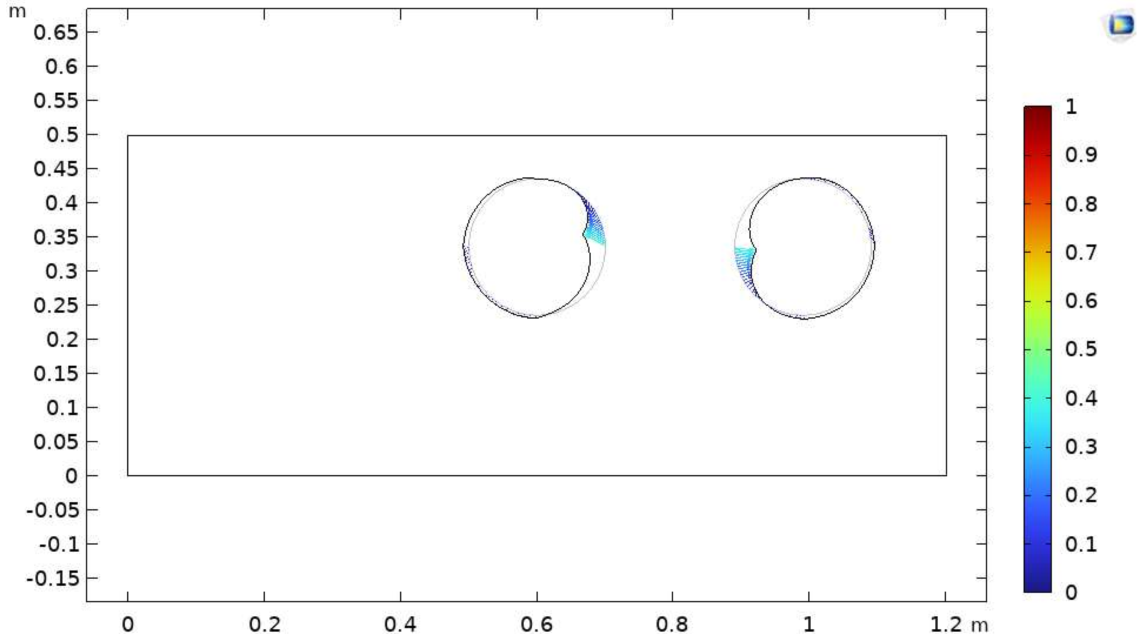

Figure 58: Boundary displacement of circles with fixed boundaries (using free-shape boundary method).

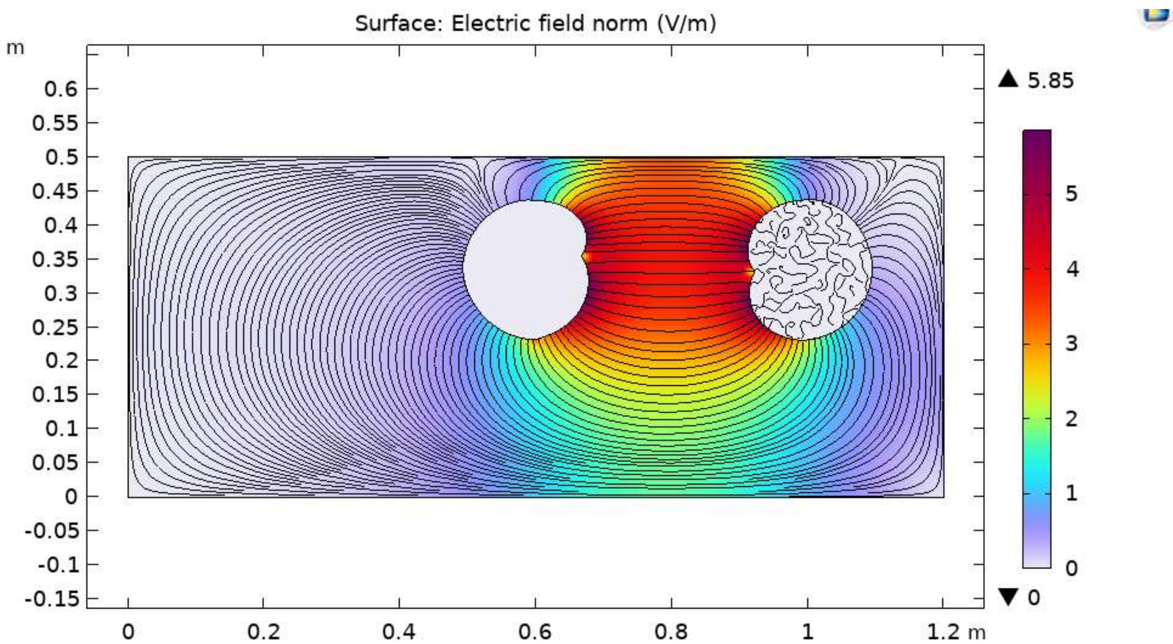

Figure 59: Shape optimization of circles (at the corner) using free-shape method.

Table 11: Results of shape optimization of circles (at the corner) using free-shape boundary method.

Minimum filter size, Rmin	dmax, [m]	Initial area, [m^2]	Optimized area, [m^2]	% change in the area	Initial max E-field, [V/m]	Optimized max E-field, [V/m]	Elapsed time, [min]
Rmin = large	0.05	0.052	0.053	1.92	6.77	5.1	6
	0.06		0.056	7.69		4,9	5
	0.07		0.057	9.60		5.9	8
Rmin = medium	0.05		0.053	1.92		6,3	7
	0.06		0.055	5.76		4.4	7
	0.07		0.056	7.69		6.4	5
Rmin = small	0.05		0.054	3.84		6.5	9
	0.06		0.055	5.76		6.7	6
	0.07		0.053	1.92		4.9	4

There is a small difference in the magnitudes of the electric field strength obtained after the shape optimization of circles regardless the method used because the type of solver used is similar however there is significant difference in the elapsed time because of dependence on the number of iterations to be used until the solution is reached, thus, the greater the number of iterations used, the longer time it takes the solver to generate a solution. In case, a quick solution is required, one can introduce constraints in the solver settings as this will limit the solver from generating random shapes.

For side-side squares at the corner of the box.

1. **Using the polynomial boundary at dmax= 0.02 and n=2**

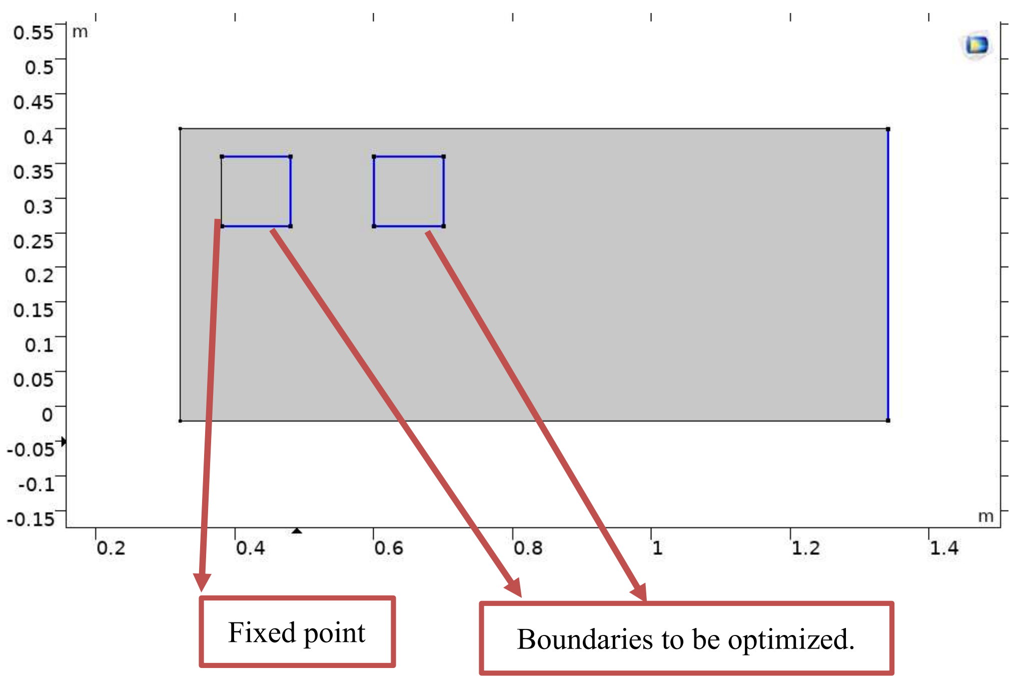

Figure 60: Boundaries selected for shape optimization.

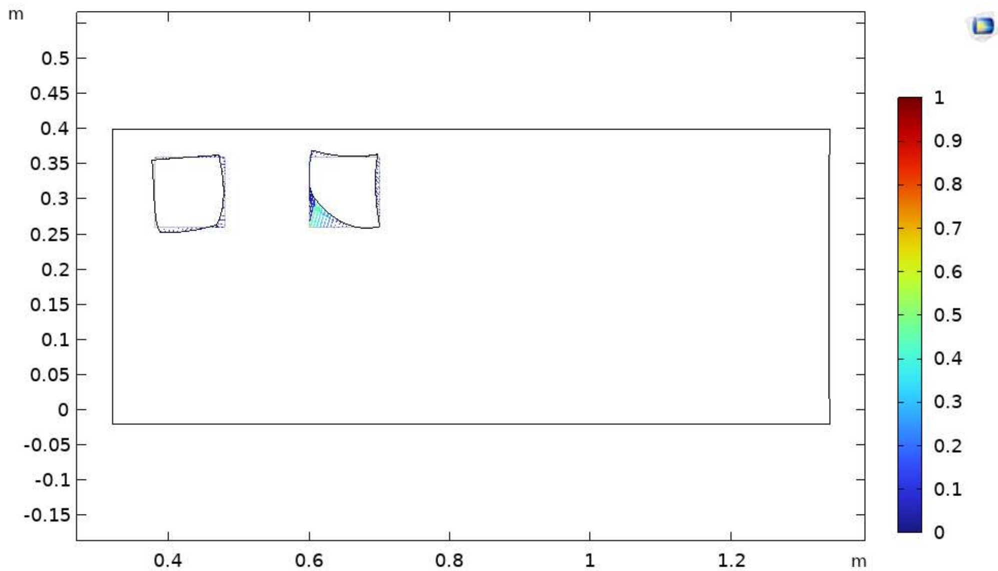

Figure 61: Boundary displacement for side-side squares (polynomial boundary).

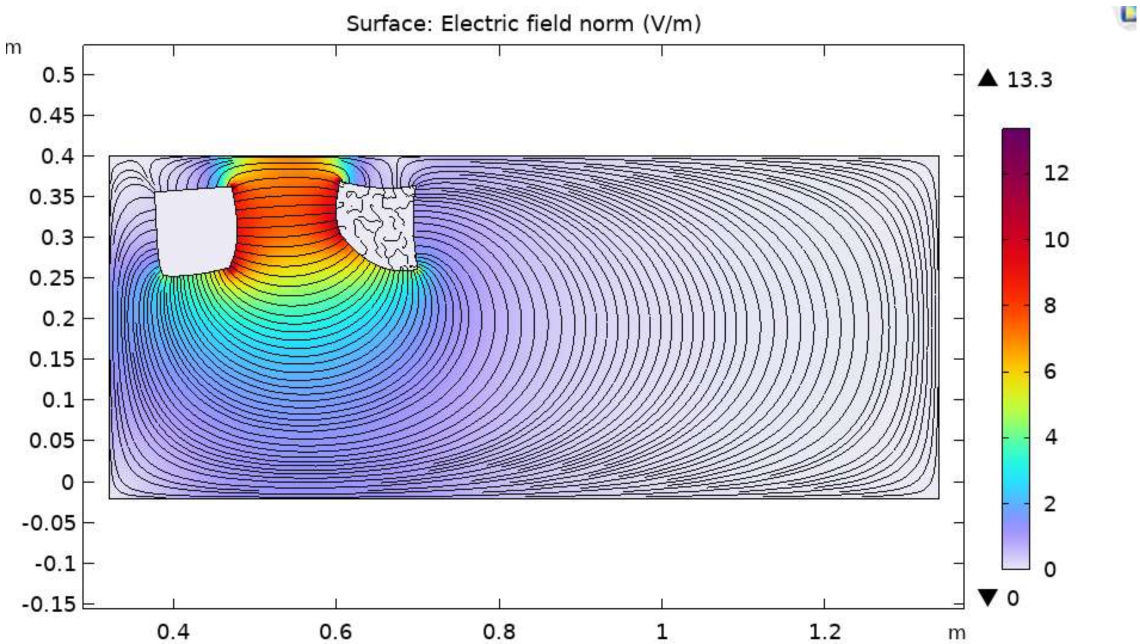

Figure 62: Shape optimization of side- side squares (at the corner of the box) using polynomial boundary.

Table 12: Results of shape optimization of side-side squares (at the corner) using polynomial boundary method.

Bernstein order,n	dmax, [m]	Initial area, [m^2]	Optimized area, [m^2]	% change in the area	Initial max E-field, [V/m]	Optimized max E-field, [V/m]	Elapsed time, [min]
	0.02		0.0210	5.0		12.2	3
n=2	0.03		0.0202	1.0		11.0	4
	0.04		0.0210	5.0		12.3	7
	0.02	0.020	0.0220	10	18.4	13.5	5
n=3	0.03		0.0205	2.5		10.1	5
	0.04		0.0208	4.0		11.1	6
	0.02		0.0210	5.0		10.5	3
n=4	0.03		0.0204	2.3		12.5	6
	0.04		0.0209	4.8		10.0	8

The polynomial boundary method of shape optimization is advantageous when applied on geometries with flat boundaries unlike the free-shape boundary method because it allows the smoothening of corners by fixing a point along the boundaries to be optimized as this allows the curving of the boundaries with respect to the fixed point hence describing why the free-shape boundary method is not applied to this geometry because the results are not satisfactory [8].

For corner-corner squares at the corner of the box,

Using polynomial boundary at dmax= 0.028 [m], n=5.

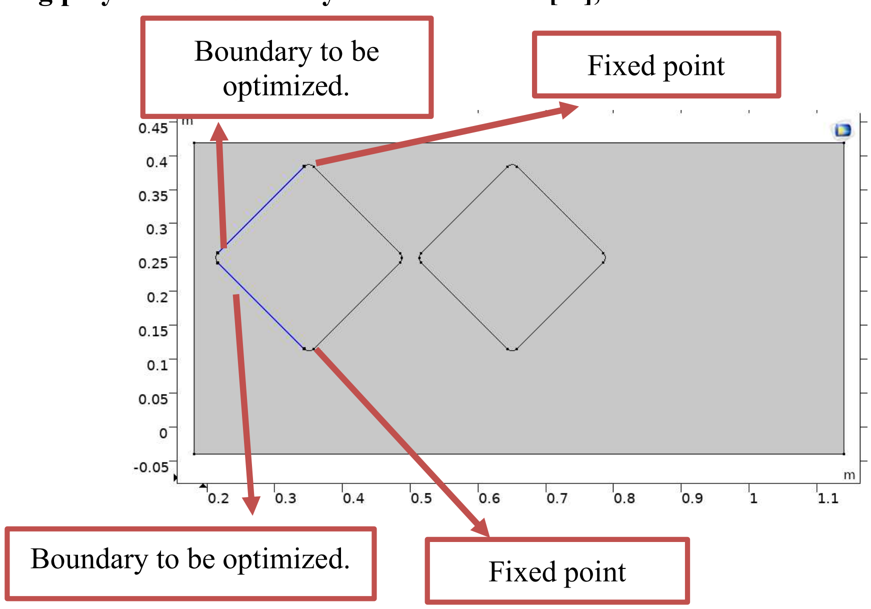

Figure 63:Boundaries selected for shape optimization.

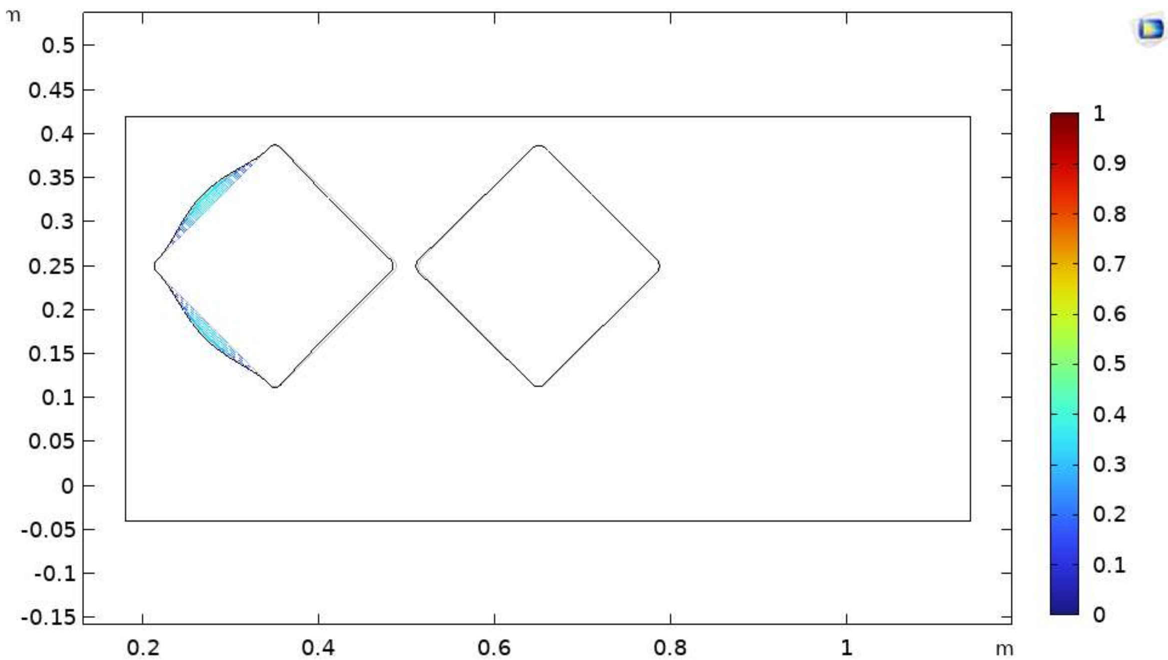

Figure 64: Boundary displacement for corner-corner squares

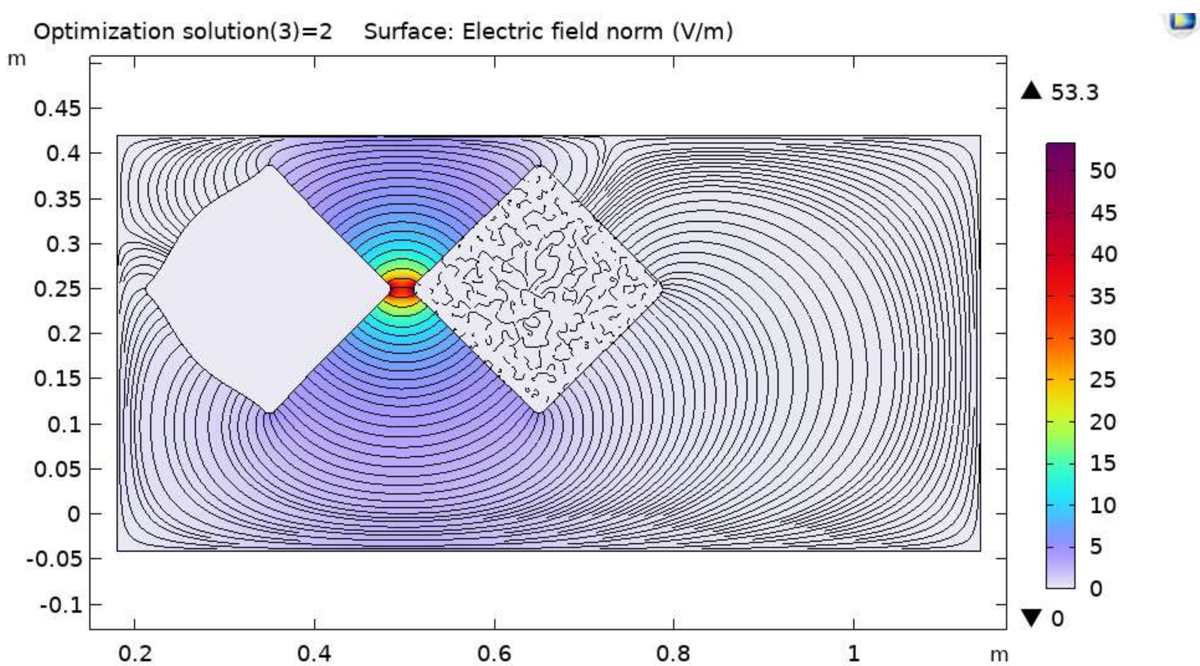

Figure 65: Shape optimization of corner-corner squares.

Table 13: Results of shape optimization of corner-corner squares using polynomial boundary method (at the corner).

Bernstein order,n	dmax, [m]	Initial area, [m^2]	Optimized area, [m^2]	% change in the area	Initial max E-field, [V/m]	Optimized max E-field, [V/m]	Elapsed time, [min]
	0.028		0.082	3.79		53,3	11
n=2	0.031		0.084	4.05		48.4	12
	0.034		0.085	7.59		43.3	14
	0.028	0.079	0.081	2.52	**53.7**	40.0	27
n=3	0.031		0.082	3.79		39.6	31
	0.034		0.083	5.05		37.9	10
	0.028		0.082	3.70		32.8	23
n=5	0.031		0.082	3.79		37.4	8
	0.034		0.081	2.52		35.7	5

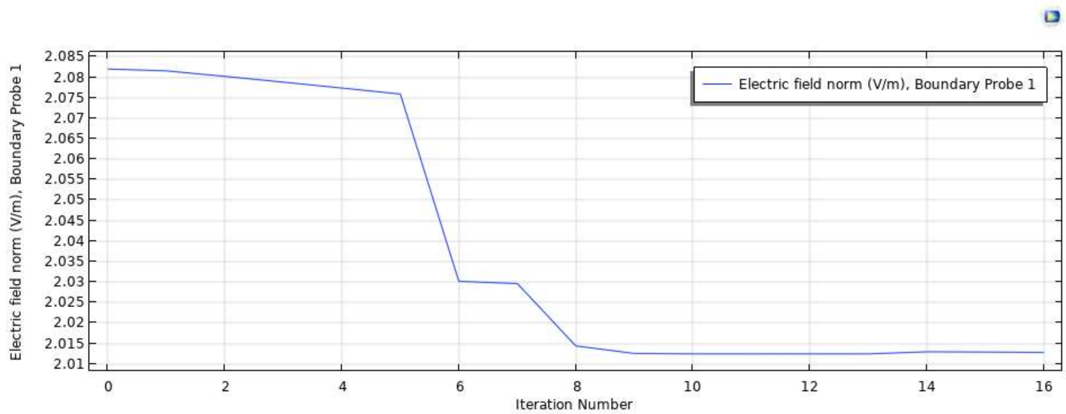

Figure 66: Electric field distribution on the surface of corner-corner squares versus iteration number.

Conclusively, different formulations of the objective function generate relatively similar results regardless of the shape optimization method used.

- When the objective function of optimization is formulated to be the E-factor; ideally the aim is to maximize it to unity, thus as the E-factor increases, the field distribution becomes uniform unlike cases when the E-factor approaches zero where the field is non-uniform; thus, causing local field intensifications on the surface of the geometry. Figure 67 describes how the formulation of the objective function (E-factor) is implemented in the solver settings.

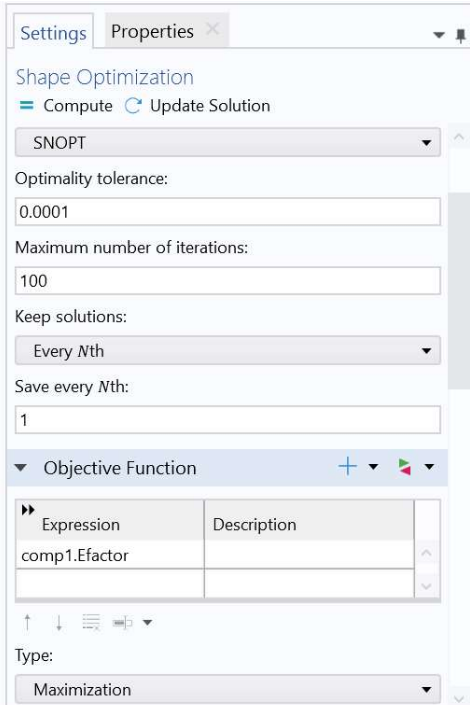

Figure 67: The formulation of the objective function (E-factor) in the shape optimization solver settings.

- The objective function can be formulated as the minimization of the maximum electric field strength as shown in figure 66 and 68.

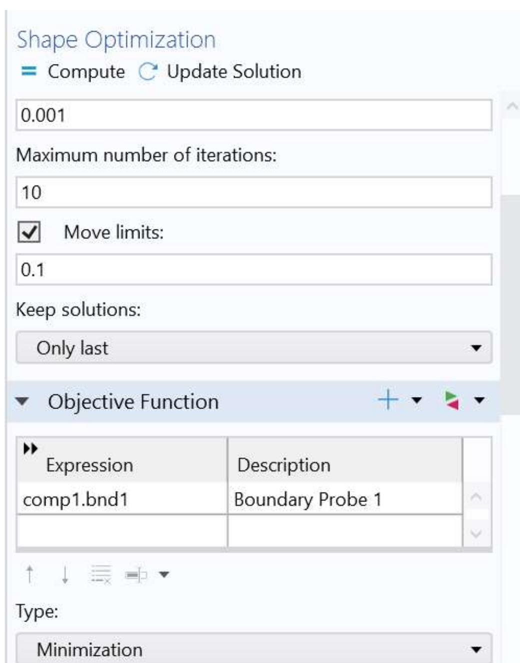

Figure 68: The formulation of the objective function (electric field strength) in the solver settings.

3.1.3 3D-voltage divider

3.1.3.1 3D-voltage divider at the center

The electrostatic field was computed in 3D whereby the materials assigned to the imported geometry are.

1. **Aluminum**: which is assigned to the cone-shaped top, toroid of the voltage divider.
2. **FR4 circuit board** is assigned to the vertical cylindrical support to the top-part.
3. **Air medium**: is assigned to the cubical box that encloses the voltage divider. As shown in figure 69 below.

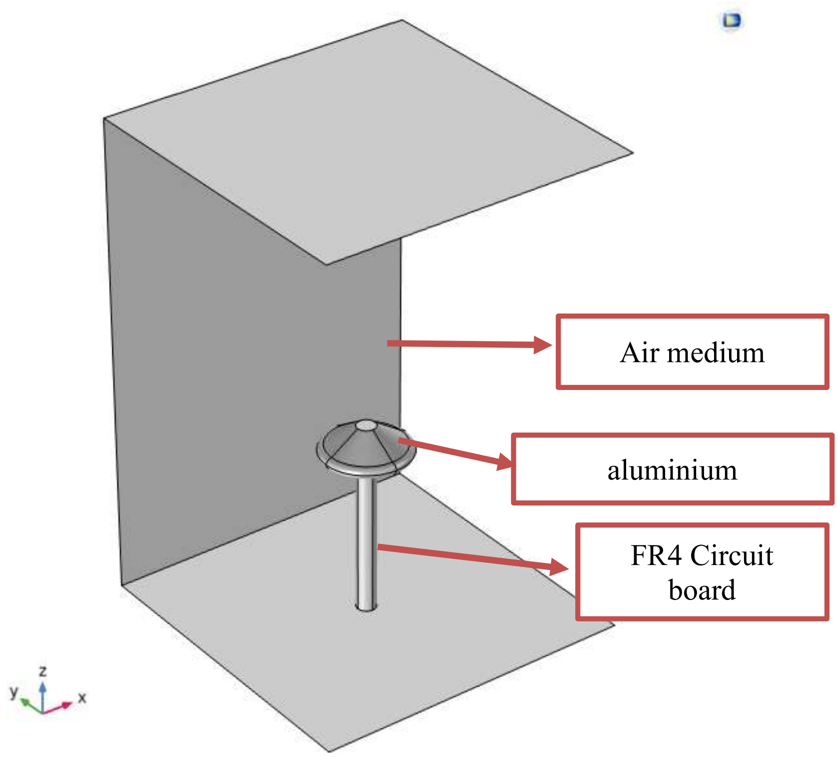

Figure 69: Test set-up of the voltage divider in COMSOL.

3.1.3.2 The boundary conditions

In the physics interface, the nodes added are the "ground" and "electric potential". These nodes are assigned to different boundaries of the finalized imported geometry whereby the cone-shaped, toroidal top part is assigned a nominal voltage of 400 [kV]. The bottom surface of the vertical cylindrical part and the walls of the cubical box are assigned to be the ground as such typically is used to ensure the safety of the measuring device and other equipment outside the HV laboratory. However, the top part of the box is set to be the zero-charge, as shown in figure 70 below.

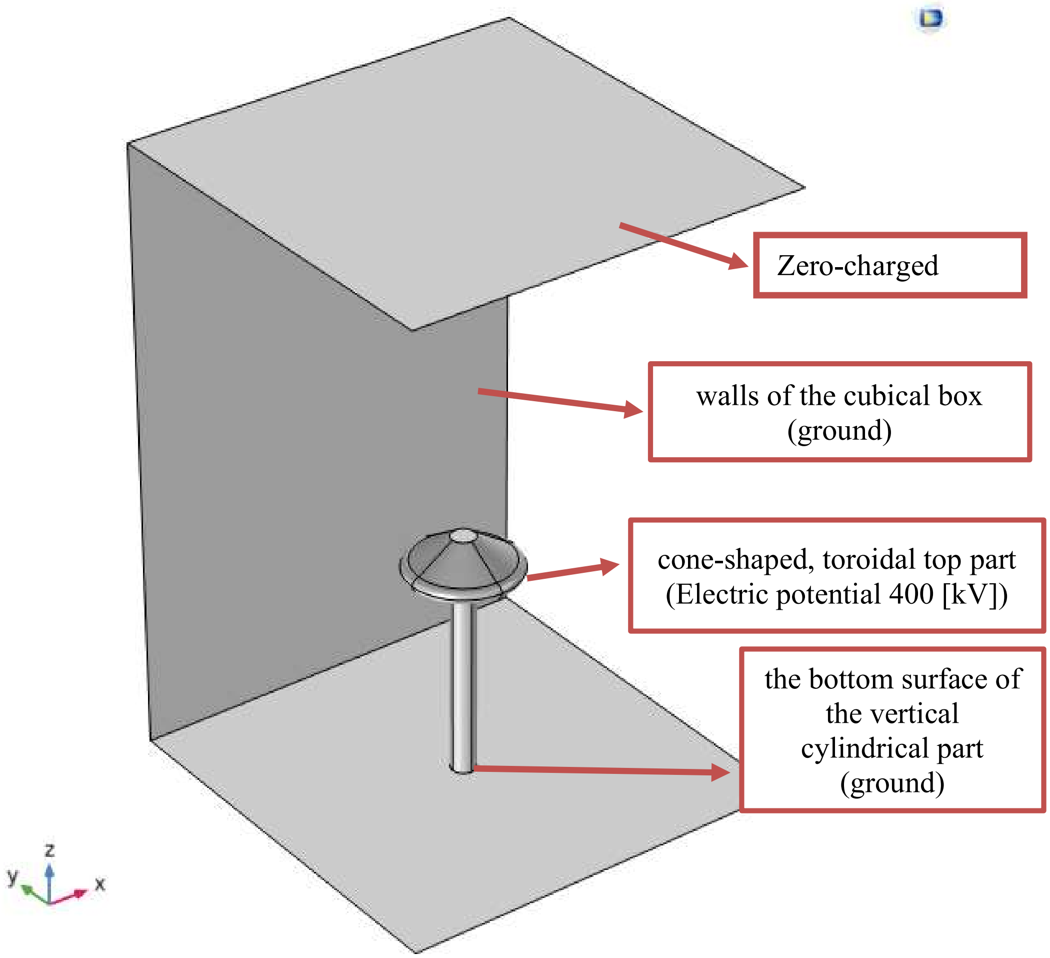

Figure 70: Finalized geometry of the voltage divider with boundary conditions.

3.1.3.3 Mesh adjustments

COMSOL provides different mesh generation options and sizes depend on the physical problem to be computed. However, depending on the users need to obtain accurate results during post-processing part, it is important to use built-in algorithms of mesh generators as a way of adjusting the mesh distribution along the areas of interest. A typical example is described in figure 71. However, for the necessity of reducing the number of degrees of freedom and the size of the problem, it is recommended to use a physics-generated mesh to avoid overwhelming the optimization solver which slows down the simulation speed to a halt.

In figure 71 it is clearly observed that the regions of interest defined as the regions where the electric field strength is expected to be enhanced requiring meshing of the boundary elements to a much finer mesh such that the results of the computation are accurate. Other regions of the box assigned to be the ground thus don’t need to be re-meshed because the field strength is expected to be lower and are of less interest in the analysis.

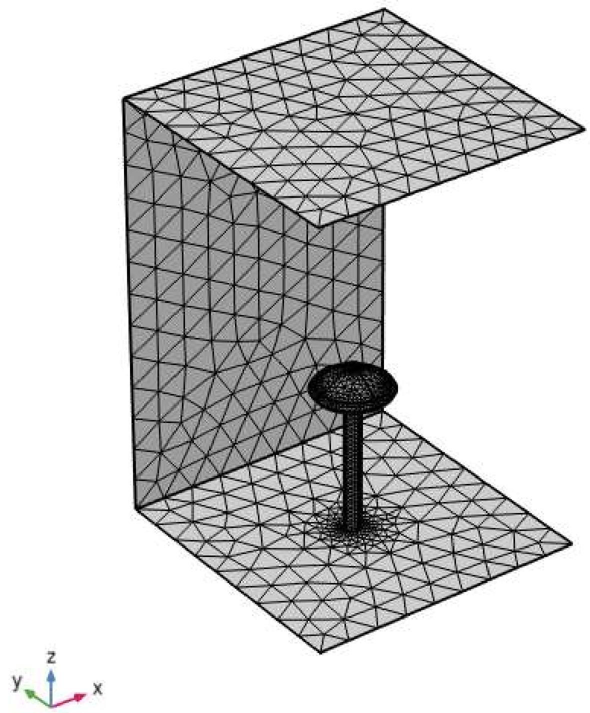

Figure 71: Meshing of the voltage divider at the center of the box.

3.1.3.4 Es-study of 3D-voltage divider (center)

The simulation results allow to establish a reference value of the maximum electric field during the optimization process. The maximum value of the electric field on the initial geometry of the voltage divider is 2.4 [kV/mm] as seen from figure 72 The voltage divider is geometrically and electrically symmetrical amongst 2 planes since it is placed at the center of the box. Furthermore, the electric field appears nearly axisymmetric since the separation distance between the high electric potential toroidal screen is far from the ground and thus the field enhancement will not be very significant. The top part of the box which can be considered as the ceiling of the high voltage laboratory, will experience negligible electric field strength as it is assigned to be zero-charged.

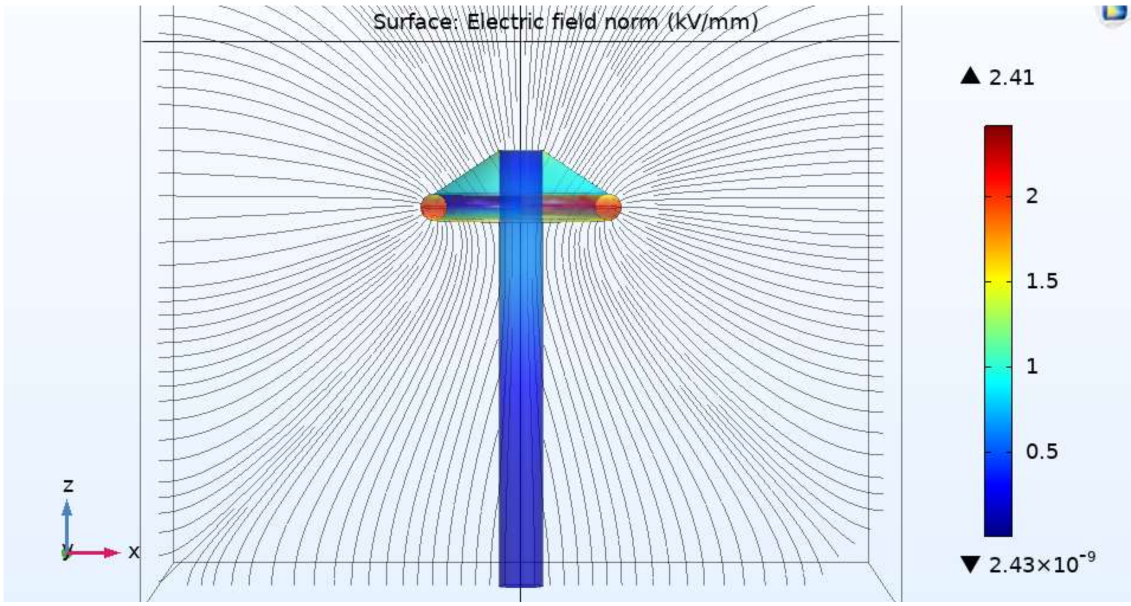

Figure 72: Es-study of voltage divider at the center of the box.

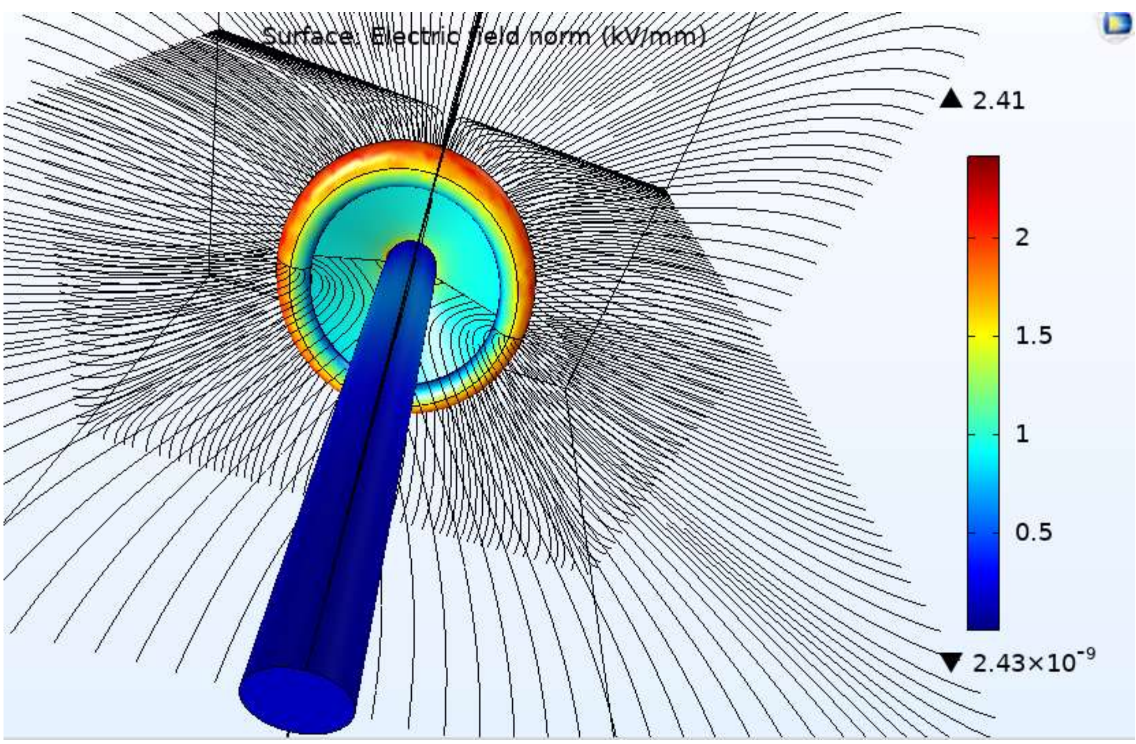

Figure 73: (Bottom view) of the es-study of voltage divider at the center of the box.

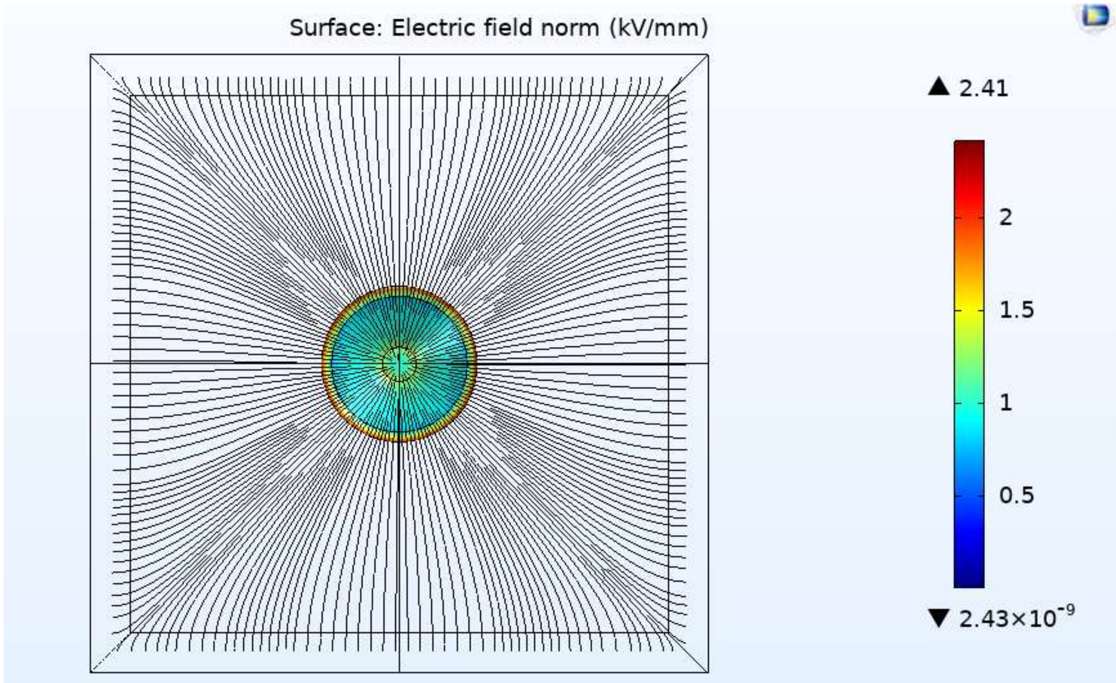

Figure 74: (Top view) of the es-study of voltage divider at the center of the box.

3.1.3.5 Shape optimization of 3D-voltage dividers at the center

The shape optimization of 3D- voltage dividers is performed by adding a "free-shape domain and the "free-shape boundary node" to perform optimization on the selected boundaries. Free-shape boundary uses features like the maximum displacement, dmax in [meters] to regulate the percentage change of the original geometry whereby the default value is dmax = 0.2 [m] which is equivalent to 5% of the boundary box. Another feature of the free-shape boundary method of shape optimization is the "minimum filter size, *Rmin*" which corresponds to 1.5 and 2 times the maximum displacement [9] [10]. Therefore, this requires a careful selection of *dmax* and *Rmin* parameters, whereby it is advisable to select a maximum displacement, *dmax* not too large or the minimum filter size, *Rmin* not too small to avoid convergence errors during the computation. Additionally, the shape optimization algorithm of 3D- voltage dividers consist of the following features:

1. **Probe selection**: An objective function is added by using a boundary probe that computes the maximum electric field strength on the boundaries of the cone-shaped & toroidal part of the 3D-voltage divider. It is used in the shape optimization solver settings as the objective function such that the maximum electric field strength is minimized.

2. **Shape Optimization solver**: A shape optimization study is performed based on the initially computed electric field strength value = 2.41 [kV/mm]. In this case the method of optimization used in this problem is "MMA" because it is characterized to be faster than the other gradient-based solver types.

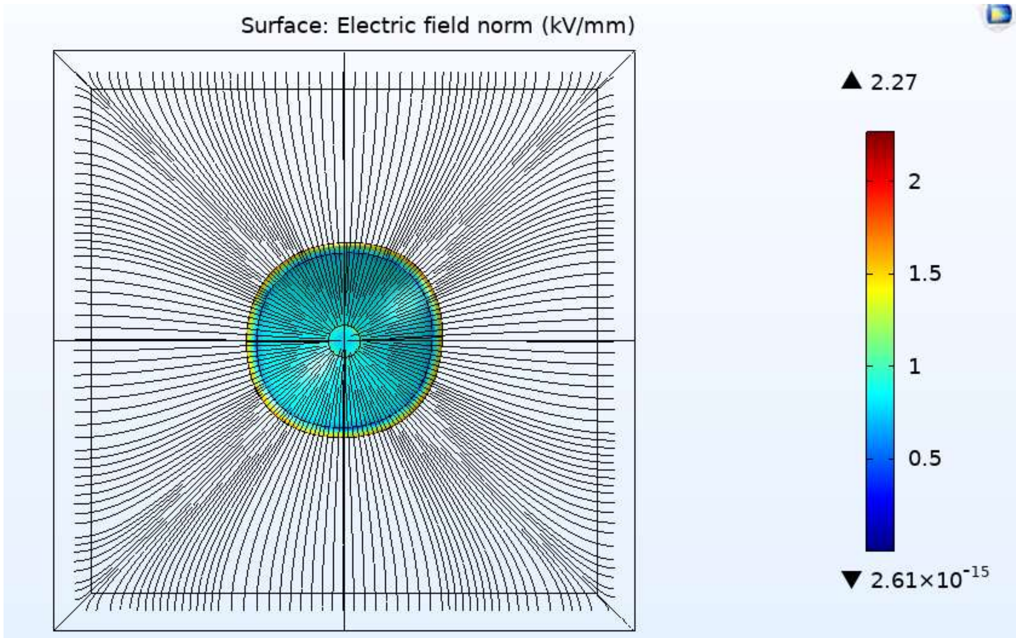

Figure 75: (Top view) of the optimized voltage divider at the center.

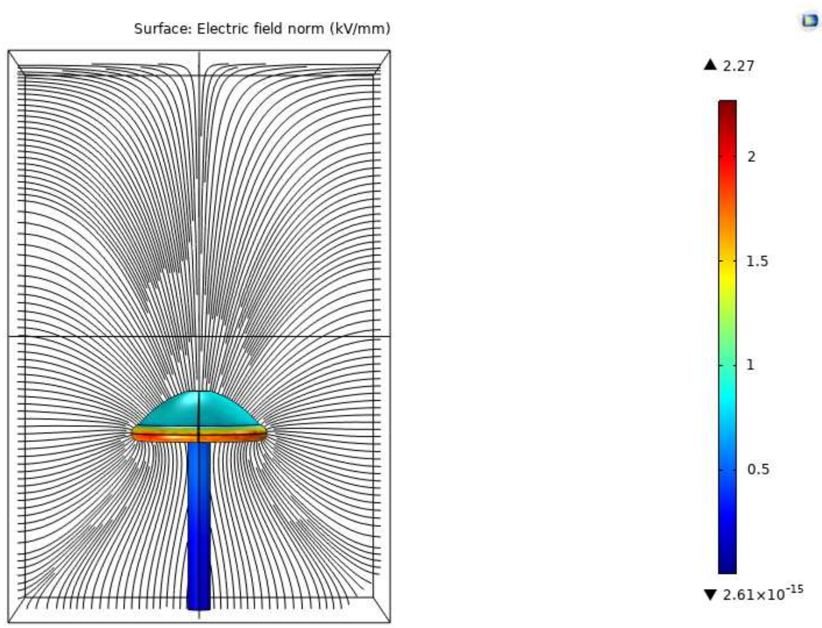

Figure 76: (Side view) of the optimized voltage divider at the center.

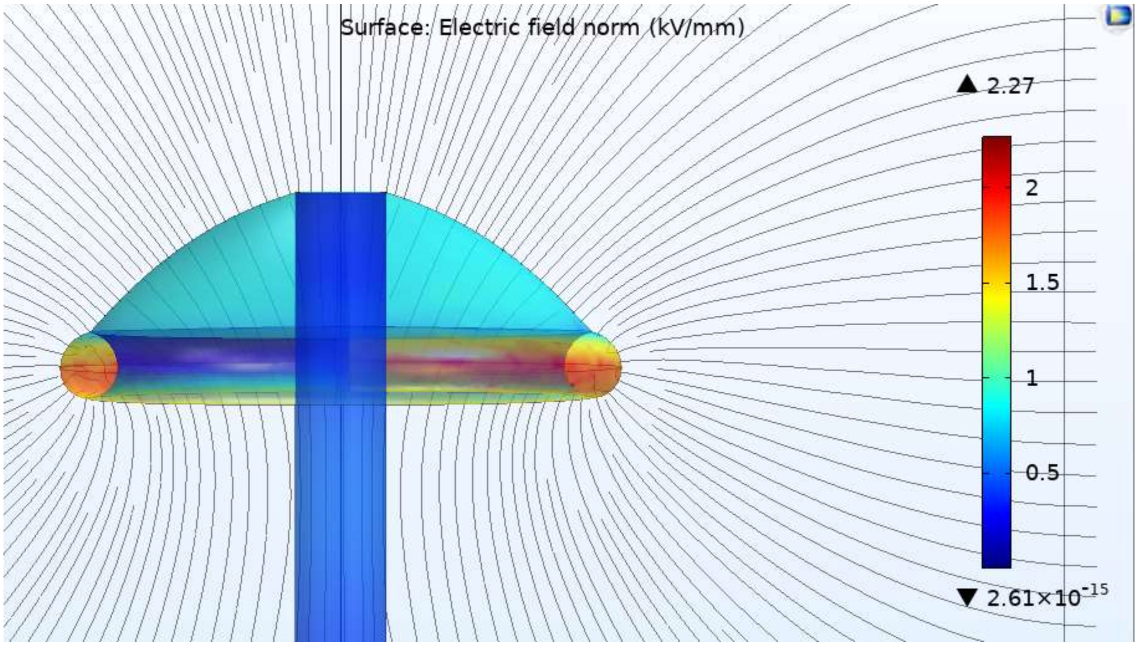

Figure 77: Inner view of the voltage divider.

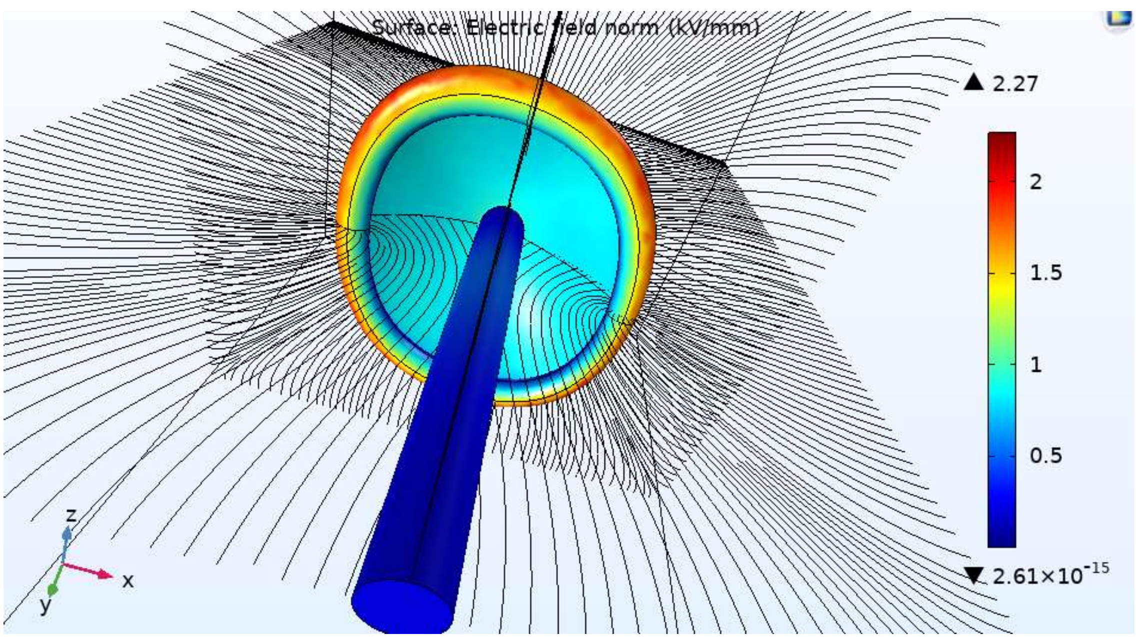

Figure 78: Optimized voltage divider (center) with dmax= 0,2 [m] and Rmin= small.

Conclusively, it is observed that the toroidal screen of the voltage divider is not subjected to significant shape deformation because of the selected minimum filter size, *Rmin= small* as this will not influence any change in the circumference of the toroidal screen.

3.1.3.6 3D-voltage divider at the corner

The electric field strength of the voltage divider is analyzed by considering two important cases, which involve the computation of electric field strength at different locations of the voltage divider which will helps drawing a conclusion about the effectiveness of the shape optimization. Hence, the magnitude of the electric field strength at the top of the toroid of the voltage divider when placed at different locations enclosed in a box is evaluated.

The procedure of performing the electrostatic study is identical to the previous case with the only aspect that changed being the location of the initial geometry as described in figure 79.

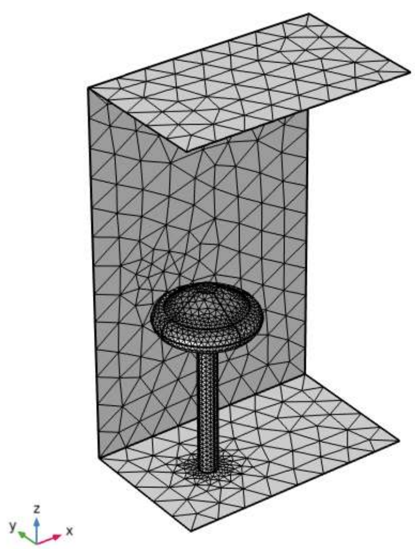

Figure 79: Meshing of the voltage divider (at the corner).

3.1.3.7 Es-study of the 3D-voltage divider (at the corner)

As the voltage divider approaches the proximity of the wall, the maximum electric field strength also increases as shown in the figure 80. Due to this proximity the field strength on the surface of the toroidal screen is expected be significantly increased, because of the field enhancements caused by the decreased distance between the grounded walls and the high voltage potential at the top part of the voltage divider. As observed during the shape optimization, when the electric field strength was minimized the overall shape of the toroidal part of the voltage divider was flattened and deformed to relieve this enhancement.

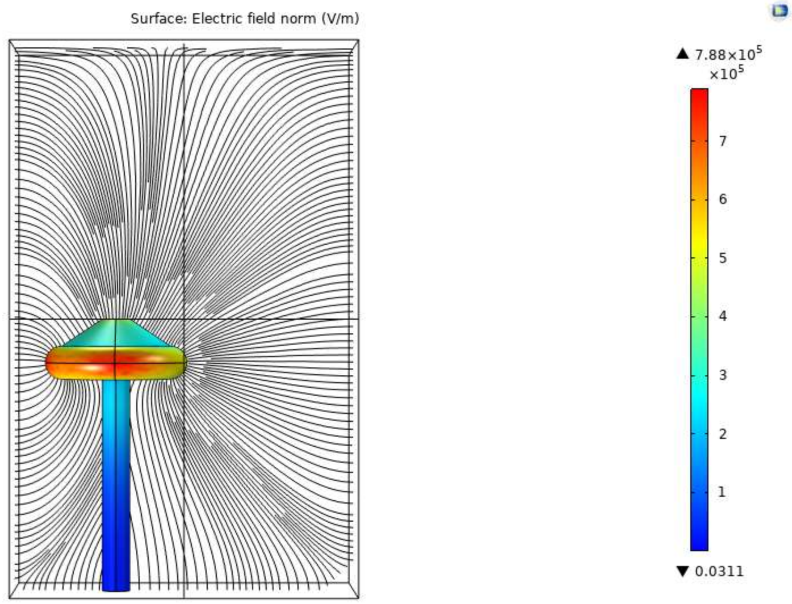

Figure 80: Es-study of voltage divider at the corner of the box.

3.1.3.8 Shape optimization of 3D-voltage dividers (at corner)

The shape optimization of the 3D- voltage divider was performed by adding a “free-shape domain and the” free-shape boundary” node for adding the control variables such as the maximum displacement, “dmax” which was set at 0.2 [m] and the minimum filtering size was selected to be small.

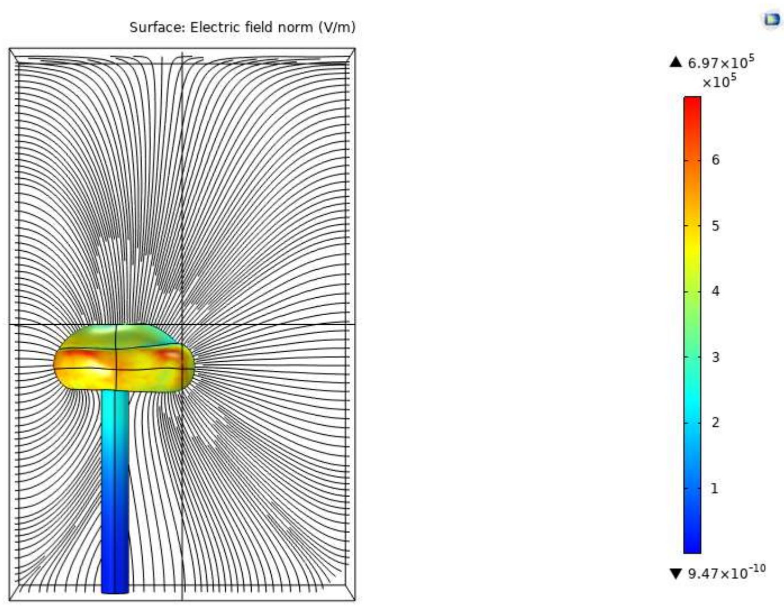

Figure 81: (Front view) of shape optimization of the voltage divider.

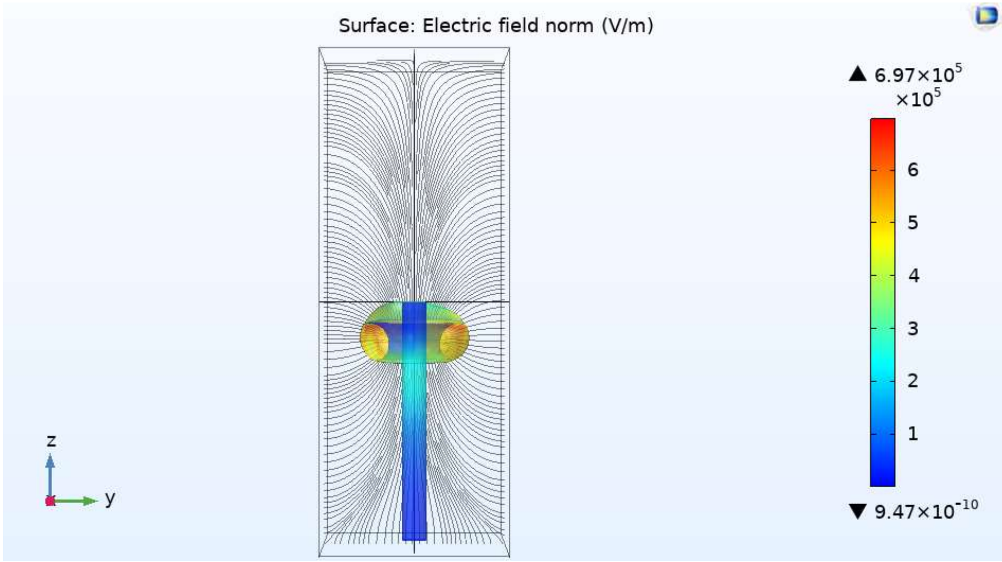

Figure 82: (Inner view) of shape optimization of the voltage divider.

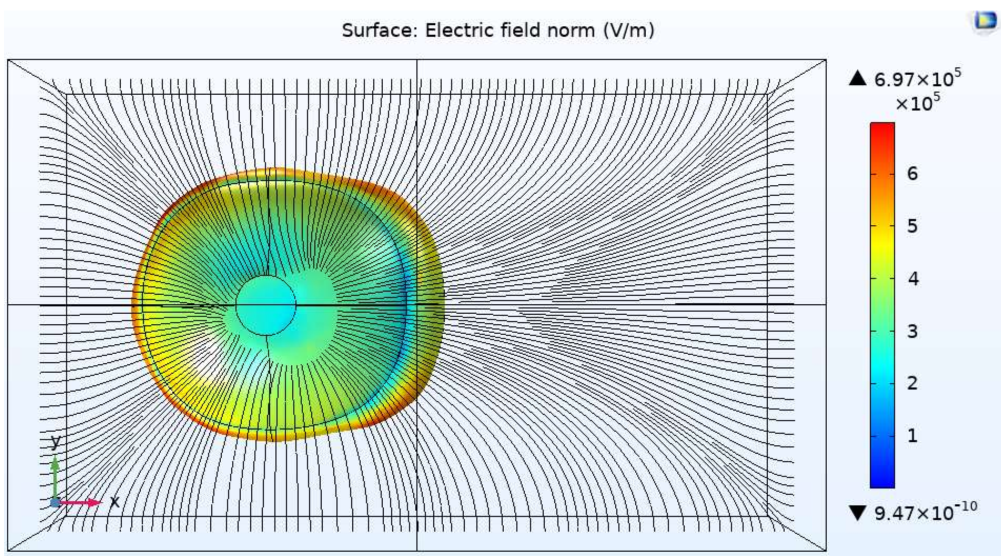

Figure 83: (Top view) of shape optimization of the voltage divider.

4 Discussion

4.1 3D-scanning

It is important take into consideration suggestions summarized below to ensure the scanning process goes smoothly, ensuring increased quality in the scans;

- If possible, it is important to perform the scanning process after clearing the space around the physical object to be scanned. Thereby other objects in proximity, or in the background which are not supposed to appear don't hinder the process of scanning. Otherwise, if a congested room or laboratory full of equipment is to be scanned as it is, the physical objects to be optimized have at least to be enough away from other equipment to avoid accidents during the scanning, and in post-processing it is possible to exclude regions not of interest.
- From a technical perspective, it is important to check the accuracy of the 3D-scanner by means of calibration. Here, commercial products typically feature built-in methodology.

4.2 Shape optimization

4.2.1 2D- circles (symmetric case)

Using the free-shape boundary method from table 3, the following aspects were observed:

- As the maximum displacement, dmax increases the percentage change in the area also relatively increases as it is the maximum displacement that determines how much the boundaries of the circle will be expanded or contracted. Thus, any form of deformation in the shape of the circle must correspond to an areal change.

Using the polynomial boundary method for 2D-circles (symmetric case) from table 4 it is observed that:

- For the first iteration at n=1 the average shape increase is *3.74%* while for the second iteration at n=2 is *3.75%*, and the third iteration is *4.29*%. This is caused by the higher the degree of the Bernstein equation, creating a more significant effect of the smoothing equations on the circle boundaries.

- As the order of the Bernstein polynomial increases, the elapsed time of computation increases accordingly, because the optimization solver is trying to generate new shapes of the boundaries that are largely dependent on the formulated equation of the Bezier curve, the latter now having a much bigger degree of freedom. Since volume constraints are not applied, it will take more time for the solutions to converge.

- The lower the order of the Bernstein polynomial, the larger the change in the overall area of the initial geometry of the circle, yielding for this case a sharper decrease in the magnitude of the maximum electric field strength.

4.2.2 2D-circles (corner)

Using the polynomial boundary optimization results in the table 10, from which the following observations were made:

- At n=2, there is not much change in the surface area even though the maximum displacement is increasing; this is because the gradient- based solver, MMA which was used in this problem takes into consideration the order of the polynomial degree, meaning that when it derivates the second degree polynomial of n=2, which can be mathematically described as a parabola, the result of the derivation will be approximately a linear function hence the boundaries will tend to be straight. Therefore, while the degree of the optimized shape tends to be reduced, it will make the optimization process more robust.

- In case significant shape changes are demanded, it is advisable to increase the degree of the polynomial, i.e., n>2. However, this increases the computation time accordingly.

4.2.3 2D-squares

4.2.3.1 Side-side (symmetric case)

The shape optimization of side-side squares, at the center of the box, using the free-shape boundary method from the table 7 yielded the following findings:

- When the minimum filter size, *Rmin* is large and the maximum displacement, *dmax* increases; the incremental surface area of the squares increases from *25%* to *37.5%,* because the solver is given more freedom to move the boundaries in any direction since the solver is using the method of iteration of points to perform optimization. This will also increase the elapsed time of the computation.

- As the minimum filter size decreases, the solution converges more quickly, which is shown by how much the elapsed time decreases, this is because the amount of iteration points that are handled by the solver are decreased thus increasing the speed of its performance.

4.2.3.2 Corner-corner (symmetric case)

For the corner-corner squares, using the polynomial boundary method with results shown in the table 8, further insight was made:

- A bigger change in surface area occurred at higher orders, i.e., at n>2, as observed in the table 8, the average increase at n=4 is approximately 9%, and at n=3 it is 6%. For this specific type of problem, “fixed points” played a key role in making the boundaries flexible to move, hence making them to be more curved after optimization, thus strongly affecting to which degree the electric field is minimized since the sharp points were eliminated at the points of interest.

4.2.3.3 Side-side squares (corner)

From table 12, showing the optimization using the polynomial boundary, it was observed that:

- The average elapsed solving time is lower compared to the other cases. This is because the solver's performance was enhanced by using a smaller tolerance in the solver settings, leading to a decrease in accumulated errors, resulting in a faster convergence time since the time steps were smaller.

4.2.3.4 Corner-corner squares (corner case)

From the table 13 it is observed that:

- The changes in the surface area resulting from the optimization are quite minimal whereby the average change in the surface area for n=2 is *3.47%*, for n=3 is *3.78%,* n=5 is *5.33%.* This shows how the boundaries of the squares resist to changes, thus requires adding features to the algorithm like adding "fixed points" to render more flexibility to the free displacement of the boundaries about the fixed point.

4.2.4 Voltage divider

The free-shape boundary method of adding control variables to the optimization problem is suitable for problems involving the 3D-geometries such as the 3D-voltage divider. The free-shape boundary method utilizes a maximum displacement, dmax which was set to a default value 0.2[m] controlling the change in the overall geometry from the initial one. The errors associated with using the free-shape boundary method arise as forementioned in the polynomial boundary method. It is recommendable to use a maximum displacement in range of 0.2 up to 0.8 [m] for the optimization problem to function smoothly without any computational errors. The convergence rate can be improved through careful selection of the initial values.

In the optimization of the 3D-voltage divider, the vertical cylinder was not subjected to shape optimization, this means that it should not appear in the selection list of boundaries to be free-shape boundary optimized. Including it could result in the deformation of the vertical cylindrical part, which is impractical in the design of the voltage divider and typically manufacturable.

5 Conclusion and suggestions for the future work

The conclusions of this work are as follows:

- Optimization tools provided in COMSOL Multiphysics have been adopted for electrostatic studies, whereby it has enabled the possibility to merge the objective functions of the shape optimization with stationary solvers hence allowing to choose a suitable optimization solver.
- Best practices for the selection of parameters of the optimization algorithms i.e., gradient based, and gradient-free solvers have been established whereby gradient based optimization solvers such as SNOPT, IPOPT are selected based on the number and complexity of constraints dealt with while MMA was selected to handle problems with many control variables such as some cases of shape optimization of 3D-voltage dividers.
- The results of shape optimization of a voltage divider show that the shape of the toroidal screen can be adapted to changes in the position of the voltage divider. The final optimized shape of the 3D-voltage divider can be manufactured using 3D-printing.

Even though, a large percentage of this project was implemented, there is still room for further studies to be performed. However, the fundamental theory and test simulations using high voltage test setups from the Chalmers High voltage laboratory have been done.

Different methods of controlling the electric field strength like using grading rings were not explored, although there was a high possibility that using these would achieve the objective of further minimizing the electric field strength below the breakdown value.

The implementation of this project in COMSOL Multiphysics has helped in providing a deep understanding of what is happening in the real world of high voltage engineering in which if the optimization module is fully explored would bring a much deeper understanding about the optimal shape for individual applications.

Lastly, the practical aspects of geometry optimization involving scanning certain setups, calculating their electric field strength, manufacturing optimized electrodes, and performing withstand tests of the printed high voltage electrodes remains a topic to be covered in future work.

References

[1] A. Küchler, " *Fundamentals-Technology- Applications*," *in High Voltage Engineering*, Schweinfurt, Germany, Springer Vieweg, 2018, pp. 8-26.

[2] E., Kuffel; W.S., Zaengl; J., Kuffel, "*High Voltage Engineering Fundamentals (2nd Edition)*," Elsevier, 2000, pp. 201-280.

[3] "*Introduction to the Optimization Module*," 1998–2020. [Online]. Available: https://doc.comsol.com/5.6/doc/com.comsol.help.opt/IntroductionToOptimizationModule.pdf.

[4] D. Kind and K. Feser, *High Voltage Test Techniques 2nd Edition*, Newnes, January 24, 2001.

[5] "Artec 3D," 2024. [Online]. Available: *https://www.creaform3d.com/en/portable-3d-scanners.*

[6] "*Optimization Module, User's Guide*," `COMSOL AB, 2022. [Online].

[7] D. T. Anton Olason, "*Methodology for Toplogy and Shape Optimization in the Design process*," Chalmers Reproservice, Göteborg, Sweden, 2010.

[8] Erik Bjerned, Mattias Persson, Axel Danielsson, "*Shape optimization of corona shield geometry*," Uppsala Universitet, Uppsala, May 2022.

[9] Rao, Singiresu S., *Engineering Optimization - Theory and Practice*, John Wiley & Sons, third edition, 1996.

[10] Niels Ottosen, Hans Petersson, *Introduction to the Finite Element Method*, Prentice Hall, 1992.

DEPARTMENT OF ELECTRICAL ENGINEERING
CHALMERS UNIVERSITY OF TECHNOLOGY
Gothenburg, Sweden 2023
www.chalmers.se

AVANCEZ
1829

CHALMERS
UNIVERSITY OF TECHNOLOGY